A STUDY OF SEMI CONDUCTION IN OXIDE SOLID SOLUTIONS.

A THESIS

SUBMITTED FOR THE

DEGREE OF DOCTOR OF PHILOSOPHY

IN THE

UNIVERSITY OF LONDON

BY

GORUR NARAYANA KRISHNA IYENGAR

Department of Metallurgy,
The Royal School of Mines,
Imperial College of Science & Technology.

January, 1967.

ABSTRACT

A study of the redox equilibria in the dilute magnesio - wustites has been made in order to understand the energy assoc - iated with the charge transfer taking place between di and tri - valent iron cations in the host lattice of magnesia. In this study measurements were of the $^{n}Fe^{+++}/^{n}Fe^{++}$ ratio in the solid solutions containing 0 - 20 mole of per cent iron oxide (FeO) in the temp - erature range 900 - 1200 ^{o}c. The oxygen partial pressures employed covered the range from equilibrium of the solid solutions with solid iron to that in equilibrium with the spinel phase (Mg Fe) Fe_2O_4. By combining these results with the literature data it is possible to make an accurate calculation of the thermodynamics of the redox equilibria in these solid solutions. The results of this calculation are compared with those for the pure Fe - O_2 binary system. The results of the present work are discussed in the light of the various defect structural models proposed for the non - stoichiometric oxides. The measurement of $^{n}Fe^{+++}/^{n}Fe^{++}$ ratio was made on the quenched samples by both colorimetric and volumetric methods.

Furthermore, measurements were made on the variation of the electrical conductivity of the solid solutions on the temperature range 800 - 1000 ^{o}c to determine the nature of the current carriers. The range of the oxygen partial pressure employed again covered the entire phase field. The results of conductivity are discussed in terms of the localized electron model.

CONTENTS

CHAPTER ONE

CHAPTER TWO

CHAPTER ONE

1. INTRODUCTION

1.1. General

According to Verwey[1] semiconductors of ionic type can be classified into three groups.

1. Non-stoichiometric compounds, e.g. FeO_{1+x}, NiO_{1+x}, TiO_{2-x} etc. where x is the degree of deviation from stoichiometry.
2. Oxide solid solutions (made by dissolution of a semiconductor in an isomorphous compound having relatively poor conductivity) e.g. Solid solutions of type Fe_3O_4-$MgAl_2O_4$, FeO-MgO, Cr_2O_3-Al_2O_3 etc.
3. Controlled valency semiconductors, e.g. $Li_xNi_{1-x}O$, $La_xCa_{1-x}MnO_3$ etc.

With an exception of the non-stoichiometric compounds, a detailed and systematic study of the electron transfer properties of the other systems is lacking. Such studies would provide the relevant quantitative information to test the validity of the assumptions which are implicit in the band[2, 3] and the electron transfer[1, 4-6] model theories. The aim of the present work has been to obtain results in order to interpret the semiconducting behaviour of the binary oxide solid solutions involving a transition metal oxide. For such investigations the system FeO-MgO was chosen because of the following attractive properties of the system.

a. Both the end members and the solid solutions[7-9] possess the NaCl crystal structure (Figs. 1(a) and (c)).

b. FeO and MgO form a continuous series of solid solutions[10] (Fig. 1(b)).

c. The mechanism of electrical conduction and the nature of the lattice disorder in wustite[8, 11-29] and magnesium oxide[30-39] is relatively clearly established.

d. The thermodynamics and various phase relations of the system has been studied in detail[9, 40-45].

e. Finally the system offers an unique opportunity for a study of the electron transfer mechanism between ferrous and ferric ions when the cation sub-lattice of wustite is diluted with magnesium ions which cannot adopt any other stable state of ionization other than Mg^{++}.

1.2. Thermodynamic and Electrical Properties of Wustite and Magnesium Oxide

1.2.a. The Wustite Field and Related Equilibria

Iron forms three oxides, wustite (FeO_{1+x} $0.06 < x < 0.15$), magnetite (Fe_3O_4) and haematite (Fe_2O_3), of which only wustite is unstable below 560°C. The classic study of Darken and Gurry[11] of the thermodynamics of the Fe-O_2 binary system clearly established, the pressure-temperature-composition limits within the wustite

FIG. 1.

Fig 1 a ROCK SALT STRUCTURE

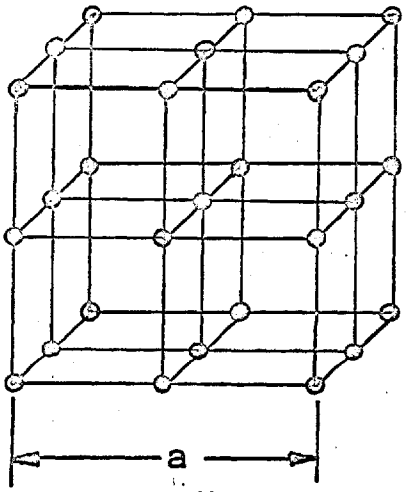

Fig 1 b.
PHASE DIAGRAM OF
FeO - MgO SYSTEM

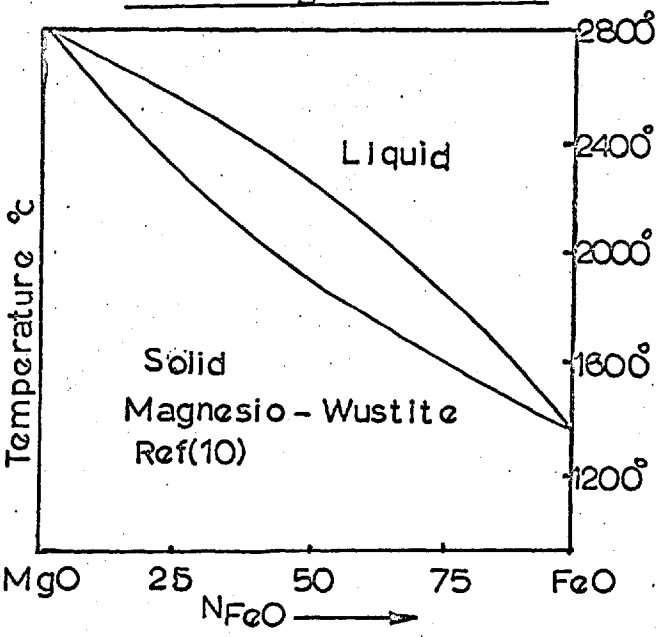

Fig 1c

VARIATION OF d-SPACING OF(200) REFLECTION
WITH COMPOSITION IN THE SYSTEM FeO-MgO

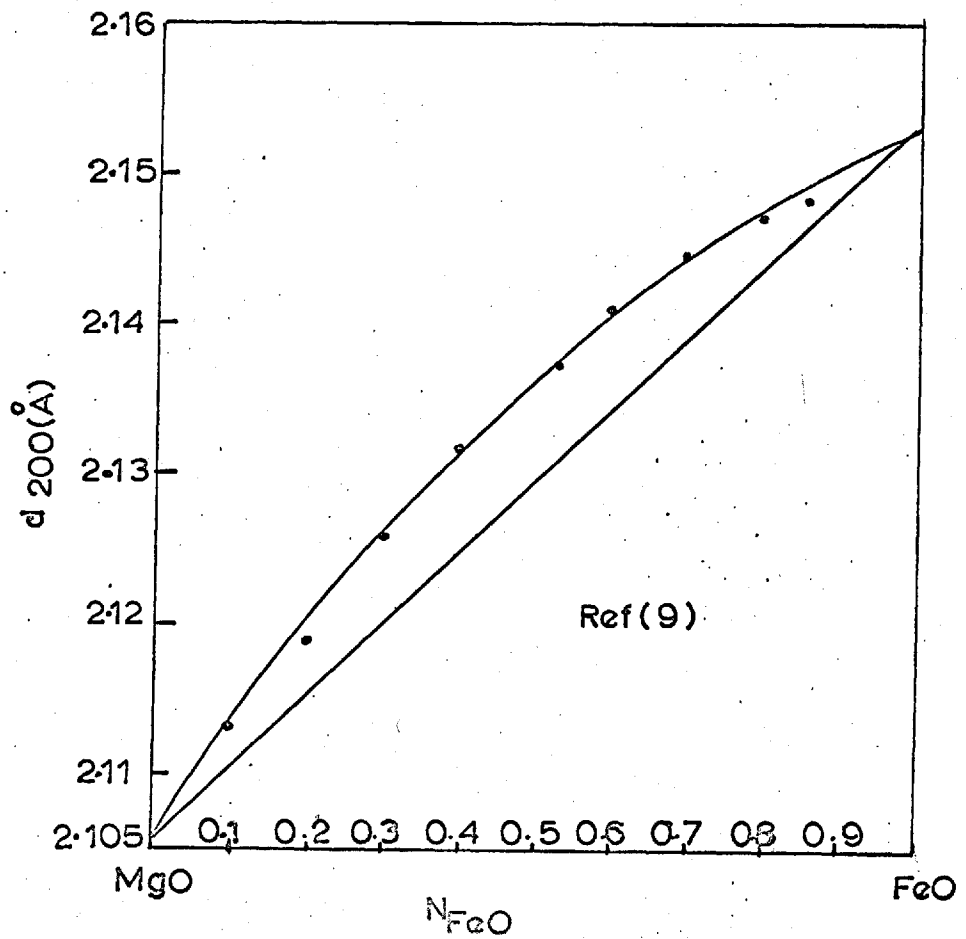

phase field, and wustite-magnetite, and magnetite-haematite phase boundaries. These workers also established that the O/Fe ratio in wustite can have values between 1.06 and 1.15 within the range of oxygen partial pressures 10^{-26} to 10^{-6} atm. and a range of temperatures 560-1400°C. From the isothermal relationships between O/Fe ratio (within the homogeneous phase field of wustite) and the oxygen activities (expressed in terms of p_{CO_2}/p_{CO} ratios), the following thermodynamic calculations were made.

a. The activity of iron (a_1) in the wustite phase using the Gibbs-Duhem equation:

$$\log a_1 = -\int \left(\frac{N_2}{N_1}\right) d \log a_2 \qquad (1.1.)$$

where N_2/N_1 = O/Fe ratio. The activity of oxygen (a_2) in the above equation is obtained directly from the CO_2/CO ratio in the gas phase which was used to establish equilibrium. Thus,

$$\ell n a_2 = \ell n a_{\frac{1}{2}O_2} = \ell n p^{\frac{1}{2}}_{O_2} = \ell n p_{CO_2}/p_{CO} - \ell n k_1 \qquad (1.2.)$$

where k_1 is the equilibrium constant of the reaction,

$$CO + \tfrac{1}{2}O_2 = CO_2 \qquad (1.3.)$$

and

$$k_1 = \frac{p_{CO_2}}{p_{CO}} \frac{1}{p^{\frac{1}{2}}_{O_2}} \qquad (1.4.)$$

b. Similarly the activity of FeO (a_{FeO}) which is equal to the product of $a_1 a_2$ was found by the use of the relation,

$$\log a_{FeO} = \log a_1 + \log a_2 = -\int \left\{ \frac{N_2}{N_1} - 1 \right\} d \log a_2 \quad (1.5.)$$

c. The heats of solution of oxygen ($\Delta\bar{H}_{\frac{1}{2}O_2}$) and iron ($\Delta\bar{H}_{Fe}$) at constant composition in wustite were obtained from the temperature coefficients of the oxygen partial pressure and the activity of iron respectively. It was found that the heat of solution of iron ($\Delta\bar{H}_{Fe}$) is small, ranging from -1430 to +380 cals. with O/Fe ratio 1.05 to 1.15, but that of oxygen had the values between -61720 cals and -63460 cals over the same composition range. The heat of solution of oxygen obtained by the other authors by indirect methods (like conductivity measurement) are found to be in good agreement with the results of Darken and Gurry.

1.2.b. The Defect Structure and the Transport Properties of Wustite

Wustite nominally FeO, but always non-stoichiometric containing excess oxygen with O/Fe ratio ranging from 1.05 to 1.15, has the NaCl crystal structure. The analysis of the chemical composition[8, 12] has shown the presence of trivalent iron ions and concentration was found to be twice as much as the stoichiometric excess of oxygen. From density measurements[8, 12]

and iron diffusion studies[13, 14] the deviation from stoichiometric appeared to be due to vacant sites in cation sublattice. From the measurements of electrical conductivity[15-20] and thermal emf [17, 20] it was found that wustite is a p-type defect semiconductor. The electrical conductivity remains p-type irrespective of O/Fe ratio within the wustite phase at all temperatures, whereas the thermal emf starts out as hole type at low oxygen pressure but changes to electron type at high oxygen pressures above 950°C. Below this temperature it remains p-type regardless of stoichiometry. Koch and Wagner[15] and J. B. Wagner et al.[20] have shown that the isotherms of conductivity as a function of oxygen pressure around 1000°C have the slope of 1/6. In the light of these findings the dissolution is represented by the equation:

$$\tfrac{1}{2}O_2^{g} = O^{=} + V_{Fe}^{++} + 2\oplus \qquad (1.6.)$$

Where the symbols $O^{=}$, V_{Fe}^{++} and $\oplus$ represent oxygen ions on the normal lattice site, a doubly ionized cation vacancy and a positive hole respectively*. From the above reaction it

---

* Ionic notation similar to that of Kroger and Vink is used here to represent the defects. Ions on crystal sites are wirtten with proper charge designations and the completely ionized vacancies are represented without any charge. However, it is clear that the completely ionized vacancies carry virtual but opposite charge. A comparison of various notations in use to represent the defects is made in the Appendix.

follows that each atom in stoichiometric excess of oxygen introduces a complementary defect pair into the wustite lattice; a cation vacancy plus two positive holes. In oxides of the transition metals, in their lower valence state, the energetically favoured trapped positive hole is likely to be a higher valent cation: $\oplus + Fe^{++} = Fe^{+++}$, the corresponding endothermic ionization energy being substantially off-set by the gain in local Madelung energy. Therefore the reaction (1.6.) can also be written as:

$$2_{Fe}{}^{++} + \tfrac{1}{2}O_2{}^{g} = O^{=} + V_{Fe}{}^{++} + 2_{Fe}{}^{+++} \qquad (1.7.)$$

Thus the solution of stoichiometric excess of oxygen in wustite involves the creation of Schottky defects in the iron sub-lattice and the simultaneous oxidation of ferrous ions to ferric in the rigid oxygen ion lattice.

Hauffe and Pfeiffer[21] applied the mass action law to the above reactions, treating the various imperfections as independent chemical entities and assuming that the defect interaction is negligible or constant and the activity coefficients of these entities are either small or constant. They obtained the following equilibrium constants for the oxygen dissolution in wustite:

$$K_2 = \frac{n_{\oplus}^{\ 2}\ n_{V_{Fe}^{++}}}{p_{O_2}^{\frac{1}{2}}} \qquad (1.8.)$$

and

$$K_3 = \frac{n_{Fe^{+++}}^{\ 2}\ n_{V_{Fe}^{++}}}{n_{Fe^{++}}^{\ 2}\ p_{O_2}^{\frac{1}{2}}} \qquad (1.9.)$$

Since two ferric ions or two holes are created for each vacancy, it follows that,

$$n_{\oplus} = 2\, n_{V_{Fe}^{++}} \qquad (1.10a)$$

and

$$n_{Fe^{+++}} = 2\, n_{V_{Fe}^{++}} \qquad (1.10b)$$

where n's with the subscript correspond to the respective defect concentrations. Using the above identities in the equations (1.8.) and (1.9.) the following relations were derived by Hauffe.

$$n_{Fe^{+++}} = n_{Fe^{++}}^{\ 2/3}\ (2k_3)^{1/3}\ p_{O_2}^{1/6} \qquad (1.11)$$

and

$$n_{V_{Fe}^{++}} = \left(\frac{k_2}{4}\right)^{1/3} p_{O_2}^{1/6} \qquad (1.12)$$

Further assuming the intrinsic hole concentration is small in wustite and the conductivity is mostly electronic, the oxygen pressure dependent conductivity can be expressed as:

$$\sigma = k' e\mu p_{O_2}^{1/6} \qquad (1.13.)$$

where σ represents conductivity (ohm.$^{-1}$cm.$^{-1}$), and e and μ stand for electronic charge and mobility (cm.^{2}/volt sec.) respectively.

Smyth[22] has recently shown that the oxygen pressure vs. O/Fe data of Darken and Gurry for wustite in the temperature range 1100-1400°C fit very well with the mass action law (Fig. 2a.), but the results of the electrical conductivity measurements as a function of oxygen pressure showed a considerable deviation from the mass action law (Fig. 2b). In the centre of the phase field the equation (1.13) is obeyed whereas the slopes of the conductivity isotherms deviate from the predictions of the mass action law both at high and low temperatures and more so at low temperatures. The slope of 1/7-1/8 and 1/5-1/3.6 have been observed between 1100-1300°C and 950-650°C respectively. Thus in the case of wustite the mass action law predicts more accurately the dependence of composition on oxygen pressure than has generally been found for the electronic conduction. According to Smyth

FIG. 2.

Fig. 2 a VARIATION OF VACANCY CONCENTRATION AS A FUNCTION OF PARTIAL OXYGEN PRESSURE

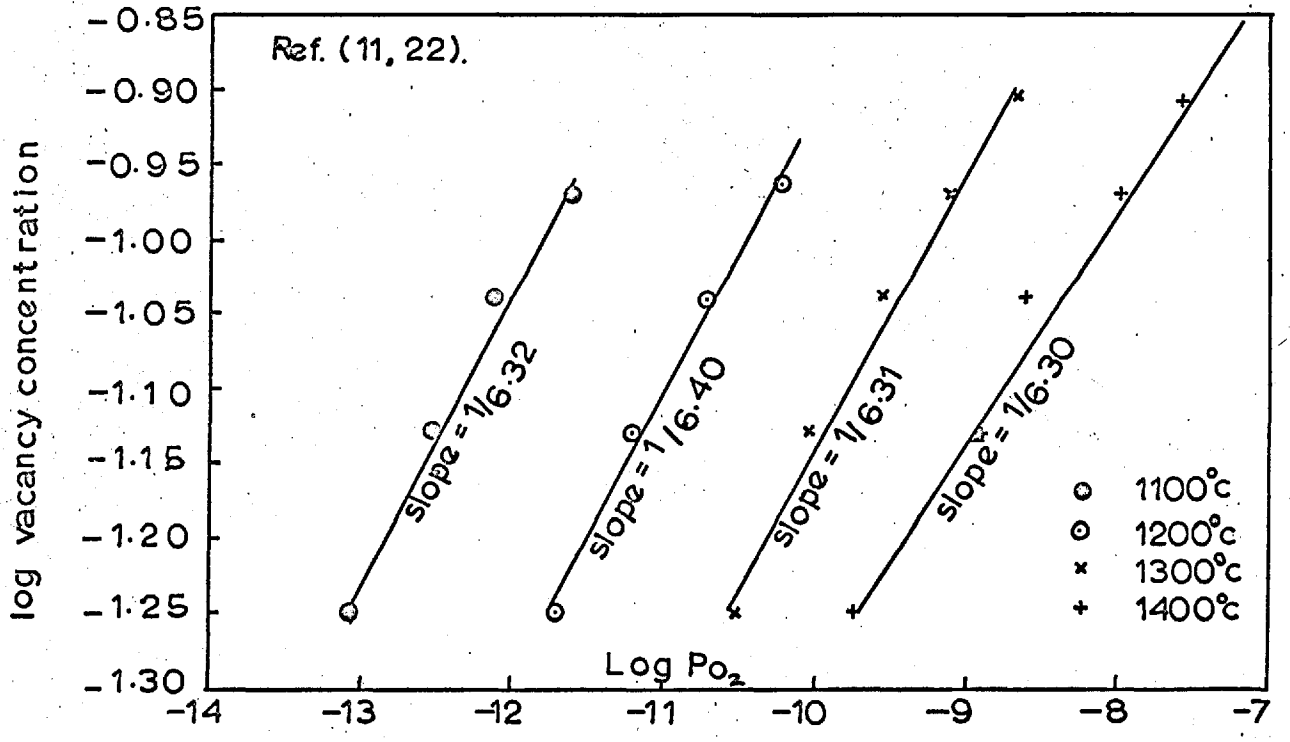

Fig. 2 b VARIATION OF CONDUCTIVITY AS A FUNCTION OF PARTIAL OXYGEN PRESSURE

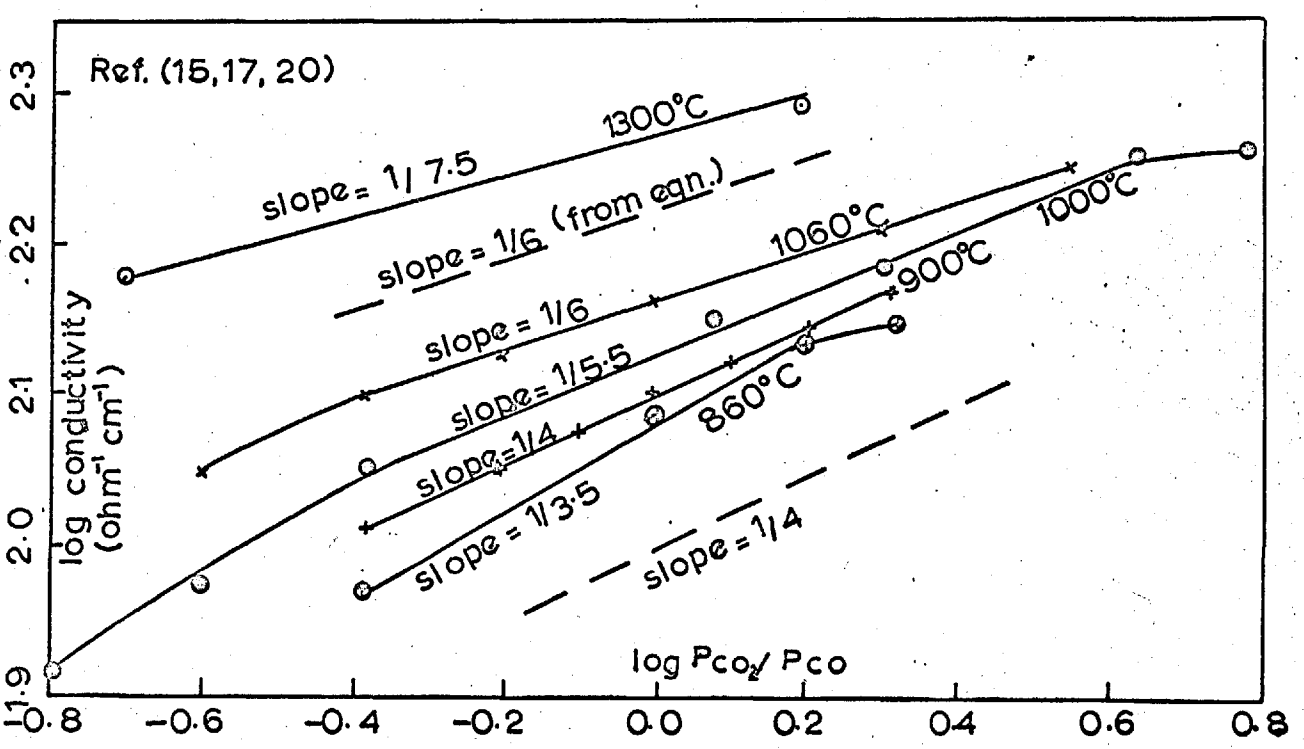

such a behaviour is to be expected since the composition is a function of the defect activity whereas the conductivity is a function of both the defect activity and the mobility. The latter is not necessarily independent of concentration.

The solid state chemists are inclined to ascribe such discrepancies as these more due to the defect interactions than the changes in the mobility of the current carriers. When the deviations from stoichiometry become large, a greater percentage of the defects will become nearest neighbours and their interactions cannot be ignored and must be then taken into account. Anderson[23] has derived the various relations for the defect concentrations involving the relevant defect interaction energy terms. In the treatment of Anderson[23] and Libowitz[24], the attractive defect interaction energies can be looked upon as the driving force for the compositional phase transformations. If the attractive defect interaction energy is high, there is a greater tendency for the defects to cluster and nucleate a new phase. On the other hand, if the attractive interaction energy is small, there is less tendency for the defects to cluster and hence the lattice can accomodate a large number of defects before it undergoes a transformation. Brebrick[25] has shown that the stability of the non-stoichiometric compounds does not only depend upon the defect interaction energy but also on the

relative stability of the adjoining phases. Compounds which have wide existence range at high temperatures, might form a series of ordered phases or contain defect complexes due to defect clustering at low temperatures. In some cases such clustering may displace some of the ions from the normal lattice sites. In cases like wustite, where the deviation from stoichiometry involve the creation of cation vacancies and concomitant increase in the ferric ion concentration, the defect clustering leads to association of the point defects and altervalent ions into complexes. In this connection the work of Ariya[26] and his associates is worth mentioning. They found that the enthalpies of formation of non-stoichiometric phases like FeO_{1+x}, TiO_{1+x}, etc., were equal, in each case, to the enthalpy of a mixture of the stoichiometric phases on either side of the non-stoichiometric compound for a given oxygen to metal ratio. So in the case of wustite, they found that the FeO_{1+x} ($0.06 < x < 0.15$) has the same enthalpy of formation as a mechanical mixture of $(1 - 2x)$ $FeO_{1.00}$ plus xFe_2O_3. In the light of what has been said above, Ariya proposed a theory of sub-microheterogeneity for non-stoichiometric compounds. According to this theory, a non-stoichiometric lower valence oxide consists of micro-domains of higher valence oxide dispersed through the matrix. Hence the defect structure of wustite is based on

the FeO matrix of NaCl lattice and consists of the micro-domains of Fe_2O_3. From entropy considerations, Ariya regards that the non-stoichiometric phases containing micro-domains thermodynamically as a single phase and their presence never vitiates the homogeneity of the host lattice. Further Brynestad and Flood[27] attempted to fit their results to the equilibria equations derived on the bases of several defect complexes in wustite lattice. They assumed that a vacancy will not have another vacancy as the nearest neighbour and two ferric ions are situated diametrically opposite to a vacancy and obtained a good agreement with this model.

An additional evidence in support of the micro-domain theory is the work of Roth[28]. In 1960, Roth, from a neutron-diffraction study, disproved the defect of structure of wustite, till then described in terms of vacant sites and corresponding proportion of ferric ions with all iron ions situated in the octahedral sites (Fig. 3a.). From intensity measurements he has shown that the wustite lattice contains iron interstials in the ratio of one interstial to two octahedral vacancies. He proposed that the defect complexes consist of two octahedral vacancies with one tetrahedral ferric iron, a distribution analogous to that in magnetite (Fig. 3b and 3c) and the overall defect reaction can be

FIG. 3

VARIOUS STRUCTURAL MODELS PROPOSED FOR WUSTITE

Fig. 3a Dissociated Model Ref. 21

$Fe^{++}\ O^{=}\ Fe^{++}\ O^{=}\ Fe^{++}\ O^{=}\ Fe^{++}\ O^{=}\ Fe^{++}$

$O^{=}\ Fe^{++}\ O^{=}\ Fe^{+++}\ O^{=}\ V_{Fe}^{++}\ O^{=}\ Fe^{++}\ O^{=}$

$Fe^{++}\ O^{=}\ V_{Fe}^{++}\ O^{=}\ Fe^{++}\ O^{=}\ Fe^{+++}\ O^{=}\ Fe^{++}$

$O^{=}\ Fe^{+++}\ O^{=}\ Fe^{++}\ O^{=}\ Fe^{++}\ O^{=}\ Fe^{++}\ O^{=}$

$Fe^{++}\ O^{=}\ Fe^{++}\ O^{=}\ Fe^{+++}\ O^{=}\ Fe^{++}\ O^{=}\ Fe^{++}$

$O^{=}\ Fe^{+++}\ O^{=}\ Fe^{++}\ O^{=}\ V_{Fe}^{++}\ O^{=}\ Fe^{++}\ O^{=}$

$Fe^{++}\ O^{=}\ Fe^{++}\ O^{=}\ Fe^{++}\ O^{=}\ Fe^{+++}\ O^{=}\ Fe^{++}$

V_{Fe}^{++} = Iron Vacancy

Fig. 3b Micro-Domain Model (After Roth) Ref. 28.

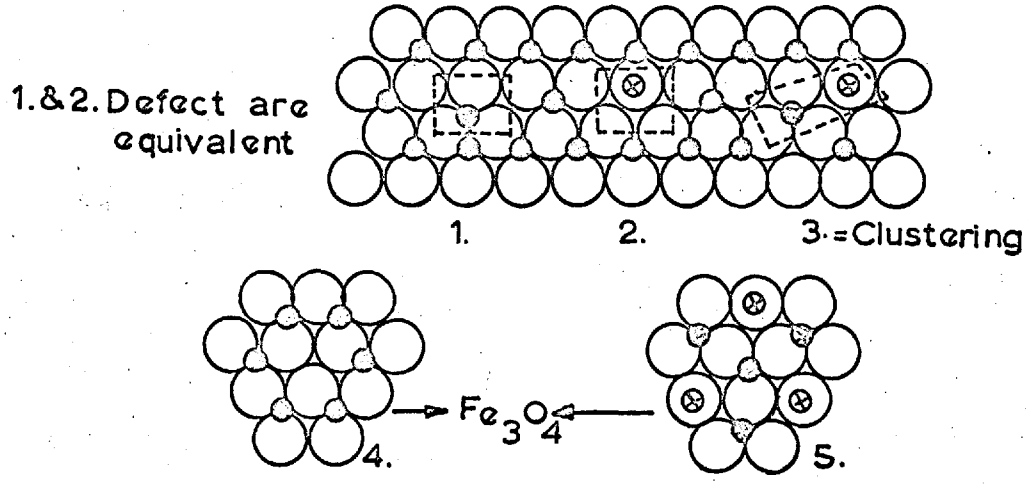

○ = Iron ion in octahedral position

⊗ = " " " tetrahedral "

written as:

$$2Fe^{++} + \tfrac{1}{2}O_2^g = O^{=} + Fe^{+++} + Fe^{+++}_{(tet)} + 2V_{Fe}^{++} \quad (1.14.)$$

where Fe^{++} and Fe^{+++} without subscripts stand for iron ions on the normal sites (octahedral) and $Fe^{+++}_{(tet)}$ represents ferric ions in the tetrahedral sites. By applying the mass action law to the above reaction and expressing the various defect concentrations in terms of the octahedral ferric ions, the relationship between the defect concentration and partial oxygen pressure can be expressed as,

$$n_{Fe^{+++}} \alpha p_{O_2}^{1/8} \quad (1.15.)$$

Since the ferric ions in the octahedral sties alone contribute to the conductivity, the oxygen pressure dependence conductivity follows the root law

$$\sigma \alpha p_{O_2}^{1/8} \quad (1.16.)$$

assuming the hole mobility is concentration independent. Since the slope of the high temperature isotherms is nearly equal to value of 1/8 as predicted by the equation (1.16.), the structural model proposed for wustite seems to be valid.

Libowitz[24] has proposed the following equilibrium in terms of the defect complexes,

$$2Fe^{++} + \tfrac{1}{2}O_2^g = (2V_{Fe}^{++} - Fe_{(tet)}^{+++}) + Fe^{+++} + O^{=} \quad (1.17.)$$

where $(2V_{Fe}^{++} - Fe_{(tet)}^{+++})$ represents the defect complex. Application of the mass action law to the above reaction yields,

$$\sigma \propto p_{O_2}^{1/4} \quad (1.18.)$$

Thus the low temperature conductivity results can be more readily interpreted in the light of the micro-domain model. However, none of the above structural models based on the concept of clustering and association of the defects predict sixth root dependence of conductivity on oxygen pressure, which in fact has been experimentally observed by already cited authors[15, 20].

Recently Raccah[29] and co-workers have reported several types of ordered wustites and have published a revised phase diagram indicating the ranges of existence of several wustites. They have developed a more detailed thermodynamic expression for the dependence of composition as a function of oxygen pressure than had previously been available. Their equilibrium

constant for the defect reaction includes the various activity coefficient terms which are composition dependent at a given temperature.

The various defect equilibria, hitherto proposed to account for non-stoichiometric behaviour of wustite can be replaced by a more general defect equilibrium of the type:

$$\tfrac{1}{2}O_2^g = O^{=} + V_{Fe}^{m}{}^{++} + m\oplus \qquad (1.19.)$$

where the exponent m denotes the degree of association between the vacancy and the holes and the equilibrium constant would become:

$$k_4 = \frac{\nu_{V_{Fe}^{m}{}^{++}} \; \nu_{\oplus}^{m} \; n_{V_{Fe}^{m}{}^{++}} \; n_{\oplus}{}^{m}}{p_{O_2}^{\frac{1}{2}}} \qquad (1.20.)$$

In the above equilibrium constant, the ν's represent the activity coefficients of various imperfections. The value of $m(0 < m < 2)$ can be determined from the slope of the property isotherm and would indicate the type of defects present under the given conditions.

1.2.c. Mechanism of Electrical Conduction in Wustite

The term semiconduction connotes a positive temperature coefficient of electronic conductivity. Semiconduction in crystal lattices is attributed to the mobile electronic or valence defects. Excess electrons in the conduction band and holes in the valence band irrespective of the source (Fig. 4a and 4b) are regarded as electronic defects and contribute to conductivity. These electrons (and holes) behave as 'free' electrons and their mobilities decrease with increase of temperature due to lattice scattering. Their electron transport properties are best represented by the band model together with its conceptual mathematical apparatus of band width, band gap (also known as forbidden gap, E_G), effective mass (m^*) and carrier mobility (μ). The number of electrons that the band can hold is inversely related to the band width. The band width and carrier mobility are independently related to the reciprocal of effective mass,

$$\frac{h}{\text{bandwidth}} < \tau \qquad (1.21)$$

$$\text{bandwidth} = \frac{2}{2m} k_0^2 \qquad (1.22)$$

$$k_0 = \pi/a \qquad (1.23)$$

FIG. 4

Fig. 4 a

INTRINSIC CONDUCTIVITY IN BAND MODEL

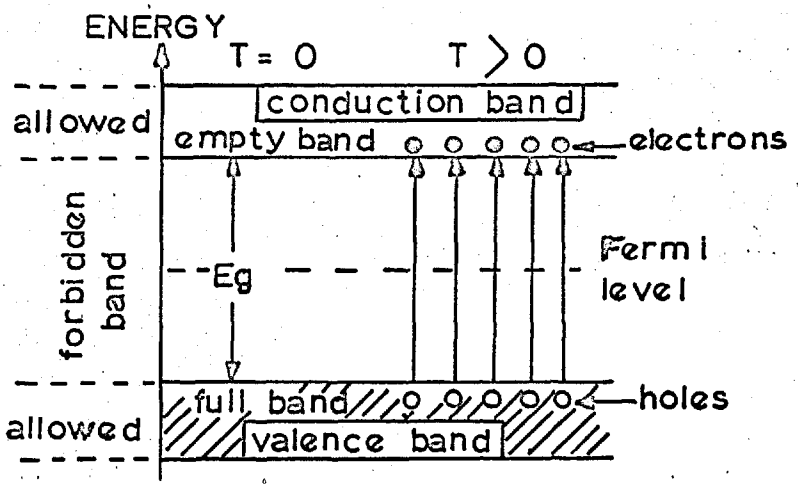

Fig. 4 b

EXTRINSIC CONDUCTIVITY IN BAND MODEL

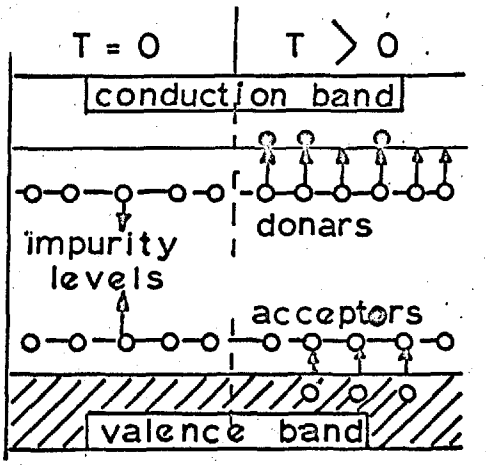

Fig. 4 c

CONDUCTIVITY ACCORDING TO ELECTRON TRANSFER MODEL

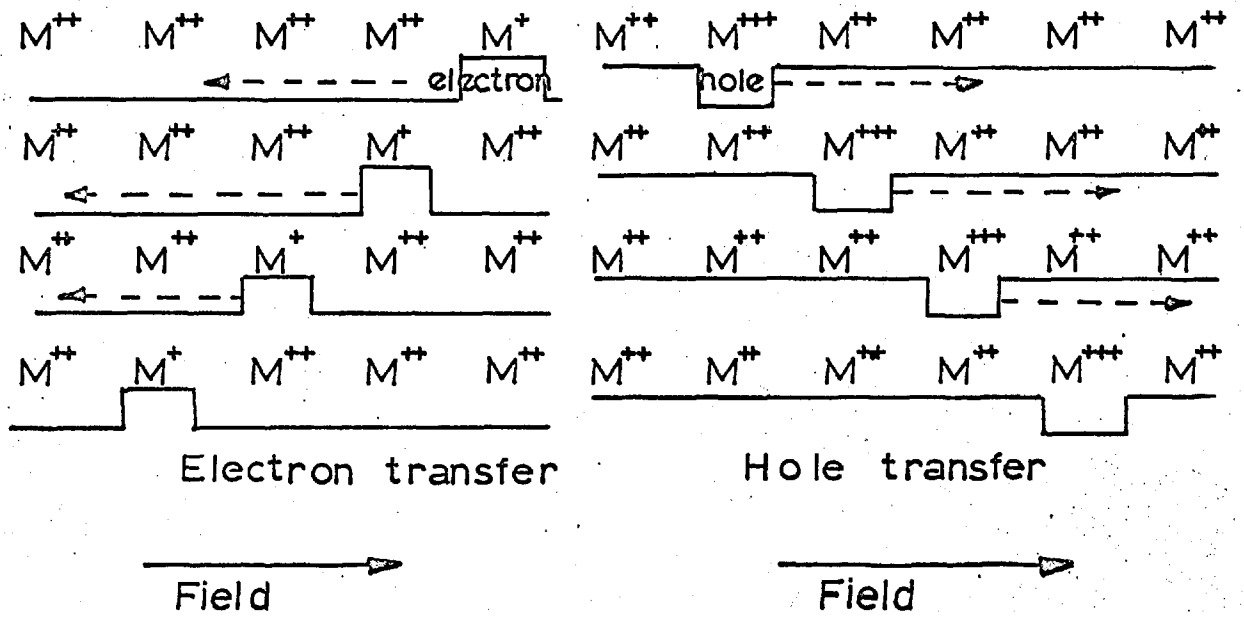

$$\hbar = h/2\pi \tag{1.24}$$

and

$$\mu = \frac{e}{m^*} \tau \tag{1.25}$$

where τ, a and h stand for relaxation time, lattice constant, and planck constant respectively.

Further, the band gap is related to the carrier concentration (n/cm.^{3}) by the reaction:

$$n = N_{eff} \exp \frac{-E_G}{2kT} \tag{1.26}$$

and

$$N_{eff} = 2\left(\frac{2\pi m^* kT}{h^2}\right)^{3/2} \tag{1.27}$$

where k is Boltzman's constant. The conductivity (ohm.$^{-1}$cm.$^{-1}$) is given by the expression:

$$\sigma = AT^{-P} N_{eff} \exp \frac{-E_G}{2kT} \tag{1.28}$$

The term AT^{-P} is to account for the decrease in the carrier mobility with temperature due to lattice scattering. Since the exponential term in the above equation varies much more rapidly with temperature (T^oK) than does the first, the above relation is reduced to the well-known form:

$$\sigma = \sigma_0 \exp \frac{-\Delta E}{RT} \qquad (1.29)$$

where the term σ_0 contains all the constants and ΔE is the energy of activation and R is the gas constant. In an ideal case, the slope of the Arrhenius plot of conductivity with the reciprocal of temperature (^oK) gives the depth of the Fermi level.

Despite the great success of the band theory in predicting and interpreting the properties of semiconductors it does not seem appropriate to apply the band theory to account for electron transport properties of oxides of the 3d transition metals.

Thus the band model predicts an extremely narrow 3d band and hence a large effective mass and under extremely low carrier mobility. Under these circumstances it is no longer meaningful to assign the width to the band and hence the 3d charge carriers should be considered to occupy energy levels localised on the cations. Further, Morin[3] has shown that the 3d orbitals beyond vanadium do not overlap in the 3d oxides to form a 3d conduction band. Therefore the charge carriers are in isolated energy states. Ions containing the localised excess charge are regarded as valence defects. They are known to occur only in the cationic sub-lattice of oxides of the transition metals. In the lower valence oxide the localized excess charge is a higher valent cation: $M^Z + \oplus = M^{Z+1}$, e.g. Fe^{+++}, Ni^{+++} in FeO_{1+x} NiO_{1+x} etc. In the case of higher valence oxide

the localised excess charge is a lower valent cation: $M^{Z+1} + \Theta = M^{Z}$, where the symbol Θ refers to electrons, e.g. Fe^{++} in Fe_2O_3. Concentration of these valence defects is a function of stoichiometry (O/Fe ratio in wustite) and impurity content (Li concentration in nickel oxide). According to Verwey[1], the conductivity in these oxides involves a thermally activated electron (or hole) transfer between the transition metal ions of the same element occurring in states of ionization differing by one unit but occupying crystallographically equivalent positions (Fig. 4c). This was further developed by Heikes and Johnston[4], Zener[5], Yamashita[6] and others[17-19] and now known by many names, e.g. electron transfer, hopping, localised electron, or shell model. The Heitler-London approach suggested by these models has been developed by Yamashita[6] to interpret the electrical conductivity in 3d oxides.

From measurements of the electrical conductivity and thermal emf . both as a function of stoichiometry and temperature, Tannhauser[17] has proposed an electron transfer model for wustite. The salient features of this model as applied to wustite is briefly as follows.

1. The thermally activated hole transfer involves an activation energy associated with the self trapping of the carriers. Such a hole conduction in wustite can be described by a diffusion

type equation.

$$\sigma = A\,(n_{\oplus})\,\exp\,-\frac{\Delta H_{m\oplus}}{RT}\cdots\frac{\Delta S_{m\oplus}}{R} \qquad (1.30)$$

where A is a constant comprising the jump frequency of the hole, the lattice parameter, electronic charge, the density of the ion pairs and the probability of finding an acceptor site for the hole, $n_{\oplus}$ denotes the hole concentration, $\Delta H_{m\oplus}$ and $\Delta S_{m\oplus}$ are the activation enthalpy and the activation entropy of movement of the holes. The plot of $\log \sigma$ vs. $1/T^{o}K$ at constant hole concentration was found to be linear as predicted by the above equation. The activation enthalpy has a value of about 1.8 k.cals (0.06 ev.) and the results of various authors are all in good agreement.

2. At constant temperature jump rate of the hole is proportional to the product of di- and tri-valent iron ions situated on the octahedral sites (normal sites) and such a hole transfer can be represented as:

$$V_{Fe}^{++} - Fe^{+++}(3d^5) + Fe^{++}(3d^6) = (V_{Fe}^{++}) - Fe^{++}(3d^6) + Fe^{+++}(3d^5) \qquad (1.31)$$

where $V_{Fe}^{++} - Fe^{+++}(3d^5)$ refers to a ferric ion situated near the

vacancy and the number of electrons in the 3d level is shown in the bracket. The energy associated with the above charge transfer process is calculated* in the manner explained in the Appendix taking the Madelung energy for wustite as 23.64 ev and dielectric constant[19] to be 20. This energy is found to be as small as 0.35 ev. Based on the reaction (1.31) Tannhauser has derived the relationship between the conductivity and product of donors and acceptors as

$$= k(T) \frac{n_{Fe^{+++}} \cdot n_{Fe^{++}}}{n_{O^{=}}^2} \qquad (1.32.)$$

$$= k(T).F \qquad (1.32a.)$$

where $n_{Fe^{++}}$ and $n_{Fe^{+++}}$ represent the ferrous and ferric ions in the octahedral sites and $n_{O^{=}}$ is the number of oxygen ions which equal the number of octahedral sites. He evaluated the F factors from stoichiometry using Roth[28] model for wustite,

$$\frac{n_{Fe^{+++}}}{n_{O^{=}}} = \frac{1}{2} \frac{n^{t}_{Fe^{+++}}}{n_{O^{=}}} \qquad (1.33.)$$

---

* A detailed calculation is given in the Appendix.

FIG. 5

Fig 5 a. VARIATION OF CONDUCTIVITY AS A FUNCTION OF: $\frac{n_{Fe^{+++}}\ n_{Fe^{++}}}{n^2_O} = F$

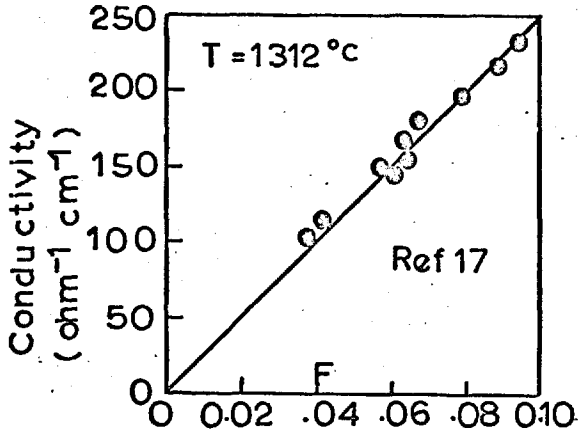

Fig. 5b. PLOT OF CONDUCTIVITY AS A FUNCTION OF: $n_{Fe^{+++}}/n_{O=}$

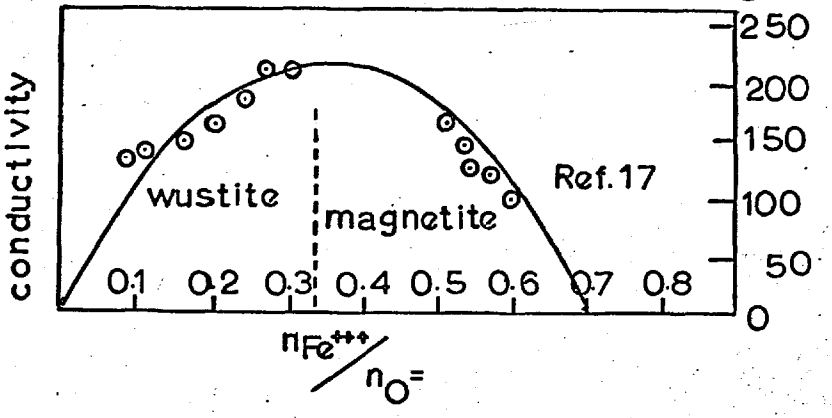

Fig. 5c ARRHENIUS PLOT OF CONDUCTIVITY AGAINST $1/T\,°K$

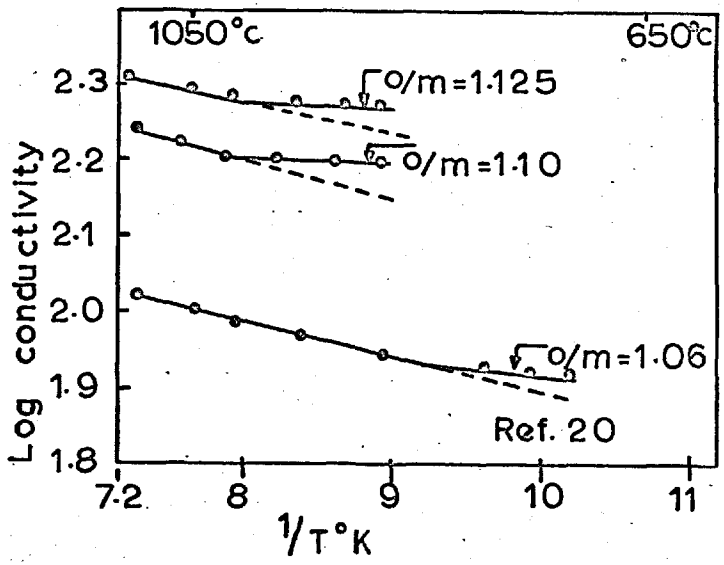

Fig. 5 d PLOT OF THERMAL EMF AS A FUNCTION OF $n_{Fe^{+++}}/n_{O=}$

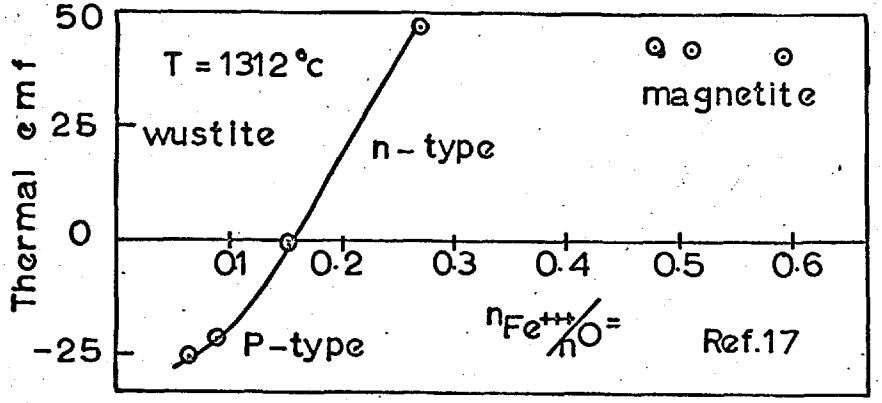

where $n^{t}_{Fe^{+++}} = n_{Fe^{+++}} + n_{Fe^{+++}_{(tet)}}$

The isothermal plots of conductivity as a function of F factors ($n_{Fe^{+++}}$. $n_{Fe^{++}}/n_{O^{=}}^{2}$) were found to be linear and conductivity vs. $n_{Fe^{+++}}/n_{O^{=}}$ parabolic (Fig. 5a and 5b) showing that the hopping model is valid for wustite.

It is interesting to note that Mikhailov et al.[19] have recently proposed the conduction model for wustite involving the formation of holes in the 2p band of oxygen lattice,

$$Fe^{+++}(3d^5) + O^{=}(2p^6) = Fe^{++}(3d^6) + O^{-}(2p^5) \qquad (1.34)$$

They have proposed the energy level diagram for wustite* similar to that proposed NiO by Morin and calculated the energy for the above transition to be 0.375 ev. From these energy calculations it seems that the charge transfer can take place in wustite by one of the two mechanisms (1.31 and 1.34) and have approximately the same energy requirements.

3. The carrier mobility is small and shows a positive temperature coefficient. According to Yamashita[6], the carrier mobility can be used to guide and determine the applicability of the band and electron transfer models. If the carrier mobility

---

* See Appendix.

is larger than 1 cm.^{2}/volt sec. the usual Bloch theory is applicable, while the Heitler-London approach is good when the mobility is smaller than 1 cm.^{2}/volt sec. Hauffe[21] calculated the mobility of the electron holes in wustite at 1000°C to be about 0.11 cm.^{2}/volt sec., thus providing another experimental support in favour of the electron transfer model.

4. Heikes and Johnston have observed the decrease in the activation enthalpy for conduction with increasing lithium content in Li doped NiO and they attribute this to changes in the elastic properties of crystal. However, in the case of wustite the data on the variation of activation enthalpy with stoichiometry are very meagre to be used for any supporting calculations. It is interesting to note that J. B. Wagner et al. have reported the appearance of changes in the slope of Arrhenius plot of conductivity vs. $1/T^{\circ}K$ at constant O/Fe ratio (Fig. 5d). The difference between the high and the low temperature slopes might be attributed to the activation enthalpy of disordering process. This needs further classification.

5. According to Heikes and Johnston the thermal emf is related to the defect concentration (c),

$$\frac{dV}{dT} = \frac{k}{e} \ln \frac{1-c}{c} - \frac{\Delta S^d}{e} \qquad (1.35)$$

where ΔS^d is the change in the entropy caused by the distortion of the lattice when the carrier is introduced. At low oxygen pressure the thermal emf in wustite is p-type as expected, but changes to n-type at high oxygen pressure before the defect concentration c exceeds the value $\frac{1}{2}$. The p-n transition within the wustite phase has been observed by Tannhauser and J. B. Wagner et al. and such behaviour is not in accord with the theory. Both the authors have neglected the contribution arising from ΔS. Tannhauser has attempted to interpret the p-n transition in thermal emf of wustite using the band model with certain assumptions. According to the band model in wustite of low oxygen content the band is full, hence the thermal emf starts out as p-type but changes to electron type with increasing excess oxygen because the band begins to empty the carriers.

Thus the electrical conduction in wustite is more satisfactorily interpreted in terms of the electron transfer model. However the band model with certain assumptions can be used to account for p-n transition in the thermal emf of wustite.

1.2.d. Transport Properties of Magnesium Oxide

Magnesium oxide is the most refractory and ionic oxide of all the alkaline earth oxides. It possess a remarkable lattice stability with no evidence of significant non-stoichiometry until very high temperatures are reached. For practical purposes MgO is classed as an insulator.

However, its electrical properties have been the subject of investigation in recent years due largely to the availability of single crystals. It has not been unambiguously established whether the magnesium oxide is an electronic or ionic conductor. Evidence for electronic and ionic conduction have come from the various sources. Lempicki[30], Yamaka and Sawamato[31], Mansfield[32] and Mitoff[33] have obtained evidence for electronic conduction. Although there is a general good agreement in the value of conduction activation energy of about 2.4 ev (57 k.cals), the absolute values of conductivity differ from author to author by as much as an order of magnitude and even more so about the nature of the current carriers. The electronic conduction in MgO is attributed to intrinsic electrons and holes[30], electrons due to excess magnesium[31], to positive holes due to excess oxygen[32] and to the presence of impurities particularly of variable valence[33]. Mitoff's results show that electronic conductivity in magnesium oxide is very much influenced by the presence of impurities and more so by their valence states.

He has shown that a different conduction mechanism occurs in MgO of higher purity than those commercially available, containing impurities like iron. Higher the purity of the crystal, lower is the conductivity, higher the conduction activation energy and smaller the dependence of conductivity with the oxygen pressure. In impure crystals, the dependence of conductivity on oxygen partial pressure is attributed to the changes in stoichiometry and the concentration of the lattice defects and such effects were found to be greater in impure crystals containing particularly iron. The effect of oxygen pressure on the conductivity in iron containing crystals has been ascribed to the change in the valence states of iron and concomitant changes in the vacancy and carrier concentrations. Cation vacancies are created at high oxygen pressures and anion vacancies at low oxygen pressures and all the defects are assumed to be associated with impurity centres. By applying the usual mass action law, he has derived the various power laws for oxygen pressure dependence conductivity and his results can be best expressed in the form:

$$\sigma = c_1 p_{O_2}^{1/n} + c_2 p_{O_2}^{-1/n} + \sigma_x \qquad (1.36)$$

Where c_1 and c_2 are constants comprising electronic charge, iron content, the carrier mobility and the relevant equilibrium

constants. σ_x is the conductivity arising due to electron and holes from sources other than impurity centres. The value of n in the above equation lies somewhere between 4 and 6.

Doubts began to haunt on the above conclusions of Mitoff when Schmalzried[34] evidenced an ionic conduction in MgO by solid state electrochemical cell technique. He used a cell of the following type (at 1100°C)

$$\text{Pt Fe/FeO} \mid \text{MgO} \mid \text{NiO/Ni Pt}$$

and obtained an e.m.f. which was close to the value predicted by the Nernst equation,

$$E = \frac{RT}{4F} \ln p_2/p_1 \qquad (1.37)$$

for an ionic conductor. In the equation E stands for emf, p_2 and p_1 are two different oxygen pressures maintained on either side of the electrolyte and F is the Faraday (23063 cals) and other symbols have usual significance. Later Mitoff[35] extended the cell measurements on single crystals of MgO in the temperature range 1000-1500°C using gaseous electrodes. He calculated the relative amounts of electronic and ionic conduction using the well known relations:

$$\sigma_i = \sigma_t t_i \qquad (1.38a)$$

and

$$t_i = E^1/E \qquad (1.38b)$$

where σ_t and t_i represent the total and ionic conductivity respectively and ti is the ionic transport number. E^1 and E are the measured and theoretical emf's (predicted by Nernst equation) respectively. The emf measurements disclosed on amphoteric conduction in MgO and ionic transport number is found to be dependent on the temperature and impurity content. The conditions which favour the electronic conductivity are:

1. High temperatures (>1300^{o}C),
2. High (1 atm.) and low oxygen partial pressures (<10^{-6} atm)
3. The presence of impurities.

Conversely low temperatures (<1300^{o}C), intermediate oxygen partial pressures, and high purity favour the ionic transport. Incidentally Pal'guev and Neuimin[36] have shown that in polycrystalline MgO ionic transport from emf measurements is nearly temperature independent its value lies very close to unity. According to Mitoff the ionic conductivity in MgO results from the magnesium ion transport, although activation energy for Mg^{++} diffusion (79 kcals = 3.3 ev) is higher than for $O^{=}$ ion diffusion (62.5 kcals = 2.7 ev). This is because the experimentally measured conductivity of

the single crystals is much closer to the value calculated from Nernst-Einstein equation,

$$\sigma_i = \frac{DnZ^2e^2}{kT} \qquad (1.39)$$

Using Lindner's[37] data for Mg^{++} ion diffusion than Kingery's[38] data for $O^{=}$ ion diffusion. In the above equation D is the diffusion coefficient, Z is the valence, e is the electronic charge and n is the number of ion pairs/cm.^{3}. Finally Davies[39] has shown that the mechanism of conduction in polycrystals of MgO is similar to that observed in single crystals. But the conductivity of polycrystalline MgO is an order of magnitude higher than that of single crystals and this is attributed to the presence of grain boundaries in polycrystals.

1.3. The Relevant Previous Work on the System FeO-MgO-O_2

1.3.a. General

The technological importance of the system FeO-MgO-O_2 has been realised both by the ceramists and metallurgists for many decades. One such example is the oxidation of magnesio-wustites which plays an important role in the behaviour of the basic refractories in the steel making processes, where iron or FeO diffusing into magnesia bricks produce magnesio-wustite and the latter undergoes a variety of oxidation-reduction cycles. Such reactions involve either intake or expulsion of oxygen resulting in dimensional changes and weakening the structure of the bricks. From this view point the phase relations and thermodynamic properties of the system have received a considerable attention but not all features of the system have been fully investigated. As the present knowledge of the electrical properties of the system remains obscure, the potential use of the system as thermistors is yet to be realised. Those aspects of the previous work on tye system FeO-MgO-O_2 which are relevant to the present study are now briefly summarised.

1.3.b. The Phase Relations in the System FeO-MgO-O_2

The temperature-composition diagram of the system FeO-MgO due to Bowen et al. is shown in the Fig. 1b. It indicates a mutual solid solubility between FeO and MgO in all proportions. Such a behaviour is not unexpected because the end members are iso-structural monoxides with NaCl lattices and the ionic radii of the cations are nearly equal. Muan[40] et al. have shown that the magnesio-wustite is stable in air only above 1000°C. Further White and co-workers[41] have shown that the magnesio-wustite in the ternary system, FeO-MgO-Fe_2O_3 has an extensive range of existence. They also showed that the additions of magnesium oxide decreased the concentration of ferric ions in the entire phase field of the magnesio-wustite and relative amounts of ferrous and ferric ions in the solid solution is dependent on temperature and Fe/Mg ratio.

1.3.c. Thermodynamics of the System FeO-MgO

The activity of FeO in magnesio-wustite as a function of composition in equilibrium with metallic iron has been investigated by Hahn and Muan[9], Berthet[42], Schmahl et al.[43], Shaskina and Gerasimov by equilibrating the oxide solid solutions with pure metallic iron in an atmosphere of known oxygen

FIG 6

ACTIVITY OF WUSTITE AS A FUNCTION OF COMPOSITION IN THE FeO – MgO SYSTEM

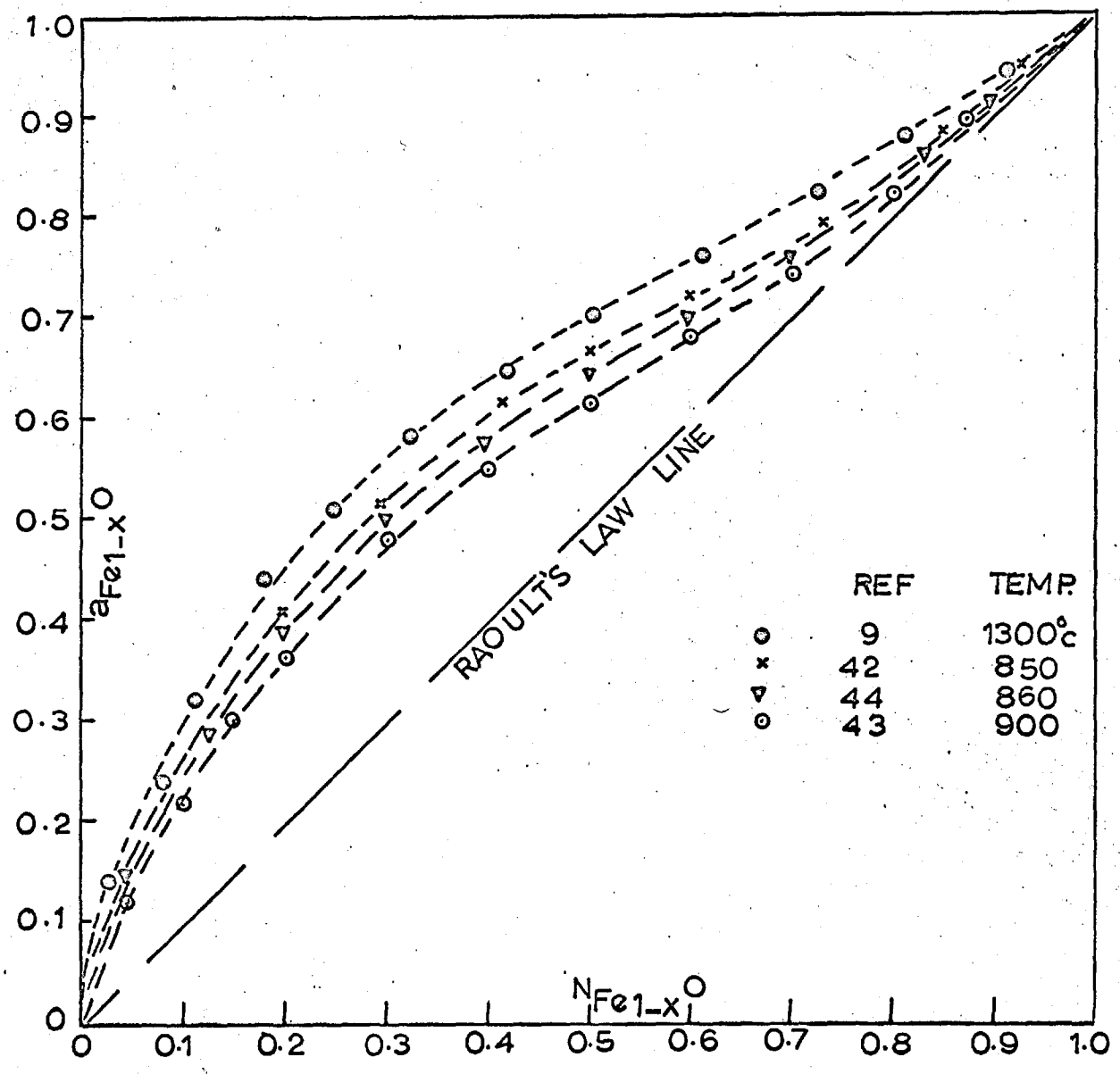

pressures. The results of the various authors are all in good agreement showing that activity coefficient of FeO is greater than unity taking wustite of minimum oxygen content in equilibrium with metallic iron at known temperature as the standard state. There also appears to be no measurable temperature coefficients of the activities within the experimental error (Fig. 6). It is interesting to note that the results of the various authors are in good accord with one another despite the different gas mixtures like H_2/CO_2, CO/CO_2 and H_2/H_2O, were employed for equilibrium studies.

1.3.d. Redox Equilibria in Magnesio-Wustite

Another aspect of the studies concern the behaviour of magnesio-wustite at higher oxygen partial pressures than those in equilibrium with iron showing the conditions for the separation of the magnesio-magnetite phase. Studies in this region have been carried out by Berthet[42], Schmahl et al.[43], Morozova[45] at temperatures between 800-1000°C and an important contribution to this group of studies is the work of Brynestad and Flood[27] which was carried out at 1400°C. Where as the low temperature results were mainly concerned with magnesio-wustites containing more than 20 Mol% FeO, Brynestad and Flood's work included some measurements on dilute

VARIATION OF O/Fe IN FeO MgO SOLID SOLUTIONS AS A FUNCTION OF H_2/H_2O RATIOS 850 Ref. 42

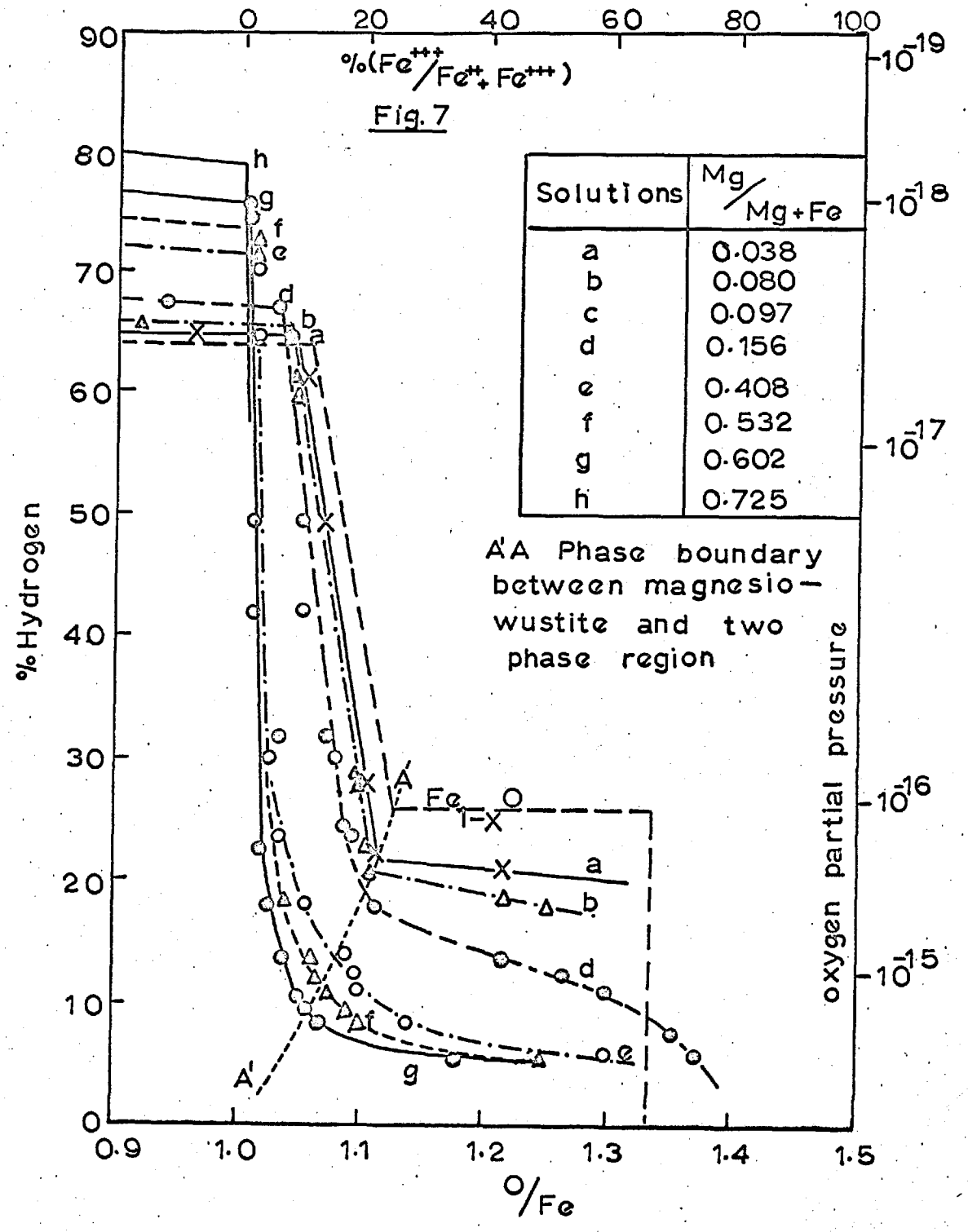

VARIATION OF $O/_{Fe}$ IN FeO MgO SOLID SOLUTIONS AS A FUNCTION OF H_2/H_2O

FIG. 8

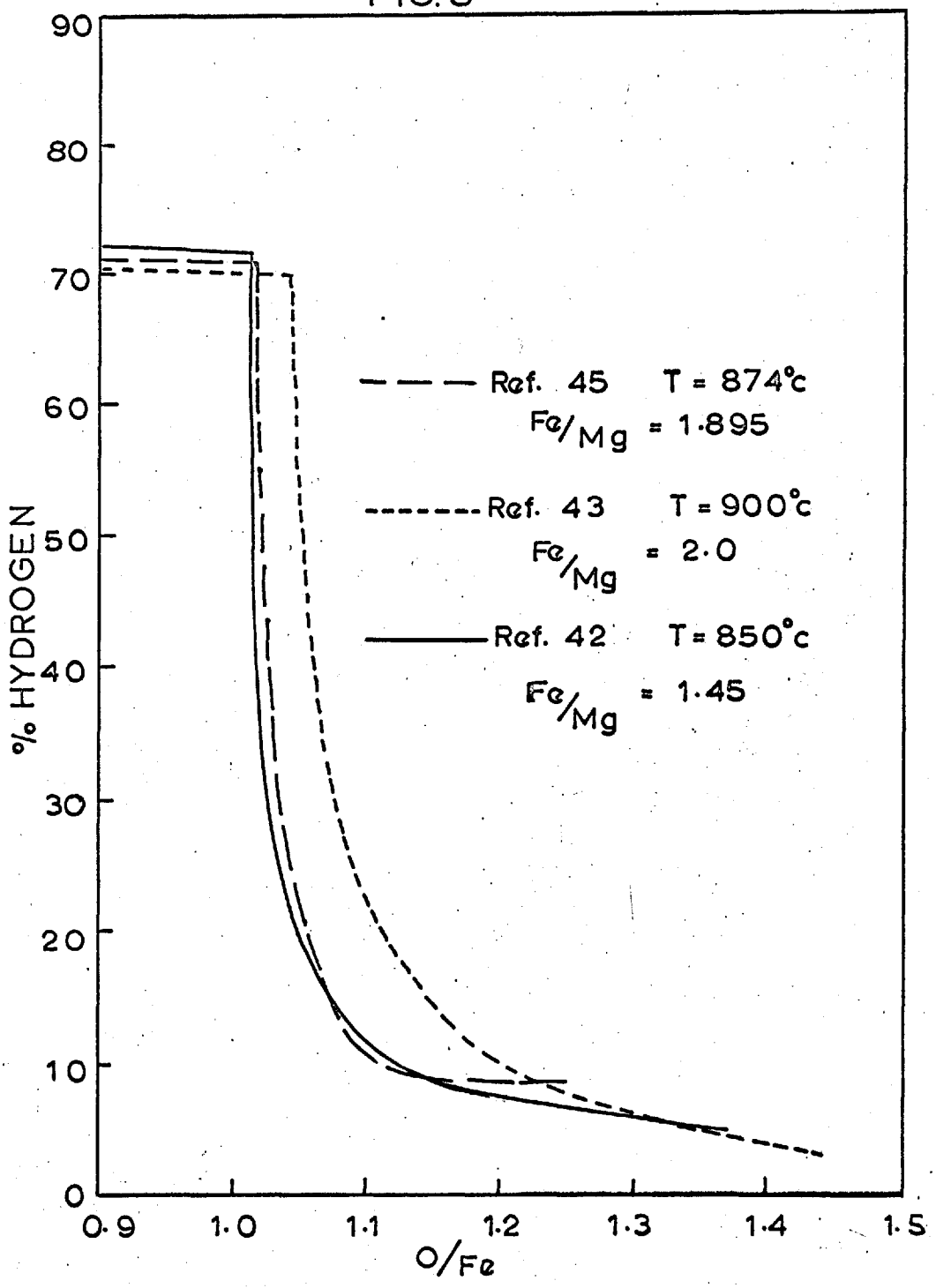

FIG. 9

RESULTS OF REDOX EQUILIBRIUM BETWEEN MAGNESIO-WUSTITE AND OXYGEN AT 1400°c

Ref(27)

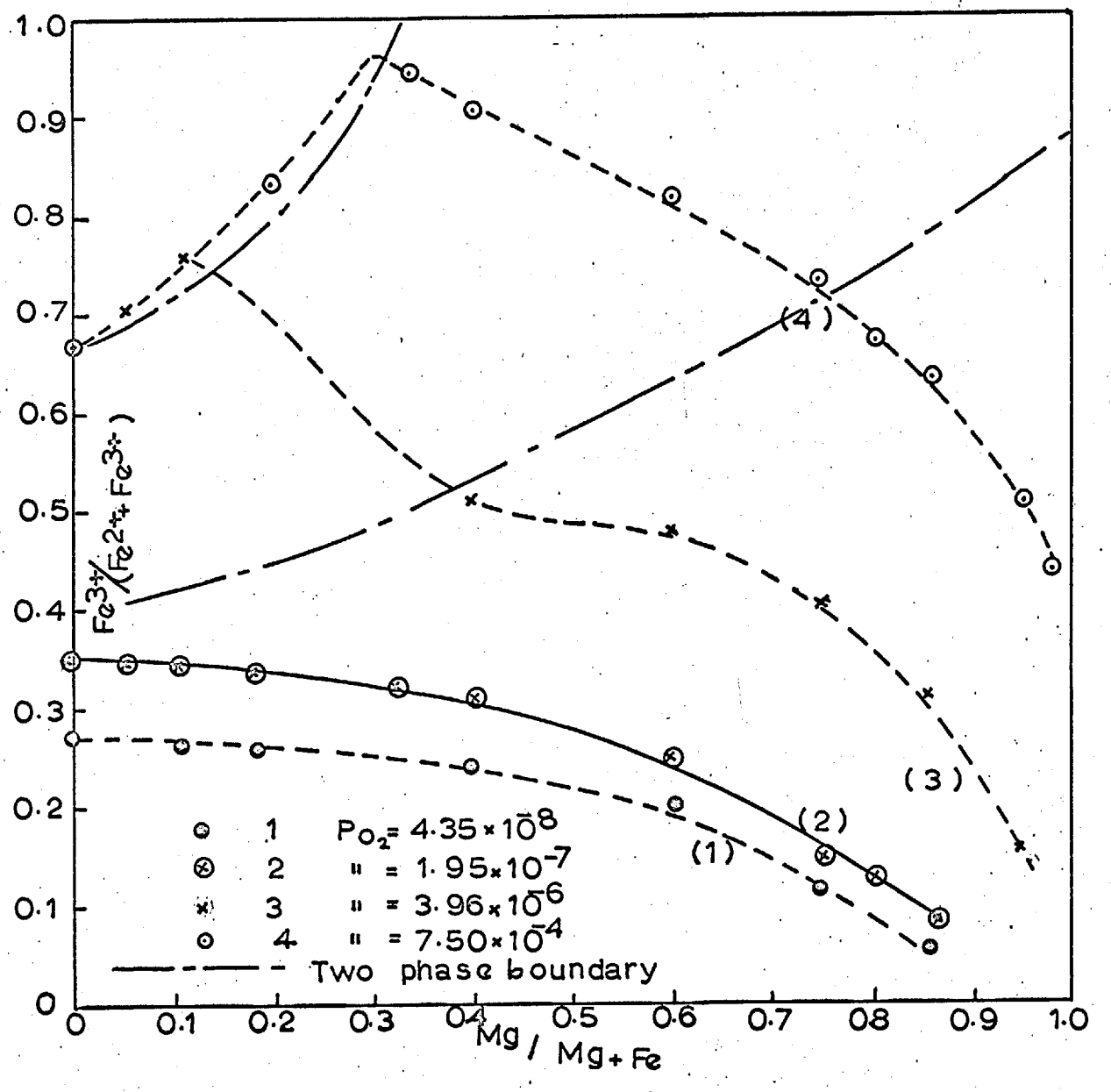

magnesio-wustites. The summary of the results on study of the redox equilibria are shown in Figs. 7, 8 and 9.
The results of all the authors possess a consistent picture, showing that, at constant temperatures, the ferric ion concentration within the phase field is a function of both the total iron content and the oxygen pressure. Of all the authors, only Brynestand and Flood have interpreted their results in terms of the association of the defects and their related equilibria. They conclude that their results can be best represented by an equilibrium constant of the type,

$$K_5 = \frac{n_{Fe^{+++}}}{n^2_{Fe^{++}}} \frac{\Sigma n+}{p^{\frac{1}{2}}_{O_2}} \qquad (1.40)$$

where n's are the ionic concentrations and $n_{Fe^{+++}}/\Sigma n+$ is the ionic fraction of the ferric ions. This result should be contracted with conclusions of Hauffe and Pfeiffer and Smyth where the defect equilibrium constant is represented by the equation (1.9) for wustite. These different conclusions are reconciled by the postulate that the ferrous vacant sites are associated with ferric ions in magnesio-wustites but not in $Fe-O_2$ system at the temperatures around $1400^{o}C$.

Finally the work of Schmahl[43] showed that the tie lines between the magnesio-wustites and magnesio-magnetites run

between constant FeO of both the phases and it was calculated that the Fe_2O_3 activity remains constant in magnesio-magnetite solid solutions in equilibrium with magnesio-wustites from pure Fe_3O_4 to $MgFe_2O_4$ at the value of 0.012 at 900°C.

1.3.e. The Information Available on the Transport Properties of the System

Except for the works of Cutler et al.[46, 47], Brindley[48] and Fine et al.[49] on the transport properties, the kinetics of oxidation and the precipitation hardening respectively, no other information concerning the transport properties of the system FeO-MgO-O_2 is available to date. To summarise the contributions of the above authors we shall begin from the work of Hansen and Cutler. They have measured the electrical conductivity of the oxide solid solutions containing various amounts of FeO (from very few P/c to 100 P/c) in the temperature range 300-700°C. Their main conclusions are briefly as follows.

1. The electrical conductivity in magnesio-wustites involve a thermally activated hole transfer similar to that observed in wustite, doped NiO as long iron-iron pairs are present as next nearest neighbours.

2. When all the 12 iron ions of the next nearest position are replaced by Mg^{++} ions, the charge transfer may take place by electron transfer mechanism or involve a completely different process.

3. The magnitude of the conductivity is dependent on the degree of dilution and at constant Fe/Mg ratio the conductivity shows a non-linear dependence on the ferric ion concentration.

4. Finally the activation energy for conduction varies from 0.1 to 0.5 ev (2.3 kcals, 11.5 kcals) for dilute solutions containing less than 15 P/c iron cations.

Further Cutler et al.[47] have shown that the solid state reaction between FeO_{1+x} and MgO involves a counter diffusion of magnesium and iron ions through a relatively rigid oxide ion lattice. The mutual diffusion coefficient increases with the cation vacancy concentration. The activation enthalpy for the diffusion process was found to be 2.05 ev (47.5 kcals) and independent of the vacancy concentration.

A study of the kinetics of oxidation of magnesio-wustite single crystals in air in the temperature range 800-1100°C has been made by Brindley et al. The rate of oxidation of magnesio-wustites containing 20-40 P/c iron cations were found to be linear with time with an activation energy of 1.4 ev (30 kcals). Whereas the magnesio-wustites of high iron content (66 P/c iron cations) were found to exhibit a parabolic oxidation

behaviour with an activation energy of 0.8 ev (18 kcals). Based on these observations these authors have proposed a variety of mechanisms for the oxidation of magnesio-wustites.

Recently Fine and Groves have demonstrated the possibility of strengthening the magnesium oxide lattice by alloying with iron. They have shown that when all the iron is in Fe^{++} state the lattice is not appreciably strengthened, but when a small amount of these ferrous ions are oxidized to ferric retaining the homogeneity of the phase the lattice is remarkably strengthened and the strengthening rate is proportional to the ferric ion concentration. They have also shown that the strengthening due to Fe^{+++} can be enhanced by ageing of the crystal in air 700-1100^{o}C. This causes a precipitation of magnesio-ferrite which possesses the crystallographic coherency with the matrix.

1.4. Research Programme

A large number of investigations have been made in recent years on the phase relations and the thermodynamic properties of the FeO-MgO-O_2 system, and as a result this technologically important system can be described fairly completely. However, there remain a few gaps in our knowledge and one of the objectives of the present study has been to provide some information so far not available, concerning the redox

equilibria in dilute magnesio-wustites. The other objective has been to study the mechanism of the electron transfer between multivalent iron cations in a host lattice such as magnesia. Measurements of the electrical conductivity and determination of Fe^{+++}/Fe^{++} ratio by chemical analysis were the methods selected to obtain the relevant data for the dilute magnesio-wustites.

CHAPTER TWO

2. EXPERIMENTAL DETAILS

2.1. General

In such ternary ionic crystals as magnesio-wustites, spinels, etc. we have to fix two independent variables in addition to the temperature to define the composition of the crystal in equilibrium with its vapour unambiguously. In the present study of the redox equilibria in magnesio-wustites, the thermodynamic state of the system has been unambiguously defined by fixing the oxygen activity in the gas phase and the Fe/Mg ratio in the solid solutions. Two experimental methods were used throughout this investigation:

1. Equilibrium studies on the solid solutions to determine the compositional changes;
2. Measurements of electrical conductivity to ascertain the nature of the current carriers.

Both sets of experiments were conducted under well defined thermodynamic conditions as previously mentioned.

This chapter describes the apparatus and experimental procedure adopted for the present work.

2.2. Gas Train

2.2.a. Flow Meters

The oxygen activity in the gas phase was accurately fixed by metering out a known volume of hydrogen and carbon dioxide or carbon monoxide and carbon dioxide into the reaction chamber and the gas train used for this purpose incorporated a capillary flow meter of the conventional pattern (Fig. 10). The monometers (F) and the blow off's contained n-dibutyl phthate. The gases were dried in the drying towers (D) packed with silica gell and unhydrous magnesium perchlorate. The flow rate of the combined gases was within the range of 120-200 ml per minute. The number of joints were kept to a minimum and connections to the furnace were made with poly-vinyl-chloride (P.V.C.) tubing. The two gases, either H_2 and CO_2 or CO and CO_2 were combined in the mixing chamber (M) and further dried over magnesium perchloride (D') and finally admitted to the reaction chamber.

2.2.b. Gases Used*

Hydrogen, carbon dioxide and carbon monoxide gases

---

* Specifications of the gases used are given in the Appendix.

FIG. 10 GAS TRAIN

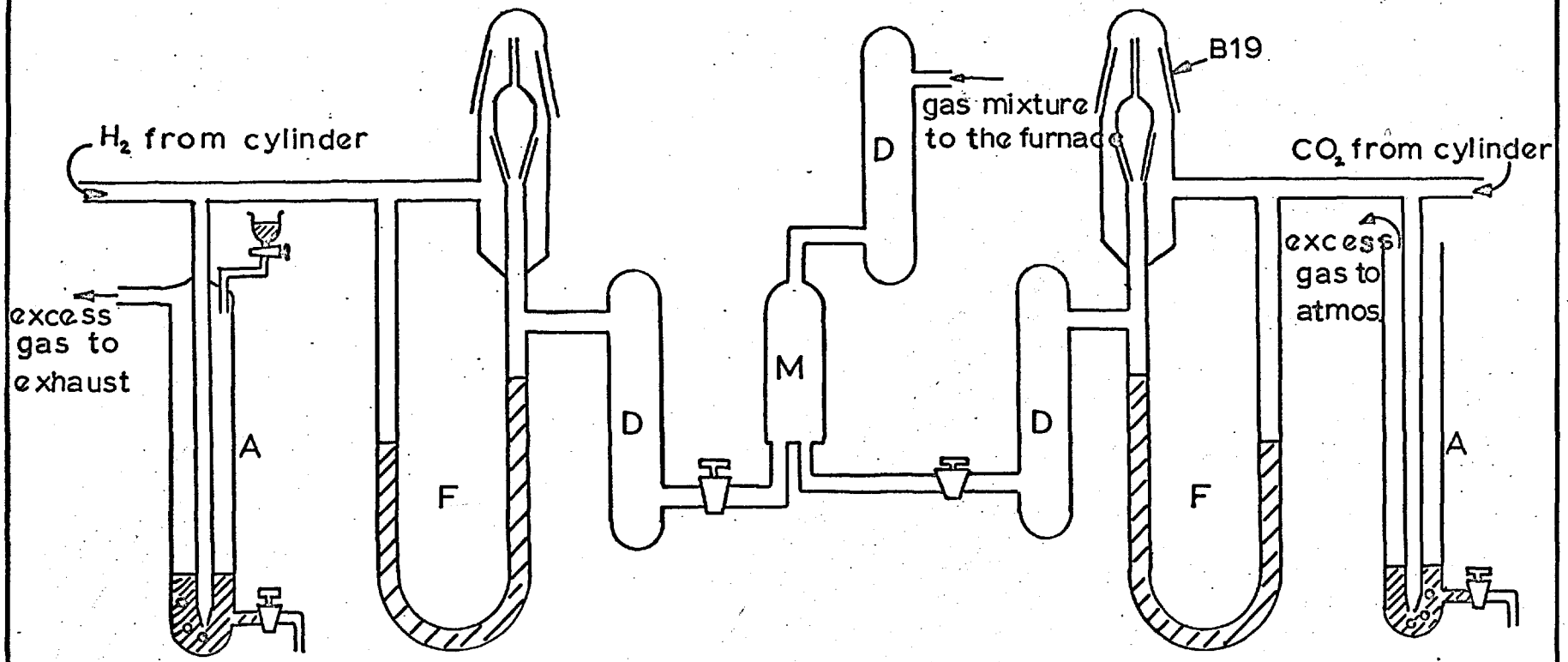

(Symbols explained in the text)

were used to control the oxygen pressures and oxygen free nitrogen for flushing and quenching. High purity hydrogen (99.95% pure) contained 10 volumes per million of oxygen and the carbon dioxide contained 0.2% of air as the major impurity. Since the flow rate of the individual gases were such that the errors introduced due to initial oxygen content was minimum.

In most of the work H_2-CO_2 gas mixtures were used. In conductivity measurements CO-CO_2 gas mixtures were also used to check any adsorption effects due to water vapour, formed in the water-gas reaction and its influence on the conductivity.

2.2.c. The Calibration of the Flow Meters

The flow meters were calibrated for different capillaries by means of a conventional soap bubble flow meter. The total deflection in the monometer was measured to an accuracy of $\pm$ 2 mm. and the reproducibility of the calibration was better than $\pm$ 1%. The calibrations were repeated at regular intervals to check the variations in the flow rates if any.

2.2.d. Measurement of Oxygen Partial Pressures by EMF Technique

The partial oxygen pressure in the gas phase at equilibrium can be calculated from the composition of the ingoing gas and the standard free energy of formation of the various gaseous species*. The Table 2.1. summarizes the range of the oxygen partial pressures used in the present work together with CO_2/H_2 ratios of the ingoing gas and the temperature of the measurement.

Table 2.1.

Range of oxygen partial pressures and corresponding CO_2/H_2 ratios.

Temperature ^oK	Oxygen partial pressure p_{O_2} atm		CO_2/H_2 Ratio	
1573	10^{-13}	10^{-12}	0.10	1.0
1473	10^{-14}	10^{-9}	0.07	40
1323	10^{-16}	10^{-11}	0.07	30
1273	10^{-16}	10^{-11}	0.10	40
1173	10^{-18}	10^{-13}	0.10	40
1073	10^{-20}	10^{-15}	0.10	45

* A detailed calculation of the oxygen partial pressures using H_2-CO_2 and CO-CO_2 gas mixtures is given in the Appendix.

Further a check on the expected oxygen partial pressures for a number of typical H_2-CO_2 gas mixtures in the temperature range 900-1200°C was made using a solid state oxygen concentration cell developed by Weissbart and Ruka[50]. For this purpose a solid oxide electrolyte (solid solution of ZrO_2-CaO) fabricated as an impermeable tube closed at one end was inserted into the equilibrium furnace. The emf of the cell,

$$O_2(p'_{O_2})\ \text{pt}\ |ZrO_2\text{-CaO}|\ \text{pt}\ O_2\ (p^R_{O_2})$$

was measured using a vibrating condenser electrometer having an input impedance of 10^{13} ohms. The emf (E) of this cell is given by the expression,

$$E = \frac{RT}{4F}\ \ell n\ \frac{p^R_{O_2}}{p'_{O_2}} \qquad (2.1.)$$

where $p^R_{O_2}$ and p'_{O_2} are the partial oxygen pressures at the two electrodes and other symbols have their usual meaning. Dry air was used as the reference electrode ($p^R_{O_2} = 2.1 \times 10^{-1}$ atm) and thus it was possible to determine p'_{O_2}, the oxygen partial pressure resulting from H_2-CO_2 gas equilibria. The results showed good agreement with those calculated from the known thermodynamic data as explained in the Appendix (Fig. 11).

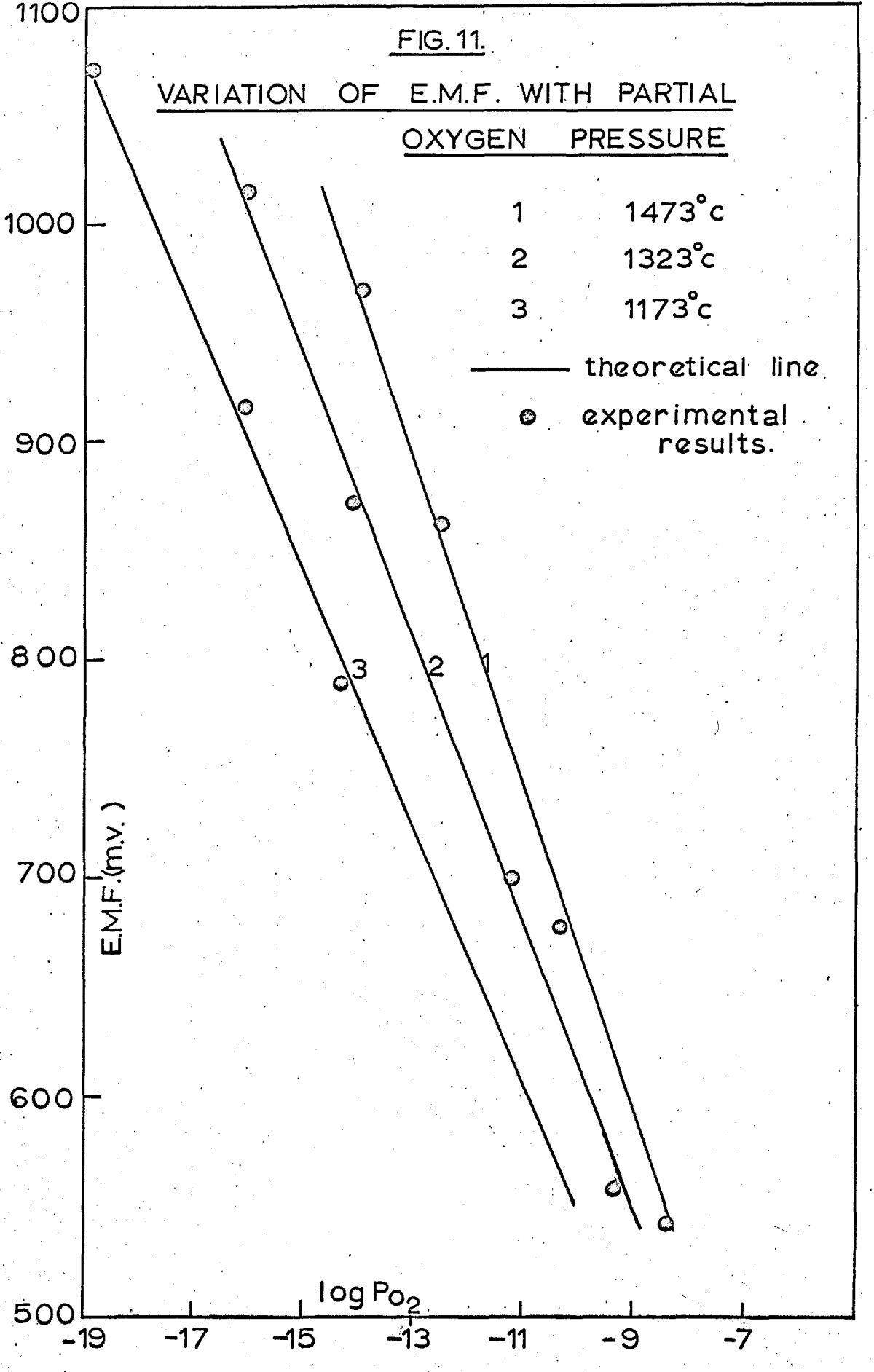
FIG. 11.
VARIATION OF E.M.F. WITH PARTIAL OXYGEN PRESSURE
1 1473°c
2 1323°c
3 1173°c
theoretical line
experimental results.
E.M.F. (m.v.)
log Po2
1100
1000
900
800
700
600
500
-19
-17
-15
-13
-11
-9
-7

2.3. Preparation of the Solid Solutions

2.3.a. Materials Used

Composition of the solid solutions was controlled by fixing the Fe/Mg ratio in the oxide mixtures. This was done by careful mixing of an accurately weighed oxide powder taking precautions to avoid any compositional changes during fabrication operations. The starting materials were 'Analar' grade magnesium oxide powder* and high purity ferric oxide**. In the initial stages of the investigation the ferric oxide was reduced to magnetite at 1200°C on an appropriate CO_2-H_2 atmosphere and was subsequently used to prepare the solid solutions. By experience it was found this initial reduction stage could be eliminated and ferric oxide was directly used in later experiments.

2.3.b. Preparation of the Oxide Powder Compacts

Appropriate amounts of the oxide powders were accurately weighed, mixed and well ground in an agate mortar. The pellets were then made by an isostatic pressing technique[51]. In this method the ceramic powder is contained in a reversible polyvinyl

---

* 'Analar grade MgO supplied from Hopkins and Williams contained 0.1% (by wt.) of iron and minor amounts of volatile impurities like arsenic, lead, etc.

** Ferric oxide supplied from L. Light and Co. Ltd. (London) and was 99.995% pure.

chloride gell which behaves as a liquid at high pressures. For this purpose a propriotary reversible gell designated vinamold 1028 was employed for the present investigation. The ancillary equipment consisted of a suitable die and punches made of EN 24 steel suitably heat-treated to withstand pressures up to 50 tons/ sq. inch. The preparation of the mould from vinamold and the pressing techniques employed for the present work were similar to those used for the fabrication of pellets of solid oxide electrolytes[52]. The pellets of dimensions 10 x 10 x 3 mm. and 4-5 diameter by 2-3 mm. thick were fabricated for the conductivity and equilibration studies, respectively. The corresponding mould dimensions were 16 x 16 x 5 mm. and 6 mm. diameter by 3-4 mm. depth, respectively, after making due allowances for the shrinkage resulting during pressing and sintering operations. The pellets fabricated by this method were free from extraneous impurities and possessed the desired geometry and enough strength. Since the mixture possessed remarkable binding properties no binder was used for the preparation of the pellets. The pellets were pressed using the pressures of the order of 15-20 tons/sq. inch and 3000-4000 lbs/inch depending upon the size of the pellets desired.

2.3.c. Sintering Procedure

The pellets were sintered at 1300°C in horizontal platinum wound furnace. The sintering furnace with all its accessaries is shown in Fig. 12. Platinum wire (18 B.S.G.) as the heating element (B) was wound round on the recrystallised alumina tube (A) of dimensions 45 cm. long, 6.7 cm. diameter and 0.3 cm. thick, at approximately 6 turns per noch at the ends and 5 turns at the centre. At the ends the Pt-13% Rh wire of the same gauge was used as the lead wires. The windings were insulated with an alumina paste. The winding tub e after drying off the water in the past was housed in a refractory tube of the same length but of 10 cm. diameter (C). The refractory tube was contained in a syndanyo box (D) packed with alumina powder. The gap between the refractory and the winding tube was also packed with alumina. The electrical leads (E) taken from the either side were properly insulated by porcelain beads and an additional pair of end plates were used to secure the leads in a proper position. The reaction tube (F) (recrystallised alumina, 75 x 4.6 x 3.9 cm.) both end open, was held in position by asbestos wool packed between the tubes at the either end. One end of the reaction tube carried a B.50 cone (G) cemented by araldite and the other end a syndanyo bung (H). The ends of the reaction tube were water cooled lead coils (I) to protect

FIG. 12. SINTERING APPARATUS

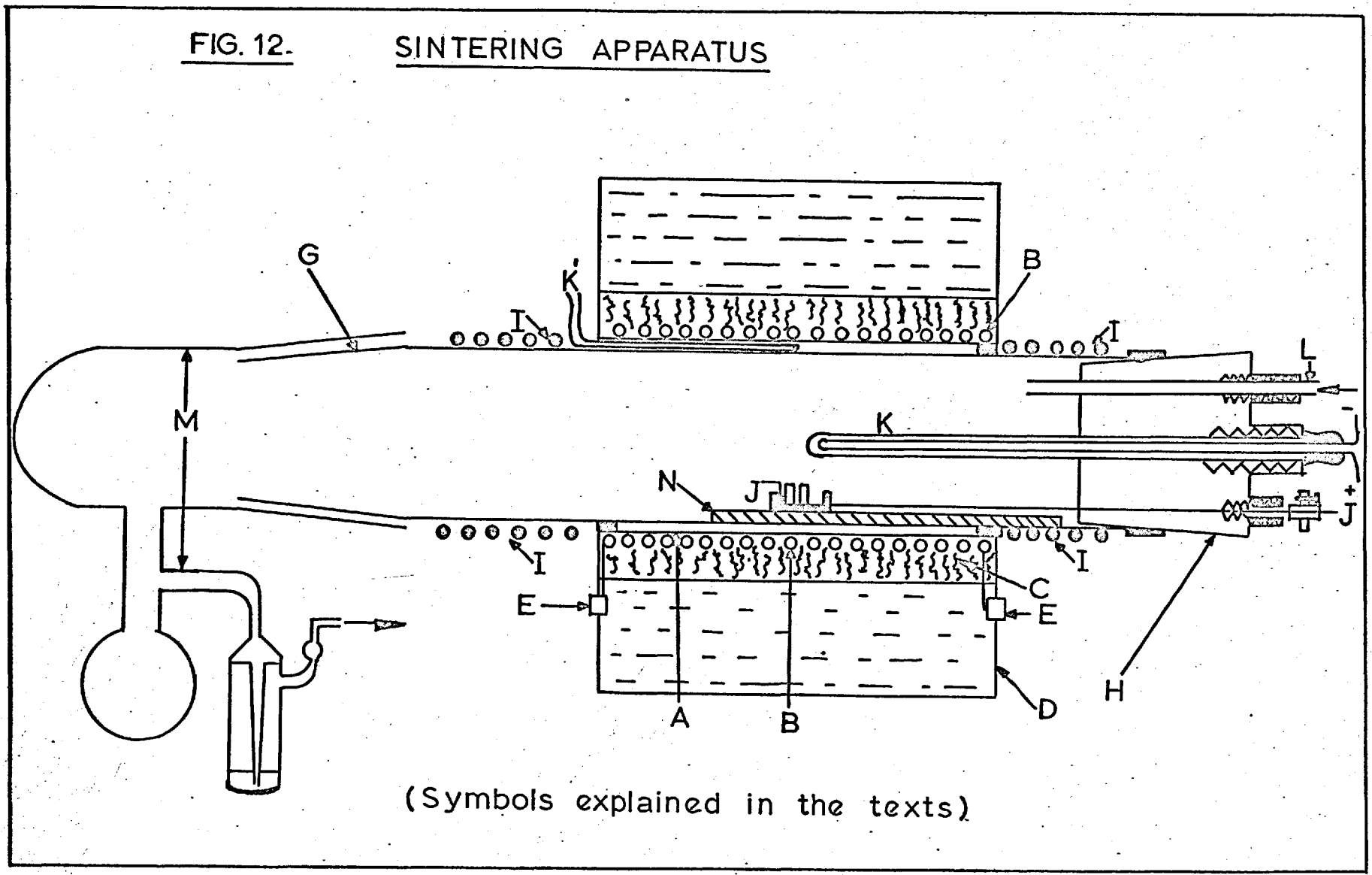

(Symbols explained in the texts)

the araldite joint and the sealing compound.** The pellets were placed on chips of thoria* contained in the platinum boat. The platinum boat was then placed in an alumina boat which carried a platinum wire (J) passing through the bung. The sample assembly was kept in a predetermined even temperature zone and this temperature was measured by means of a thermocouple (K) placed very near the boat. The furnace temperature was controlled ($\pm$ 1^{o}C) by a Mark IV Kelvin and Hughes proportional instrument using a Pt-Pt-13% Rh thermocouple (K') adjacent to the windings. The H_2-CO_2 gas mixture of known composition was passed through the gas inlet (L) at a total flow rate of 150-200 ml/min. and the outgoing gas was lead to exhaust through the bubbler fitted to a B.50 socket with a trap (M) to condense the water formed during the reaction.

The samples were then sintered for 48-72 hours in an atmosphere, the oxygen activity of which was just enough to preserve the magnesio-wustite from reduction to metallic iron. The oxygen partial pressure in equilibrium with magnesio-wustite and iron was calculated using the following solid-gas equilibrium:

$$2FeO_{(\text{solid solution})} = 2Fe_{(\text{metal})} + O_2^{g} \qquad (2.2.)$$

** Thoria prevented the reaction between the Pt and the samples.

* Sealing compound used was supplied from Midland Silicones Ltd., Glamorgan.

Thus the activity of 'FeO' in the solution (a_{FeO}) relative to 'pure' FeO in equilibrium with metallic iron can be expressed as:

$$a_{FeO} = \left(\frac{p_{O_2}}{p^e_{O_2}} \right)^{\frac{1}{2}} \qquad (2.3.)$$

where p_{O_2} and $p^e_{O_2}$ are the oxygen partial pressures in the gas phase in equilibrium with Fe/FeO.MgO solid solution and Fe/FeO (pure) respectively. Using the following thermodynamic data, from Kubaschewski and Evans[53] for the standard free energy of formation for wustite ($FeO_{1.06}$):

$$\Delta G^o_{FeO} = -124{,}100 + 29.9\ T \qquad (2.4.)$$

and Hahn and Muan[9] results for the activity of FeO in the solid solutions, the oxygen partial pressure in equilibrium with Fe/FeO.MgO solid solution at 1300°C were calculated. The corresponding or slightly higher CO_2/H_2 ratio in the ingoing gas was maintained during sintering. At the end of the sintering schedule, the sample assembly was slowly drawn to the cold end of the furnace by means of the platinum wire along the gutter (N). The furnace was flushed with nitrogen fore 10-15 minutes before the samples were taken out. These samples were subsequently used for equilibration and conductivity

measurements. It was found that the higher sintering temperatures (>1300°C) and longer sintering schedule (beyond 48 hours) did not appreciably improve the characteristics of the material. The samples as drawn from the furnace were preserved in the desiccator.

2.4. Equilibration and the Analysis of the Solid Solutions

2.4.a. Furnace Assembly

The apparatus used for equilibrating the samples is shown in Fig. 13. Equilibration was carried out in a vertical kanthal wound furnace (A) with Kanthal A as the heating element. The ends of the reaction tube (B) were water cooled (C) to protect the araldite joints. The samples were placed in a gold or platinum container (D), welded to the Pt-13% Rh wire, which was threaded through the gas-tight rubber teat (E) and fitted to the socket (G). The temperature of the samples was measured by means of the reference thermocouple (F). H_2-CO_2 gas mixture of known composition was admitted to the reaction chamber from the top and the furnace gases left the furnace from the bottom (G). At the end of the run the samples were rapidly quenched in oxygen-free nitrogen.

FIG. 13. EQUILIBRATION APPARATUS

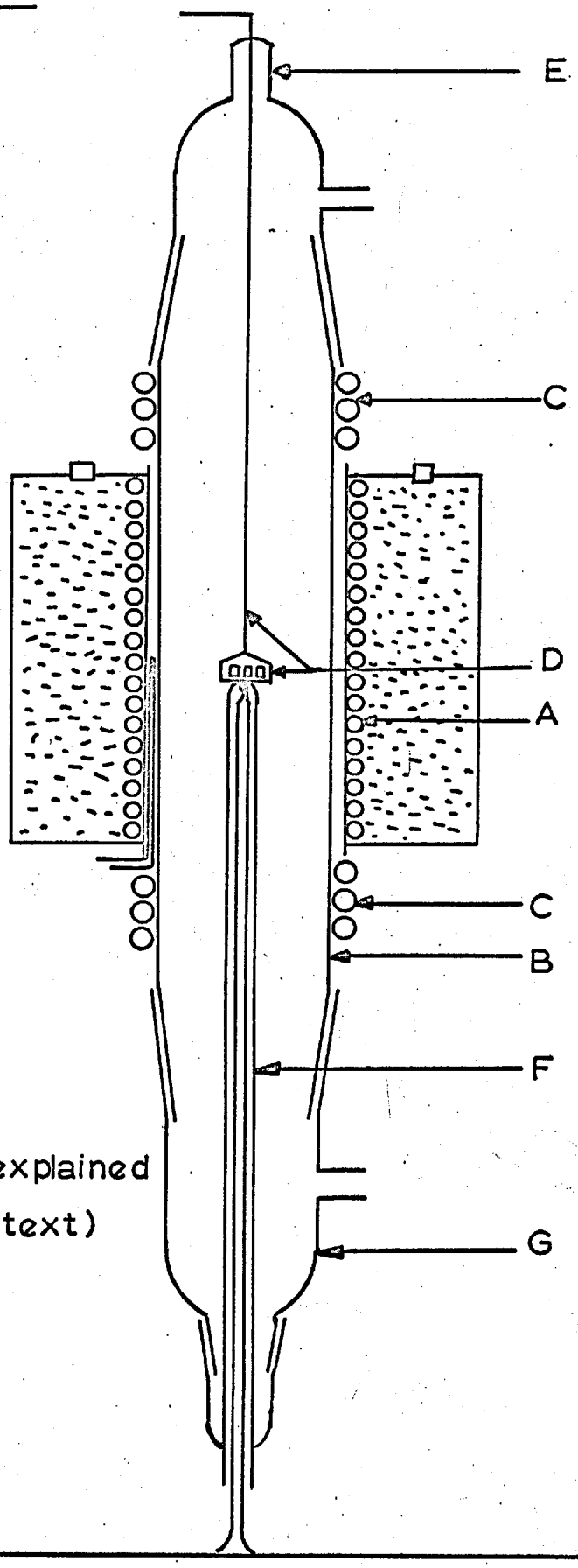

(Symbols explained in the text)

2.4.b. Heat-treatment of the Samples

The samples as sintered, were found to contain the precipitated spinel phase. Since the sintering apparatus was not designed to control the cooling rate, amount of the spinel precipitated could not be controlled. Hence the samples were heat-treated at 1000°C in a just-oxidising atmosphere for 48-60 hours to complete the dissolution of the spinel and then rapidly quenched in N_2. These samples were subsequently used for equilibration experiments.

2.4.c. Approach to Equilibrium

The solid solutions containing 3.2, 5, 7.5, 10 and 20 mole per cent of FeO were equilibrated with a number of known oxygen partial pressures at temperatures 900°, 1050° and 1200°C. Periods of equilibration up to 72 hours were studied in order to establish the time to reach equilibrium and 48 hours was found to be sufficient. The equilibrated samples were quenched in nitrogen and immediately analysed for ferrous and ferric iron content.

2.4.d. Chemical Analysis

The quenched samples were powdered and then dissolved in hot concentrated hydrochloric acid (Analar) under an atmosphere of nitrogen. The cooled solution was analysed for ferrous and ferric iron either by a colorimetric method* using O-phenanthroline as a complexing agent for ferrous iron or a volumetric method* using potassium dichromate solution of suitable strength as the titrant. In both methods, the ferrous iron and the total iron as ferrous was determined and the concentration of ferric iron was obtained by difference. Although no direct analysis for magnesium oxide content was made, we had an indirect check on the composition of the sample by knowing the weight of the sample and the total iron content.

The analysis of the samples equilibrated at 900°C were made by both methods and the results obtained from the two methods agree very well to within $\pm$5% total iron content.

Since the colorimetric method was much more involved compared with the volumetric method, the analysis of the samples equilibrated at higher temperatures was carried out mostly by the volumetric method. Further, a series of checks was made on the reliability of the methods, by analysing magnetic and metallic iron under similar conditions. It was found that the

---

* Analytical details are given in the Appendix.

ratio of Fe^{+++}/Fe^{++} obtained for magnetite was within the range 1.99-2.01 (i.e. $\pm$ 0.51 error) and the ferric iron content in the solution prepared by dissolving pure iron was found to be less than 0.5%. The observations clearly indicate that the analytical procedure did not affect the Fe^{+++}/Fe^{++} ratio in the samples.

2.5. Conductivity Measurements

2.5.a. Surface Preparation

The sintered samples were polished with appropriate grades of SiC paper followed by a polishing with different grades of diamond paste. Adequate contact was ensured by giving them a final polish with 4 micron grade diamond paste. The traces of the polishing material were removed by washing the pellets in acetone. These clean and dry pellets were subsequently used for the conductivity measurements.

2.5.b. Electrode Materials

The selection of the electrode material for the measurement of the electrical conductivity was based on thermodynamic consideration. Obviously platinum could not be used because the system

Fe-Pt exhibits a marked negative deviation[53,54] from Raoult's law. The partial heat of solution of iron in platinum rich iron alloys is negative (about -17 Kcals)[54]. Further preliminary measurements of conductivity using platinum electrodes clearly revealed the interaction between Pt and the sample. This was disclosed by irreproducible and often erratic conductivity results. The problem of electrode material was satisfactorily overcome using gold electrodes. Advantage was taken of the positive deviation of the system Fe-Au from Raoult's law and the partial heat of solution of iron in gold rich iron alloys being positive (+5 Kcals)[55]. It was found by experience that the use of gold foils as an intermediate barrier between the solid solution and the platinum electrode enabled good results to be obtained.

2.5.c. Conductivity Apparatus

Two terminal A.C. conductivity measurements were made in a horizontal platinum wound furnace* fitted with the conductivity sample holder illustrated in Fig. 14. The design of the sample holder was similar to that employed by Steele[52] for the conductivity measurements of solid oxide electrolytes but with

cont. on page 67

* Used for sintering the solid solutions (Section 2.3.c.)

FIG. 14 CONDUCTIVITY APPARATUS

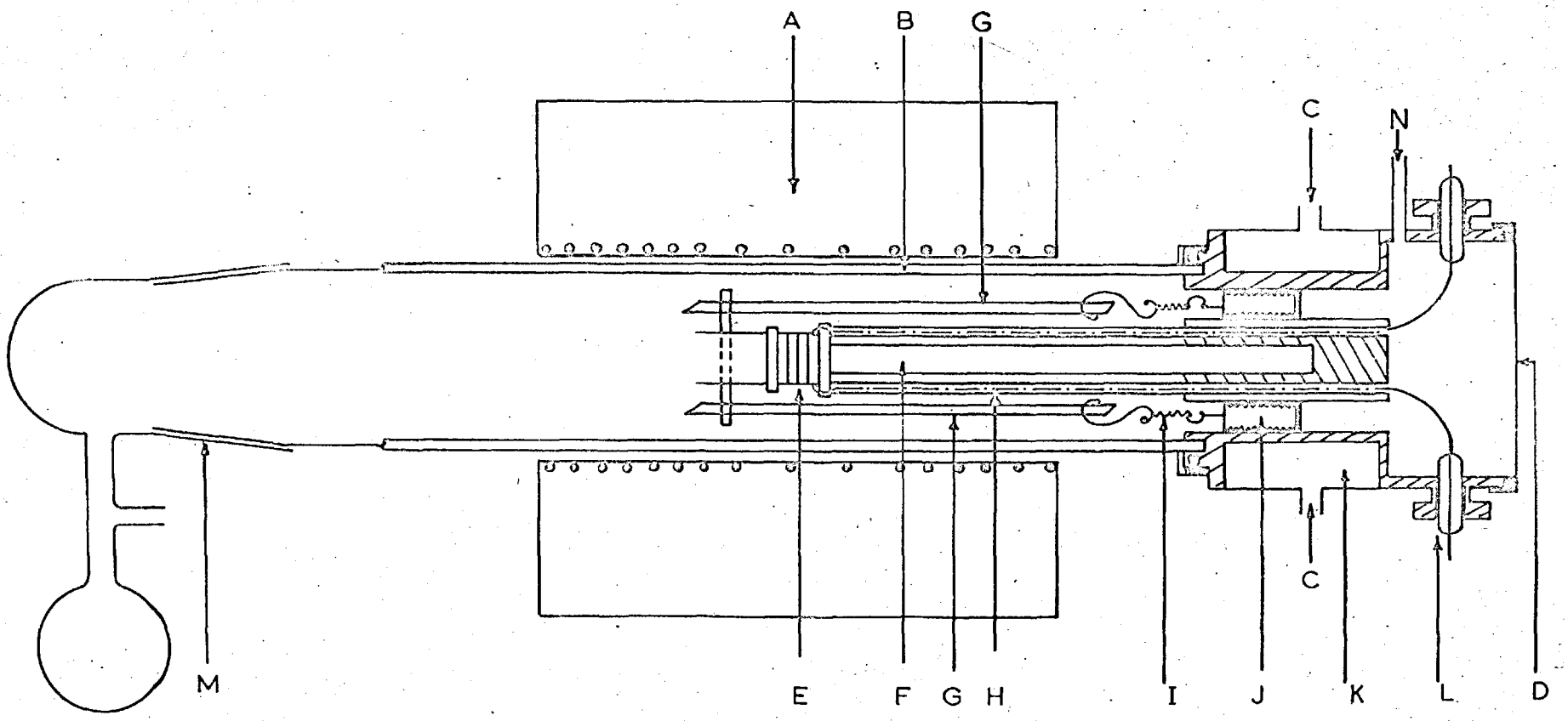

Reference Fig. 10

A - Platinum wound furnace.

B - Reaction tube.

C - Water cooling.

D - Sample holder.

E - Sandwich assembly.

F - Supporting rod (Al_2O_3).

G G - Guide rods.

H - Electrode leads.

I - Spring loading.

J - Adjustable screws.

K - Water cooling chamber.

L - Platinum leads.

M - B-50 cone-socket fitted with a water trap and gas out-let.

N - Gas in-let.

the following modifications.

1. The tension of the spring loading was varied by means of the adjustable screws.

2. The sample holder was able to accommodate 3-4 samples in the form of a sandwich assembly. Thus the conductivities of a number of samples (up to 4) of different compositions were recorded simultaneously in each run.

2.5.d. Approach to Equilibrium

The solid solutions were treated in a just-oxidising atmosphere at 1000°C for 60-72 hours to complete the dissolution of the spinel and to establish a good electrical contact between sample and electrode. Then conductivity data were recorded at temperatures 1000, 900 and 800°C and the range of the oxygen partial pressures employed covered the homogeniety range, from equilibrium of the solid solutions with solid iron to that in equilibrium with the spinel phase. At each temperature, the samples were subjected to a number of oxidation reduction cycles till consistent and reproducible results were obtained. The reproducibility was within $\pm$ 10%. Equilibrium was attained within 12-14 hours during the oxidation cycle and 16-18 hours in the reduction cycle. On many occasions the samples were equilibrated overnight or 24-36 hours to confirm the

attainment of the equilibrium.

The A.C. conductivities were measured using a "Rank Cintel capacitance-resistance" bridge at a constant frequency of 1592 C.P.S. However, a series of measurements with a variable frequency A.C. bridge* established that within the frequency range 500-33200 C.P.S. the conductivity was relatively independent of frequency. Conductivity measurements were made on solid solutions containing 1**, 1.75**, 2.5, 3.2, 4, 5, 7.5, 10 and 20 mole percent FeO.

---

* This instrument was assembled in the laboratory and incorporated variable resistors which could be adjusted till the bridge is balanced using a cathode ray oscilloscope.

** Prepared using spectroscopic pure magnesium oxide.

CHAPTER THREE

RESULTS AND DISCUSSION (PART ONE)

3.1. General

The present results of the equilibration studies on the MgO-FeO-O_2 system have been analysed in the light of the various structural modes proposed for non-stoichiometry of oxides and oxide solid solutions. Results of Brynestad and Flood, Berthet, Schmahl et al. and Morozova have also been included to understand the redox properties of the system across a wide composition range. The behaviour of the system FeO-MgO-O_2 has been compared to that exhibited by $MgO-MnO_{1+x}$ [56] and ThO_2-UO_{2+x} [57, 58].

3.2. Presentation of the Results

Tables 3.1, 3.2 and 3.3 contain the results of the equilibration studies, together with the errors involved and the analytical method adopted for the determination of ferrous and ferric iron content in the solutions. Though the function $\eta Fe^{+++}/\eta Fe^{++} + \eta Fe^{+++}$ was operational, this seems to possess a very little significance from the defect chemistry point of view. Therefore these results have been plotted in terms of $\eta Fe^{+++}/\eta^2 Fe^{++}$ or $\eta Fe^{+++}/\eta Fe^{++}$ ratios as a function of oxygen pressures. The tabulated results are the average value of minimum two measurements.

Table 3.1.

Results of Chemical Analysis at 1173°K.

Composition Mole %FeO	$(\eta Fe^{+++}/\eta Fe^{++} + \eta Fe^{+++})$ x 100 at specified oxygen partial pressures 10^{-18}	10^{-17}	10^{-16}	10^{-15}	10^{-14}	10^{-13}	Analytical Method	Errors ± % $\eta Fe^{+++}/\eta Fe^{+++} + \eta Fe^{++}$	Total Iron
3.2	2.7	2.72	2.9	7.5	21.75		Colorimetric	10	·7
	2.8	2.77	2.7	7.7	22.00	-23	Volumetric	10	·8
5	4.1	4.0	4.2	22	22.75		Colorimetric	10	·7
	4.2	3.9	4.0	23	24.00	-27	Volumetric	10	·7
7.5	1.71	2.19	3.0	13.75	17		Colorimetric	10	·7
	2.0	2.2	3.0	14	16.1	21.5	Volumetric	10	·7
10	2.42	3.5	4.5	42	44		Colorimetric	5 to 10	·5
	2.5	3.8	5	41	46	48.00	Volumetric	5 to 10	·5
20	2.41	3.5	4.5	50.4	49.7		Colorimetric	5 to 10	·5
	2.5	3.7	4.6	48.0	50	50.5	Volumtric	5 to 10	·5

Note: period of equilibration up to 72 hours.

For detailed results see Tables VI.1-12

Table 3.2.

Results of Chemical Analysis at 1323°K.

Composition Mole %FeO	$(\eta Fe^{+++}/\eta Fe^{++} + \eta Fe^{+++}) \times 100$ at specified oxygen partial pressures 10^{-16}	5×10^{-15}	5×10^{-14}	5×10^{-13}	5×10^{-12}	5×10^{-11}	5×10^{-10}	Method of Analysis	Errors ± % $\eta Fe^{+++}/\eta Fe^{+++}+\eta Fe^{++}$	Total Iron
3.2	2.4	2.2	2.30	-	5.50	11.5	12.9	Volumetric	± 5-10	10
5.0	3.8	3.9	4.0	3.9	7.20	7.2	17.5	Volumetric	± 5-10	10
7.5	4	4.0	4.4	4.12	8.00	10.7	16.5	Volumetric	± 5-10	·7.5
10.0	1.10	1.8	2.5	3.30	7.35	12.5	15.0	Volumetric	± 7.5	·5
20.0	1.2	1.20	3.00	5.10	15.00	28	58.2	Volumetric	7.5	·5

For detailed results see Tables VI. 13-17.

Table 3.3.

Results of Chemical Analysis at 1473°K.

Composition Mole %FeO	$(\eta Fe^{+++}/\eta Fe^{++} + \eta Fe^{+++})$ x 100 at specified oxygen m partial pressures 10^{-14}	$5x10^{-13}$	10^{-11}	10^{-10}	10^{-9}	10^{-8}	$5x10^{-8}$	Method of Analysis	Error ± % $\eta Fe^{+++}/\eta Fe^{+++} + \eta Fe^{++}$	Total Iron
3.2	-	2.5	2.7	2.7	6	12.5	17.5	Volumetric	5 to 10	1·0
5	-	3.9	3.91	4.30	8.5	14.1	1¾.1	Volumetric	5 to 10	1·0
7.5	-	3.0	3	3	6.8	15	28	Volumetric	5 to 10	·5
10	3	3.3	3.6	-	12.5	31	46	Volumetric	5 to 10	5
20	4.20	4.16	4.16	8.50	28.01	33	50	Volumetric	5 to 10	5

For detailed results see Tables VI.18-22

3.3. Discussion

3.3.a. Dependence of Ferric Ion Concentration on Oxygen Partial Pressure at Constant Temperature

The preseent work has revealed that the dependence of the function $\eta Fe^{+++}/\eta^{m}Fe^{++}$ (where m is equal to either one or two) on the oxygen partial pressure in dilute magnesio-wustites is quite complex (Figs. 15, 16 and 17). In the temperature range investigated, the dependence of this ratio $\eta Fe^{+++}/\eta^{m}Fe^{++}$ upon the oxygen partial pressure for all the solid solutions studied, exhibited a transition ingoing from the low oxygen partial pressure to high oxygen partial pressure and the table 3.4. summarises the slopes of the various isotherms.

Such a complex dependence of the defect concentration on the oxygen partial pressure and temperature may be reconciled as follows.

1. The results of the oxygen pressure-independent region are attributed to an intrinsic mechanism in which the oxygen plays no part in the formation of the positive holes. The possible ways by which this can occur include the disproportionation reactions.

$$2Fe^{++} = Fe^{+++} + Fe^{+} \qquad (3.1.)$$

or $$3Fe^{++} = 2Fe^{+++} + Fe^{o} \qquad (3.2.)$$

FIG. 15

VARIATION OF THE $\frac{n_{Fe^{+++}}}{n^2_{Fe^{++}}}$ AS A FUNCTION OF OXYGEN PARTIAL PRESSURE

Nos.	TEMP °K	SOURCE
1, 5, 9,	1173	Present work
2, 6, 10,	1323	"
3, 7, 11,	1473	"
4, 8, 12,	1673	(Ref. 27)

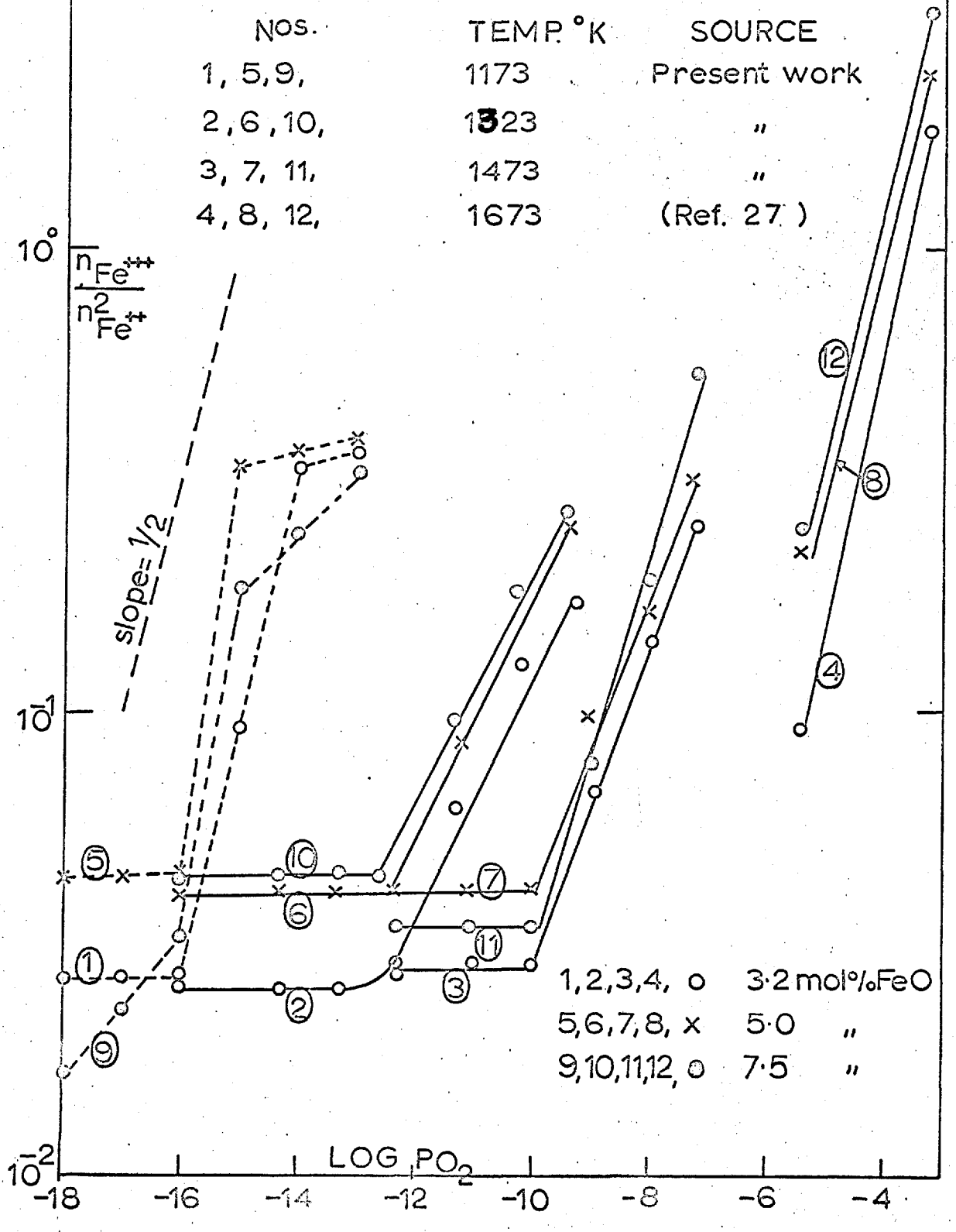

FIG. 16

VARIATION OF $\frac{n_{Fe^{+++}}}{n_{Fe^{++}}}$ RATIO AS A FUNCTION OF OXYGEN PARTIAL PRESSURE

Nos.	TEMP. °K	SOURCE
1, 4, 7,	1323	Present work
2, 5, 8,	1473	" "
3, 6, 9,	1673	Ref. 27.

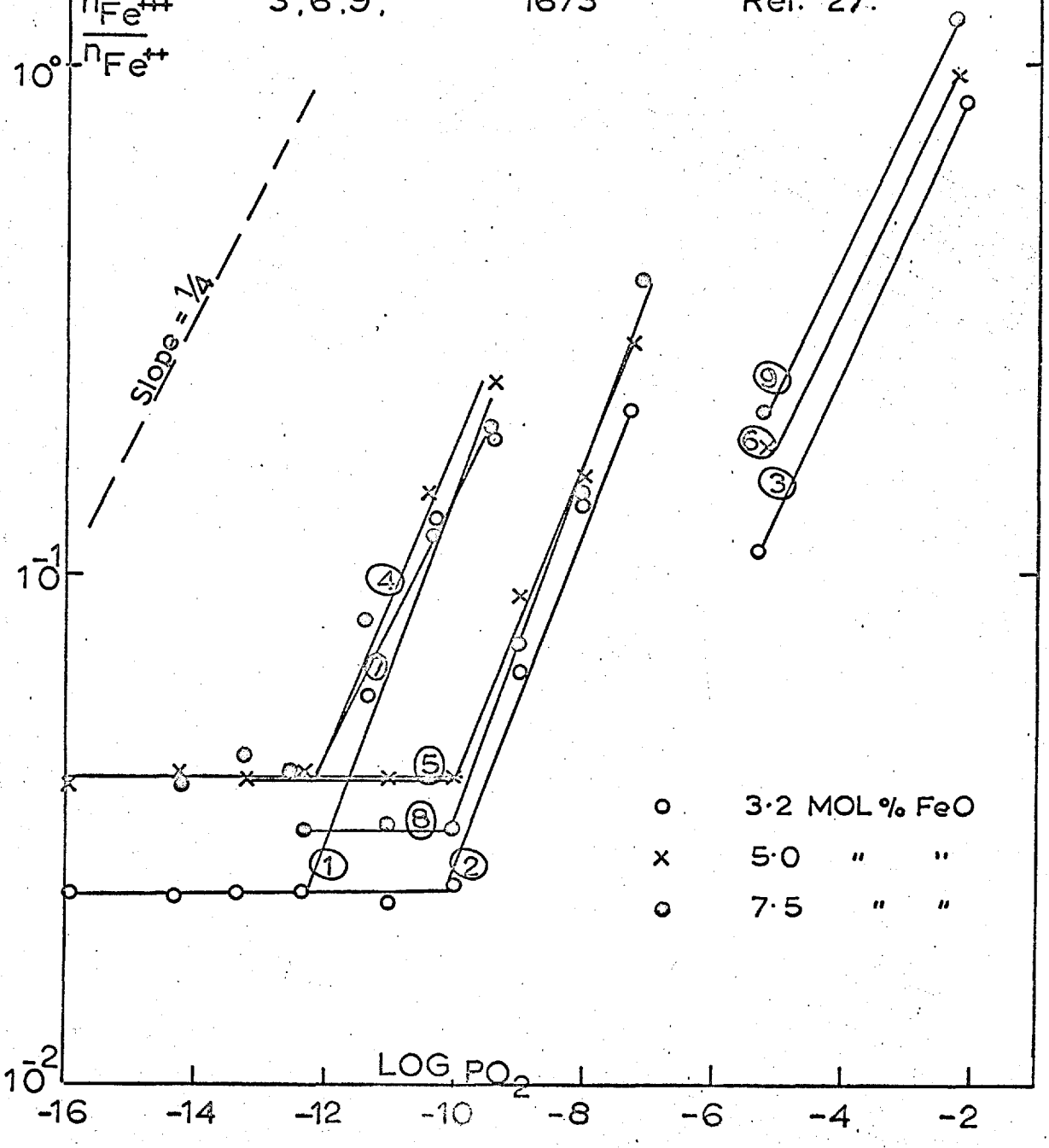

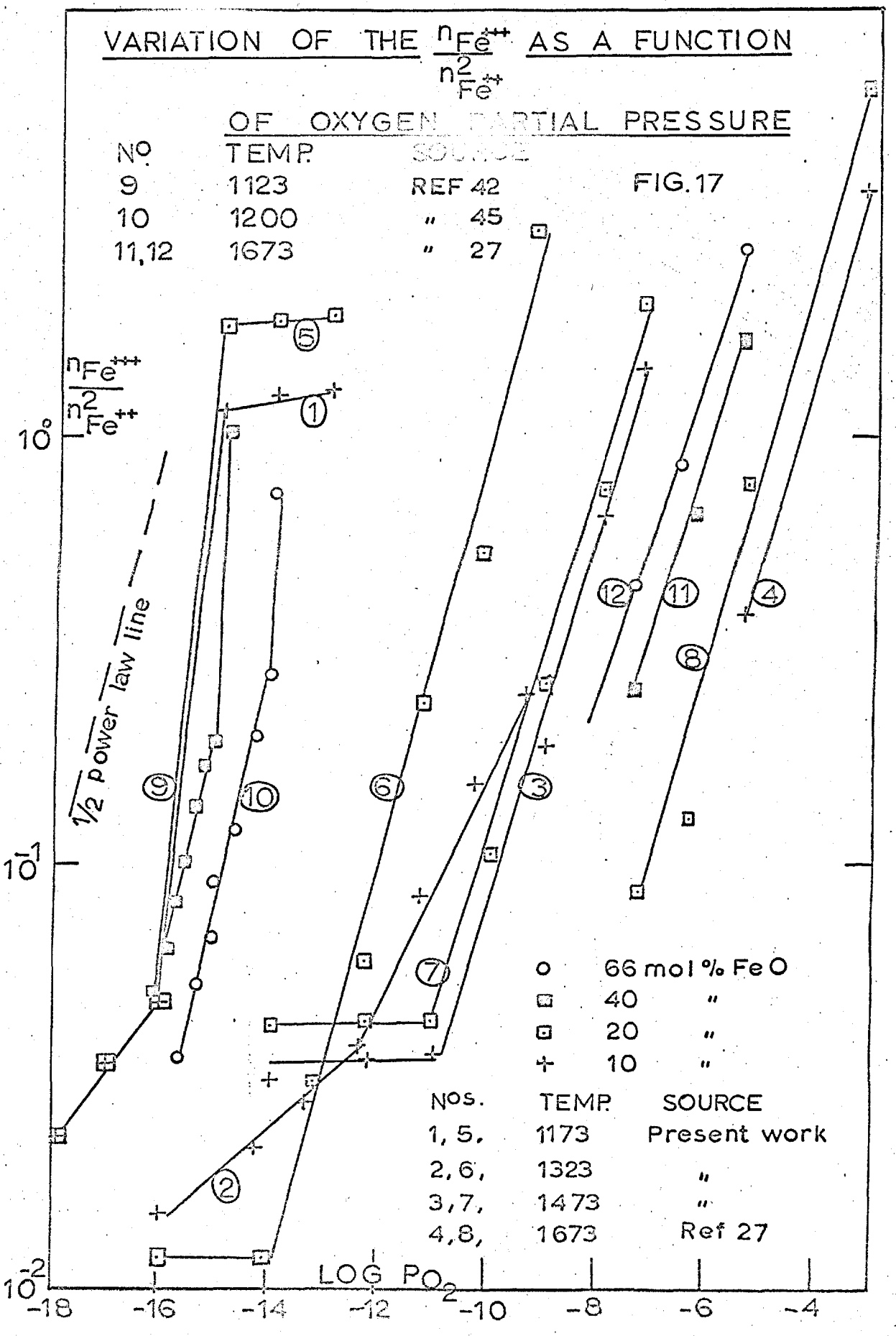
VARIATION OF THE $\frac{n_{Fe^{++}}}{n^2_{Fe^{++}}}$ AS A FUNCTION OF OXYGEN PARTIAL PRESSURE
FIG. 17
No. TEMP. SOURCE
9 1123 REF 42
10 1200 " 45
11,12 1673 " 27
$\frac{n_{Fe^{++}}}{n^2_{Fe^{++}}}$
10^0
10^{-1}
10^{-2}
1/2 power law line
o 66 mol % Fe O
□ 40 "
⊡ 20 "
+ 10 "
Nos. TEMP. SOURCE
1, 5, 1173 Present work
2, 6, 1323 "
3, 7, 1473 "
4, 8, 1673 Ref 27
LOG P_{O_2}
-18 -16 -14 -12 -10 -8 -6 -4

Table 3.4. Slopes of the Isotherms.

Composition Mole %FeO	Temperature ^{o}K	Slope	
		Low oxygen pressure	High oxygen pressure
3.2, 5	1173	I	$>\frac{1}{2}$
7.5, 10, 20	1173	1/6	$>\frac{1}{2}$
40*	1123	-	$-\frac{1}{2}$
66**	1200	-	$\frac{1}{2}$
3.2, 5, 7.5	1323	I	$\frac{1}{4}$
10	1323	1/6	$\frac{1}{4}$
20	1323	I	$\frac{1}{2}$
3.2, 5, 7.5	1473	I	$\frac{1}{4}$
10 and 20	1473	I	$\frac{1}{2}$
3.2, 5, 7.5	1673***	-	$\frac{1}{4}$
10, 20, 40, 60	1673	-	$\frac{1}{2}$

* Results of Berthet Reference.[42]

** Results of Morozova.[45]

*** Results of Brynestad and Flood.[27]

I independent of oxygen partial pressure.

Such intrinsic reactions involving the formation of univalent or zero valent iron has already been proposed by Orton et al.[59] and Flood and Hagemark[60]. Orton et al. have detected e.s.r. lines corresponding to Fe^{+} in those MgO crystals which were either heat-treated in magnesium vapour or irradiated with X-rays or ultra-violet rays and have accounted for the presence of Fe^{+} according to the electron-transfer reaction. Further Flood and Hagemark have shown that the disproportionation reactions (3.1. and 3.2.) become particularly important in the molten FeO-O_2 gas equilibrium for compositions close to stoichiometric FeO (i.e. at low p_{O_2} levels).

The present work indicates that such reactions would be suppressed at high concentrations of extrinsic positive holes and only be expected to be predominant at low iron content and low oxygen pressures. The present results also indicate that the oxygen-independent region extends to higher total iron contents and the temperature is increased.

2. The solid solutions containing 7.5, 10 and 20 mole percent FeO, at low temperatures show an identical power dependence at low oxygen partial pressures with a slope equal to 1/6. Such a dependence suggests a fairly dissociated vacancy-ferric ion model and indicates that the defect equilibrium in these magnesio-wustite solid solutions is similar to that of the pure wustite phase. Thus at low defect concentrations (i.e. low Fe^{+++}

content relative to total iron content) the semiconduction model proposed for wustite seems to be valid for dilute magnesio-wustites. From a structural point of view such a behaviour is not unreasonable because magnesio-wustites containing more than 8 mole percent of FeO possess at least one iron-iron pair in the next nearest position. Further support for this conclusion is provided by the conductivity results discussed in the section 4.

3. In the high oxygen partial pressure region for all the solid solutions, the ratio $n_{Fe^{+++}}/n_{Fe^{++}}$ is dependent upon oxygen pressure and has a value of either one-half or one-quarter. These observations indicate that the fully dissociated ferric-ion vacancy model does not seem to apply for dilute magnesio-wustites at high oxygen partial pressure. Moreover, the solid solutions containing upto 7.5 mole percent FeO showed a transition in the high oxygen partial pressure region from a half power dependence at low temperatures to quarter-power dependence at high temperatures. Magnesio-wustites containing 10 and 20 mole percent FeO exhibit a half power dependence at all temperatures investigated.

Further, the redox results of Berthet Morozova and Brynestad and Flood clearly indicate that the half-power law is consistently obeyed by the solid solutions containing more than 10 mole percent of FeO regardless of the temperature

of the measurement. To interpret these results, one can adopt the model proposed by Brynestad and Flood in which a cation vacancy is associated with the ferric ions according to the defect equilibria

$$2Fe^{++} + \tfrac{1}{2}O_2^g = Fe^{+++}_2 - V_{cation} + O^{=} \qquad (3.3.)$$

$$\text{Alternatively } 2Fe^{++} + \tfrac{1}{2}O_2^g = Fe^{+++} - V_{cation} + Fe^{+++} + O^{=} \qquad (3.4.)$$

The two equilibria have to be considered because the slopes of the isotherms indicate that the degree of association of the defects is a function of total iron and the temperature. Brynestad and Flood have derived an equilibrium constant for the reaction (3.3.), treating the defects in magnesio-wustites as a mixture of monomers and trimers. Considering the $Fe^{+++}_2 - V_{Fe}^{++}$ as a trimer, with each vacancy surrounded on the average, by two ferric ions, and each Fe^{+++} surrounded by more than one vacancy, then in the regions of high magnesium oxide content the complexes are well separated from each other. Assuming that the thermodynamics of the system is determined by the entropy changes only, they have derived the following equilibrium constant for the reaction (3.3.):

$$K_1 = \frac{\eta_{Fe^{+++}}}{\eta^2_{Fe^{++}}} \frac{\Sigma\eta_+}{P_{O_2}^{\frac{1}{2}}} \left[\frac{1}{1 - \frac{1}{3}\frac{\eta_{Fe^{+++}}}{\Sigma\eta_+^2} V_{cation}}\right]^4 3.\left(\frac{8}{9}\right) \qquad (3.5.)$$

where $\Sigma\eta_+$ is the total number of cation sites. At large magnesium oxide contents the above expression can be reduced to

$$K_2 = \frac{\eta_{Fe^{+++}}}{\eta^2_{Fe^{++}}} \frac{\Sigma\eta+}{P_{O_2}^{\frac{1}{2}}} \qquad (3.6.)$$

Plots of $\eta Fe^{+++}/\eta^2 Fe^{++}$ ratio as a function of oxygen partial pressure for the solid solutions containing upto 66 mole percent FeO are shown in Figs. 15 and 16. The slope of the isotherms in the high oxygen pressure region for magnesio-wustites containing 10 and 20 mole percent FeO is very nearly equal to half and also for the concentrated solid solutions in all the oxygen pressure range. Thus the experimental results confirm the complex model concept.

Similarly on equilibrium constant for the reaction (3.4.) at very high MgO content can be represented by:

$$K_3 = \frac{\eta^2_{Fe^{+++}}}{\eta^2_{Fe^{++}}} \frac{1}{P_{O_2}^{\frac{1}{2}}} \qquad (3.7.)$$

The above equation predicts a quarter power dependence of the ratio $\eta Fe^{+++}/\eta Fe^{++}$ upon the oxygen partial pressure which has

actually been observed for solid solutions containing up to 7.5 mole percent of FeO. From the present work on the study of the redox equilibria in dilute magnesio-wustites, there appears that high temperatures and low iron contents favour the dissociation of trimers to dimers ($Fe^{+++}-V_{cation}$) and even to monomers (i.e. fully associated ferric ion vacancies). In contrast at high FeO contents, it may be concluded that the complete association of the defects is favoured.

Recently Cutler et al.[56] have shown that the non-stoichiometric behaviour of MgO-MnO solid solutions is similar if not identical to FeO-MgO solid solutions and at constant temperature and oxygen partial pressure, the concentration of the trivalent manganese varies as a square of Mn^{++} in solid solutions containing up to 40 mole percent FeO. These authors have accounted such a behaviour by the postulate that Mn^{+++} ions are associated with cation vacancies and such associations are favoured the higher the MnO concentrations in the solid solutions. Further, they also conclude that high thermal energy and low manganese content tends to promote the dissociation of the defect complexes.

3.3.b. The Calculation of the Partial Heat of Solution of Oxygen

Data for the composition-oxygen partial pressure-temperature relationships enable the partial molar heat of solution of oxygen in the solid solutions to be calculated. Thus we may write reaction between the equilibrium constant and the partial molar heat of solution of oxygen ($\Delta\bar{H}_{\frac{1}{2}O_2}$) as

$$\Delta\bar{H}_{\frac{1}{2}O_2} = \left(\frac{\delta \ell n K_2}{\delta 1/T}\right)^{(Fe/Mg+Fe)} \qquad (3.8.)$$

$$\frac{\eta_{Fe^{+++}}}{\eta^2_{Fe^{++}}}$$

alternatively

$$\Delta\bar{H}_{\frac{1}{2}} = \left(\frac{\delta \ell n K_3}{\delta\ 1/T}\right)^{(Fe/Mg+Fe)} \qquad (3.9.)$$

$$\left(\frac{\eta_{Fe^{+++}}}{\eta_{Fe^{++}}}\right)^2$$

where K_2 and K_3 are the equilibrium constants given by the equations (3.6.) and (3.7.) respectively. Since the differentials on the right side of the expressions were taken at a constant ferric to total iron content ($\frac{\eta_{Fe^{+++}}}{\eta_{Fe^{++}} + \eta_{Fe^{+++}}} = 16.5\%$), the slope of the plot of log p_{O_2}* against $1/T^{o}K$ yields the heat of solution of oxygen. The results are shown in Fig. 18 and also

---

* See bottom of next page.

FIG.18

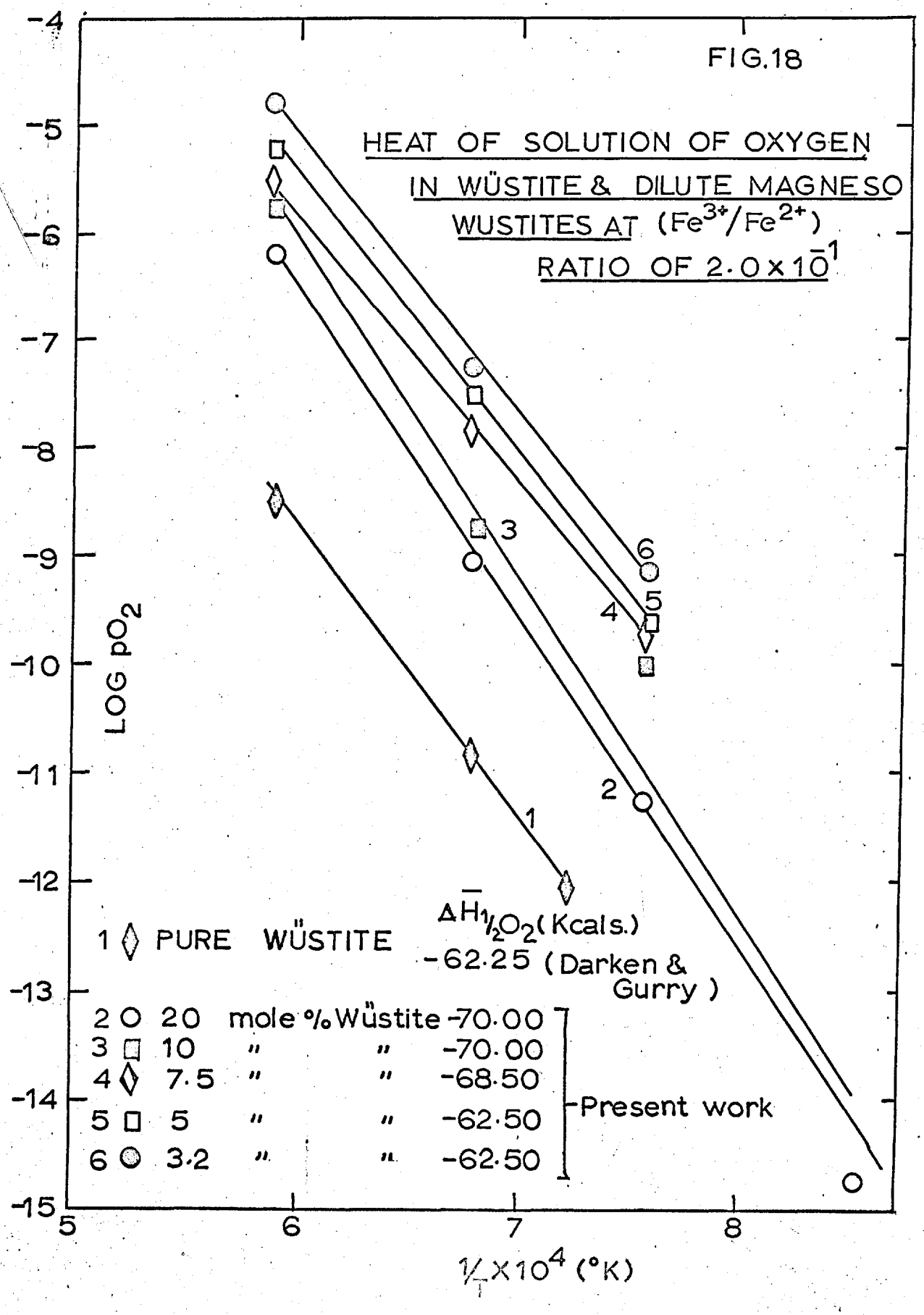
HEAT OF SOLUTION OF OXYGEN IN WÜSTITE & DILUTE MAGNESO WUSTITES AT (Fe^{3+}/Fe^{2+}) RATIO OF 2.0×10^{-1}
LOG pO_2
$1/T \times 10^4$ (°K)
$\Delta \bar{H}_{1/2O_2}$ (Kcals.)
1 ◊ PURE WÜSTITE -62.25 (Darken & Gurry)
2 ○ 20 mole % Wüstite -70.00
3 □ 10 " " -70.00
4 ◊ 7.5 " " -68.50
5 □ 5 " " -62.50
6 ○ 3.2 " " -62.50
Present work

summarised in the following table (3.5.).

Table 3.5.

$\Delta\bar{H}_{\frac{1}{2}O_2}$ values for magnesio-wustites.*

Concentration Mole percent FeO	$\Delta\bar{H}_{\frac{1}{2}O_2}$ Kcals ($\pm$ 5 Kcals)
3.2	-62.5
5	-62.5
7.5	-68.5
10	-70
20	-70
40	-61
60	-59.5
100	-62.5 $\pm$ 1 Kcal.

* The oxygen partial pressures for solid solutions 3.2, 5 and 7.5 in equilibrium at this defect concentration were obtained from the isothermal plots of $\eta_{Fe^{+++}}/\eta_{Fe^{+++}}$ against p_{O_2}, $\eta_{Fe^{++}}/\eta_{Fe^{+++}}$ ratio being equal to 2.0×10^{-1}. For solid solutions containing more than 10 mole percent, the corresponding p_{O_2} values in equilibrium at the same defect concentration were derived from interpolation from the isothermal plots of $\eta_{Fe^{+++}}/\eta^2_{Fe^{++}}$ vs. p_{O_2}.

These results show that the heat of solution of oxygen is approximately constant across a whole range of composition up to and including the binary Fe-O_2 system within the error limits of $\pm$ 5 Kcals. These results also indicate that the energy changes associated with the dissolution of oxygen in excess of stoichiometric ratio in wustite and magnesio-wustite are comparable. This conclusion is not unreasonable as can be seen in the following discussion of the various energy terms which contribute to the overall partial molar heat of solution of oxygen.

1. The dissociation energy and the electron affinity of oxygen for the incorporation of wustite and magnesio-wustite lattice are the same in both cases.

$$\tfrac{1}{2}\, O_2^{g} = O^{=} + 2\oplus \qquad (3.10)$$

2. The change in the local Madelung energy partially offsetting the endothermic change resulting from changes in the valence state of iron $Fe^{++} + \oplus = Fe^{+++}$, might be the same in the solid solution and the pure wustite phase. This is not unreasonable because the end members and the solid solution possess the NaCl crystal structure and the dielectric constant of the end members is approximately the same.

3. Since the energy required to create the thermal defects

(Schottky defects) in both the lattices (MgO and FeO) is the same, so the energies for the formation of cation vacancies and the energy of relaxation around the altervalent ions (Fe^{+++}) must be similar in wustite and magnesio-wustite phase.

Further the calculation of the partial heat of solution of oxygen in the system MgO-MnO shows that $\Delta\bar{H}_{\frac{1}{2}O_2}$ is nearly independent within the composition range 10-40 mole percent MnO (Fig. 19). Thus additional experimental evidence in support of the present observations is provided.

All these findings support Brynestad and Flood's assumption that the thermodynamics of the ternary system like FeO-MgO-O_2 is determined more by the entropy changes than the variations effects across the composition range. It also suggests that in the future the knowledge of the thermodynamics of the binary metal-oxygen system may be very valuable guide to such properties as the electrical conductivity and diffusion of cations in quite complicated systems. This is because the redox energies of multivalent cations may not change significantly and the energies of vacancy formation may also be similar in those complex solutions in which the simple non-stoichiometric oxide can enter to a substantial extent.

These conclusions are only considered appropriate when the defect mechanism of a non-stoichiometric solid solution is that involving vacant cation sites and higher valent cations.

FIG.19

HEAT OF SOLUTION OF OXYGEN IN MgO–MnO SOLID SOLUTIONS

$$K = \left\{ \frac{n_{Mn^{3+}}}{n^2_{Mn^{2+}}} \right\} \frac{Mn}{Mg}$$

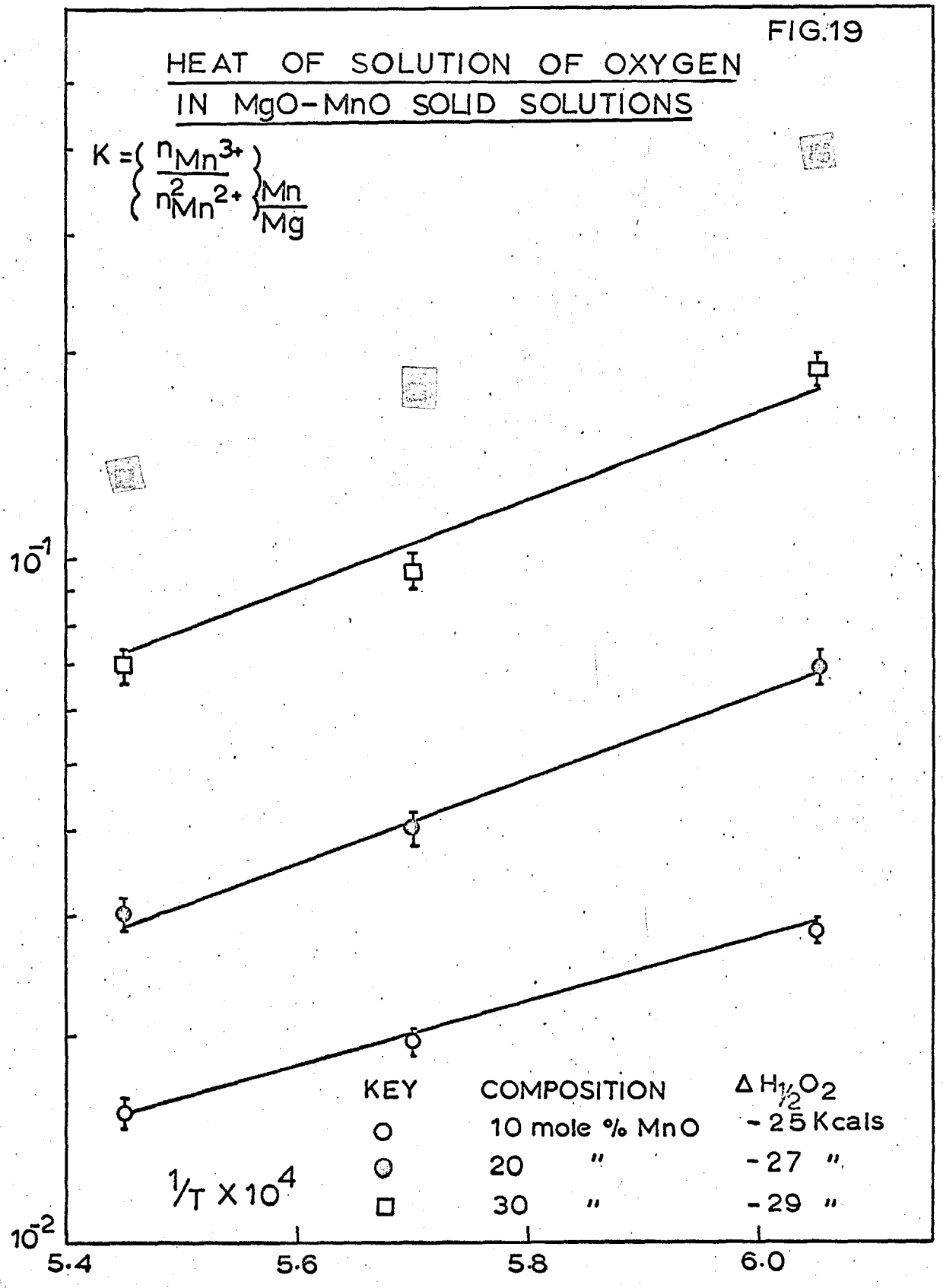

In other systems such as those containing UO_2 (ThO_2-UO_2) where the defect is an interstitial oxygen ion, the thermodynamic properties have been found to vary across a range of solid solutions due to the change in the inter-action energy of the interstitial particle with its environment[57, 58].

3.3.c. Defect Structure of the Solid Solutions

Since the complex model concept explains very satisfactorily the non-stoichiometric behaviour of the solid solutions of MgO-FeO, such defect complexes as $Fe_2^{+++}V_{cation}$ etc. should lead to formation of micro-domains of a higher phase as proposed by Ariya[26] for non-stoichiometric lower valent oxides. The process of oxidation of magnesio-wustites to the non-stoichiometric state leads to the formation of ferric ions which behave as if they are clustered in pairs around a vacant site and Mg^{++} ions as if a 'molecule' of $MgFe_2O_4$ being immersed in the matrix, analogous to Fe_3O_4 in wustite. Further Groves and Fine[49] have shown that ageing the crystals of MgO containing iron causes the precipitation of magnesio-ferrite and there is no evidence for the formation of an intermediate coherent precipitate of non-equilibrium structure such as found in age hardening of metal-alloy systems. This interesting experimental observation supports the present view that the

domains resembling the regions of magnesio-ferrite are already latent in the non-stoichiometric solid solutions and ageing of these crystals involve a slight re-arrangement of the ions in the cationic sub-lattice to form a coherent precipitate. Thus the micro-domain theory originally developed to describe the non-stoichiometry of the oxide phases can be said to account for the non-stoichiometric behaviour of such binary metal-oxygen systems as magnesio-wustites.

3.3.d. The Separation of Magnesio-Magnetite Phase

Finally a purely thermodynamic calculation can be made of the equilibria between magnesio-wustites and magnesio-magnetites. As was mentioned earlier, the results of Schmahl et al., indicated that the $Fe_3O_4/MgFe_2O_4$ ratio is very nearly the same in the spinel phase as is the FeO/MgO ratio in the wustite solid solution with which it is in equilibrium. It is therefore possible to make an approximate calculation of the oxygen pressures at which the magnesio-magnetite phase should separate from any given magnesio-wustite phase using the thermodynamic data for the reaction.

$$3FeO + \tfrac{1}{2}O_2 - Fe_3O_4 \quad K_3 = \frac{a(Fe_3O_4) \text{ magnetite}}{a^3\{FeO\} \text{ wustite } p\tfrac{1}{2}O_2} \qquad (3.11.)$$

where $a(Fe_3O_4) \simeq X(Fe_3O_4)$ in the magnesio-magnetite and

$$X(Fe_3O_4)_{\text{magnesio-magnetite}} = X\{FeO\}_{\text{magnesio-wustite}}$$

$$\text{Hence } K_4 = \frac{X\{FeO\}_{\text{magnesio-wustite}}}{a^3\{FeO\}\ p^{\frac{1}{2}}O_2} \qquad (3.12.)$$

For this reaction, Richardson and Jeffes[53] give the equation

$$\Delta G^\circ = -74,\ 620 + 29.90\ T \text{cal.} \qquad (3.13.)$$

The equation for K_4 involves the mole fraction of wustite and the cube of the activity of wustite in the magnesio-wustite in equilibrium with the magnesio-magnetite phase. If we now assume that γFeO is always so close to unity that any variation of this value may be neglected, say between 0.5 and 2, then

$$K_4 = \frac{1}{X^2\{FeO\}} \quad \frac{1}{p^{\frac{1}{2}}O_2} \qquad (3.14.)$$

at the phase boundary.

The results for the oxygen pressures at which phase separation should occur at 1050°C and 1200°C are shown in Fig. 20 and it can be seen that these values are higher than those at which a large Fe^{+++}/Fe^{++} ratio was obtained in all of the dilute solid solutions studied here. This suggests that a substantial

FIG. 20

PLOT OF THE VARIATION OF CALCULATED OXYGEN PRESSURE FOR THE SEPARATION OF THE MAGNESIO–MAGNETITE FROM THE MAGNESIO–WUSTITES AS A FUNCTION OF IRON CONTENT

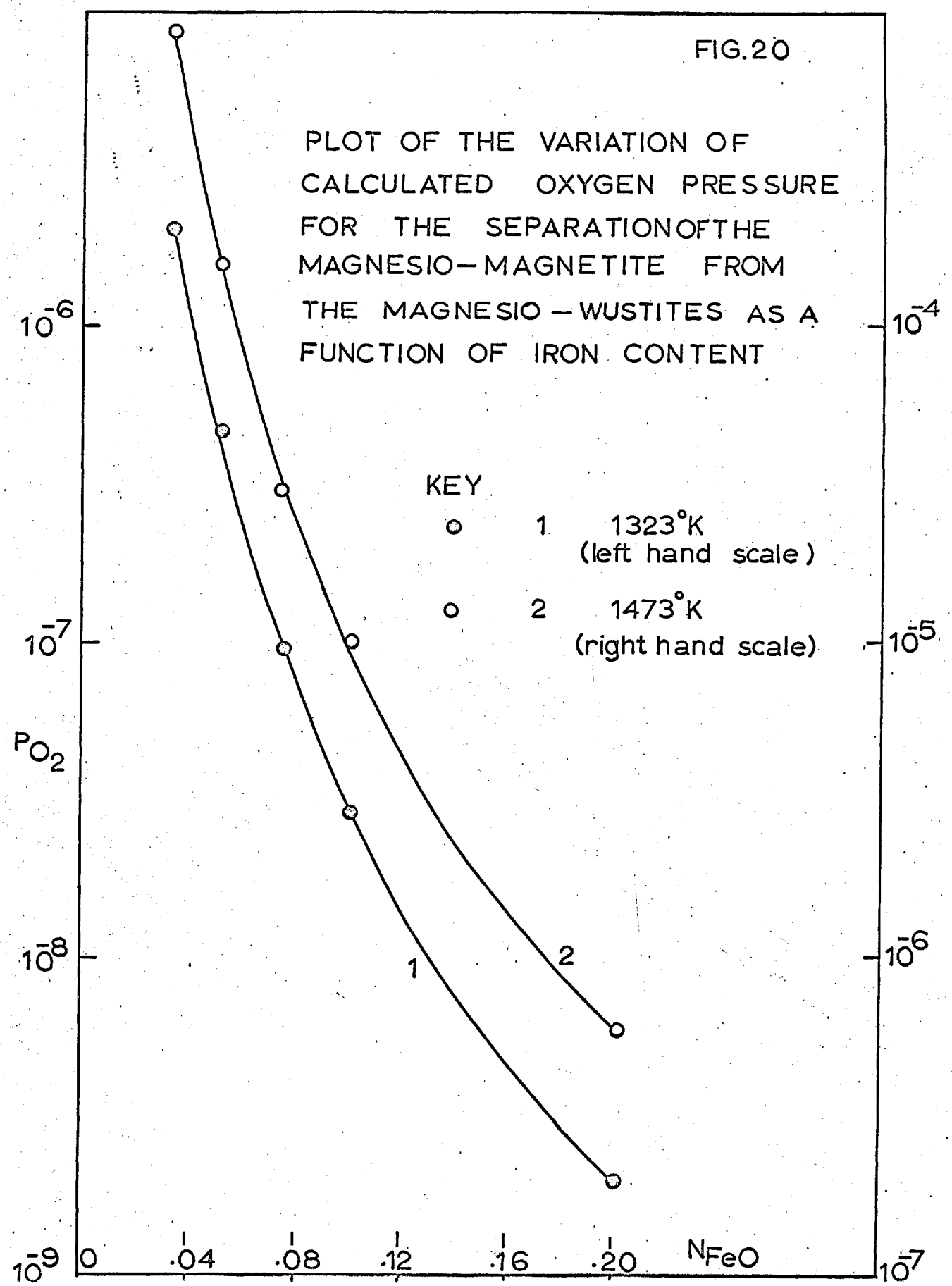

solid solution range exists between magnesio-wustites and magnesio-magnetites in this dilute solution range.

CHAPTER FOUR

4. Results and Discussion (part-two).

4.1 General.

The electrical conductivity data have been obtained for the solid solutions (MgO - FeO) as a function of composition, temperature and oxygen partial pressure. These results together with the data obtained from the equilibration studies (i.e. variation of ferric ion concentration as a function of composition, temperature and oxygen partial pressure) have been analysed in the light of the semi-conduction theory[1,3-6,17] proposed for oxides of the transition metals of iron-group. The results cutler etal[46] have also been included wherever necessary.

4.2 Presentation of the Results

Tables[4.1,4.2,4.3] summarize the typical conductivity results together with the extent of reproducibility during the oxidation-reductions cycles. Measurements were made of the conductivity of the solid solution containing 1 20 mole per cent FeO. A few conductivity measurements were made as a function of frequency and established that the conductivity is almost independent of frequency (Fig. 21). All measurements were initially made using H_2 - CO_2 gas mixtures and certain of the runs were duplicated in CO - CO_2 atmosphere. It was found that the atmosphere had no significant influence on the conductivity results ($\pm$ 10%). Thus suggesting that the conductivity due to mobile protons

TABLE 41

CONDUCTIVITY RESULTS

Temperature 1273°K

Composition Mole % FeO	σ ohm^{-1} cm^{-1} at stated oxygen pressures. 10^{-16}	10^{-15}	10^{-14}	10^{-13}	10^{-12}	10^{-11}	$10^{-1.0}$	Reproducibility ± %
1.0	3.5×10^{-7}	3.6×10^{-7}	2.8×10^{-7}	3.6×10^{-7}	3.8×10^{-7}	3.8×10^{-7}		± 5
1.75		2.4×10^{-6}	2.8×10^{-6}	3.6×10^{-6}	4.2×10^{-6}	5.8×10^{-6}		± 5
2.5			2.4×10^{-5}	2.9×10^{-5}	3.1×10^{-5}	3.4×10^{-5}		± 5
2.75		1.28×10^{-5}	1.7×10^{-5}	2.1×10^{-5}	3×10^{-5}	4×10^{-5}		± 5
3.2	8×10^{-7}		9×10^{-7}		9.7×10^{-7}		10^{6}	± 5
5.0	3.1×10^{-5}		4.8×10^{-5}		7.1×10^{-5}		1.6×10^{-4}	± 5

TABLE 4.2

CONDUCTIVITY RESULTS — Temperature 1173°k

Composition	σ — ohm^{-1} cm^{-1} or stated oxygen partial pressures							Reproducibility
Mole % FeO	10^{-18}	10^{-17}	10^{-16}	10^{-15}	10^{-14}	10^{-13}	10^{-12}	± %
2.5	1.6×10^{-5}	2.15×10^{-5}	2.2×10^{-5}	2.4×10^{-5}	3×10^{-5}	3.3×10^{-5}		± 5
3.2	5.5×10^{-7}		5.7×10^{-7}		5.8×10^{-7}		7.0×10^{-7}	± 5
5.0	1.30×10^{-5}		3×10^{-5}		7.18×10^{-5}		1.2×10^{-4}	± 5
7.50	4×10^{-5}		1.1×10^{-4}		5.1×10^{-4}		1.62×10^{-3}	± 10
10.00	1.1×10^{-3}	1.8×10^{-3}	3.9×10^{-3}	6.1×10^{-3}	8.7×10^{-3}	1.11×10^{-2}		± 10
20.00	1.3×10^{-2}	2.16×10^{-2}	3.37×10^{-2}	5×10^{-2}	7.64×10^{-2}	9.6×10^{-2}		± 10

TABLE 4.3

CONDUCTIVITY RESULTS

Temperature 1073°k

Composition	σ — Ω^{-1} cm^{-1} at stated oxygen partial pressures								Reproducibi
Mole % FeO	10^{-20}	721×10^{-20}	10^{-19}	10^{-18}	10^{-17}	10^{-16}	10^{-15}	10^{-14}	± %
2.5		1.01×10^{-5}		1.2×10^{-5}	1.3×10^{-5}	1.4×10^{-5}		1.6×10^{-5}	± 5
3.2	3×10^{-7}		3.1×10^{-7}	3.5×10^{-7}		4×10^{-7}		5×10^{-7}	± 5
5.0	1.8×10^{-5}					6.85×10^{-5}		9.5×10^{-5}	± 5
7.50	4.20×10^{-5}			9.25×10^{-4}		2.49×10^{-4}		8.75×10^{-4}	±10
10		1.6×10^{-3}		2×10^{-3}	3×10^{-3}	5×10^{-3}	48×10^{-3}	5×10^{-3}	±10
20		1.2×10^{-2}		2×10^{-2}	4×10^{-2}	5×10^{-2}		5×10^{-2}	±10

FIG.21

CONDUCTIVITY AS A FUNCTION OF FREQUENCY

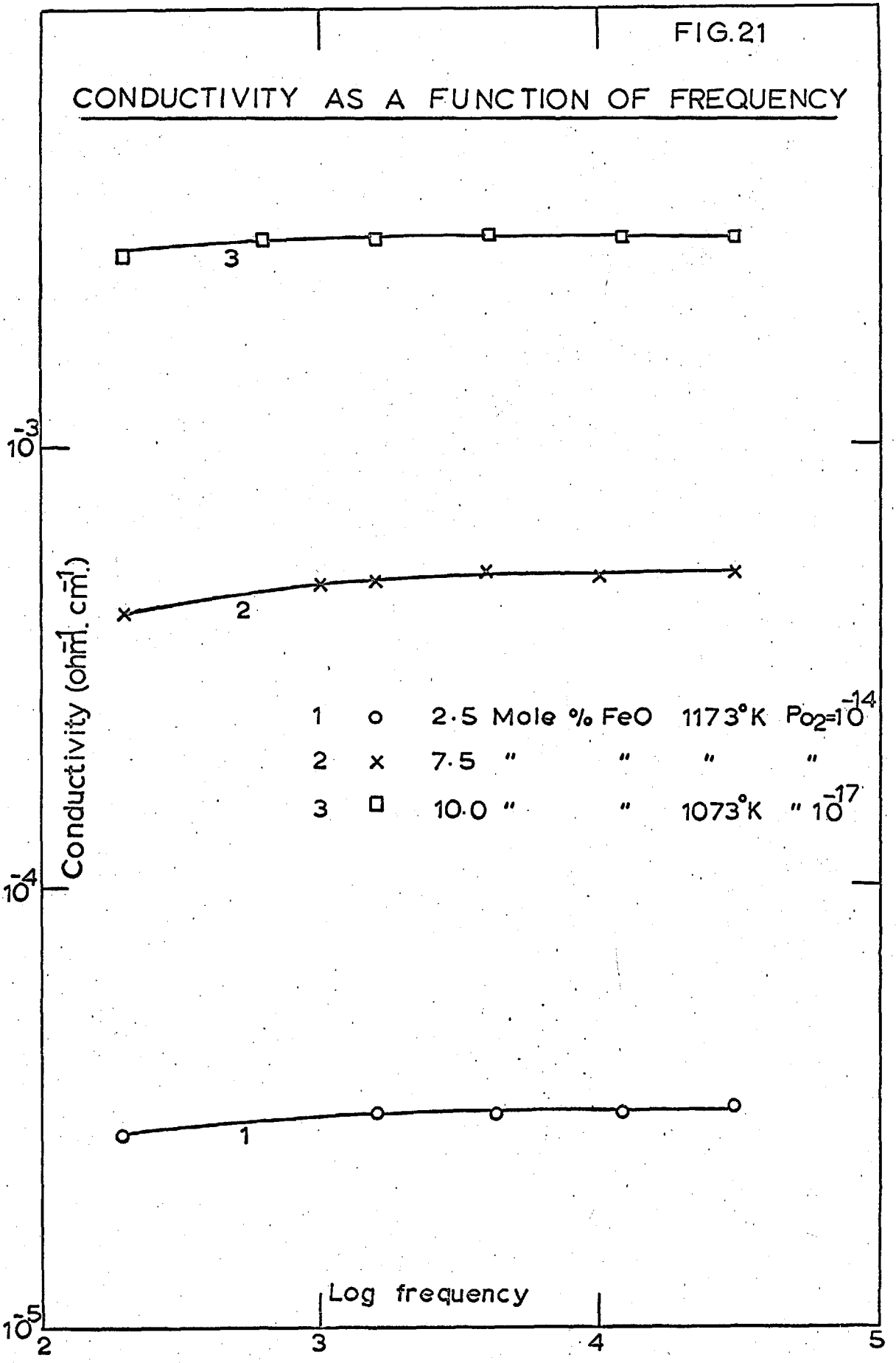

arising from the following defect reaction is negligible.

$$2H_2O^{g} = 2H^{+}_{(mobile)} + 2OH^{-} + V_{cation} \qquad (41)$$

Further consideration of the conductivity measurements required information about the relative amounts of electronic and ionic conductivity. It is difficult to determine precisely these relative amounts as the required data for such calculations are missing. Ionic conductivity arises due largely to the cation transport[33,37]. Oxygen ion conductivity is assumed to be negligible because both the end members and the solid solutions possess a relatively rigid face-centred cubic oxygen lattice.

Mitoff[33,35] has shown (see Chapter 1, Sec. 1-2d) that the impurities decrease the ionic transference number and favour electronic conduction. Therefore one could expect a maximum ionic contribution in those solid solutions containing very small ammounts of iron. Since no data are available on the cation diffusion in these solid solutions, use has been made of Lindner's data[37] for Mg^{++} ion diffusion* and Wuensch and Vasilos[59] for Fe^{++} ion diffusion** in the magnesium oxide to calculate the ionic conductivity. The calculated ionic conductivity using Nernst - Einstein relation lies in the range $1.5 - 2.5 \times 10^{-8}$ ohm^{-1} cm^{-1} at temperatures around $1000^{o}c$ indicating that the ionic transport numbers in the dilute solid solutions do not exceed the value 5×10^{-2}. These calculations though approximate give a

arising from the following defect reaction is negligible.

$$2H_2O^{g} = 2H^{+}_{(mobile)} + 2OH^{-} + V \qquad (41)$$

Further consideration of the conductivity measurements required information about the relative amounts of electronic and ionic conductivity. It is difficult to determine precisely these relative amounts as the required data for such calculations are missing. Ionic conductivity arises due largely to the cation transport[33,37]. Oxygen ion conductivity is assumed to be negligible because both the end members and the solid solutions possess a relatively rigid face-centred cubic oxygen lattice.

Mitoff[33,35] has shown (see Chapter 1, Sec. 1-2d) that the impurities decrease the ionic transference number and favour electronic conduction. Therefore one could expect a maximum ionic contribution in those solid solutions containing very small ammounts of iron. Since no data are available on the cation diffusion in these solid solutions, use has been made of Lindner's data[37] for Mg^{++} ion diffusion* and Wuensch and Vasilos[59] for Fe^{++} ion diffusion** in the magnesium oxide to calculate the ionic conductivity. The calculated ionic conductivity using Nernst - Einstein relation lies in the range $1.5 - 2.5 \times 10^{-8}$ ohm^{-1} cm^{-1} at temperatures around $1000^{o}c$ indicating that the ionic transport numbers in the dilute solid solutions do not exceed the value 5×10^{-2}. These calculations though approximate give a

strong indication that the conductivity in these solid solutions is mostly electronic.

$$\left[* \quad D^{MgO}_{Mg^{++}} = (0.249) \exp \frac{-3.37}{kT} \text{ ev} \quad \text{Ref. 37} \right.$$

$$\left. ** \quad D^{MgO}_{Fe^{++}} = 8.85 \times 10^{-5} \exp \frac{-1.81}{kT} \text{ ev} \quad \text{Ref. 59} \right]$$

4.3 Discussion

4.3 (a) Dependence of Conductivity on the Oxygen Partial Pressure.

Figures 21 to 25 describe the variation of the electrical conductivity with the oxygen partial pressure for the solid solutions containing up to 20 mole per cent FeO. The slopes of the isotherms are summarized in the table 4.4.

From the table 4.4 and the isothermal plots, it can be inferred that most of the solid solutions exhibit a p-type semiconducting behaviour. The magnitude of the power dependence of conductivity with the oxygen partial pressure depends upon the total iron content and the temperature. A variety of power dependence ranging from 1/10 - 1/3 has been observed. The solid solutions containing less than 5 mole per cent FeO show a power dependence of 1/8 - 1/10 which is very much smaller than expected for the compound semiconductors deviating from stoichiometry when the intrinsic electronic disorder is small. The above results suggest that the various defect equilibria envisaged so far to account for the p - type electronic conductivity in oxides are not applicable for the dilute magnesio. wustites containing

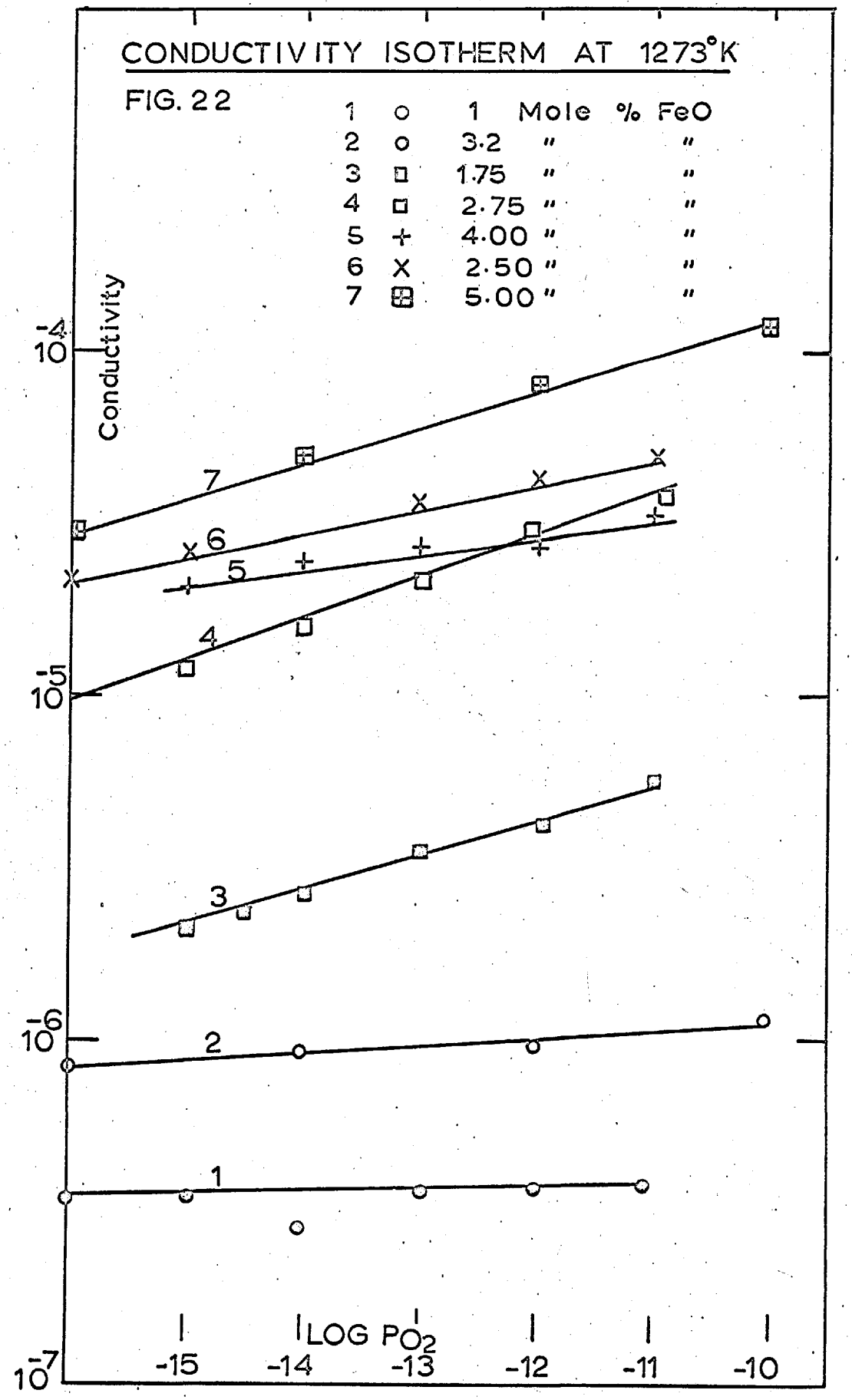
CONDUCTIVITY ISOTHERM AT 1273°K
FIG. 22
1 o 1 Mole % FeO
2 o 3.2 " "
3 □ 1.75 " "
4 □ 2.75 " "
5 + 4.00 " "
6 X 2.50 " "
7 ⊞ 5.00 " "
Conductivity
10^-4
10^-5
10^-6
10^-7
LOG PO2
-15
-14
-13
-12
-11
-10

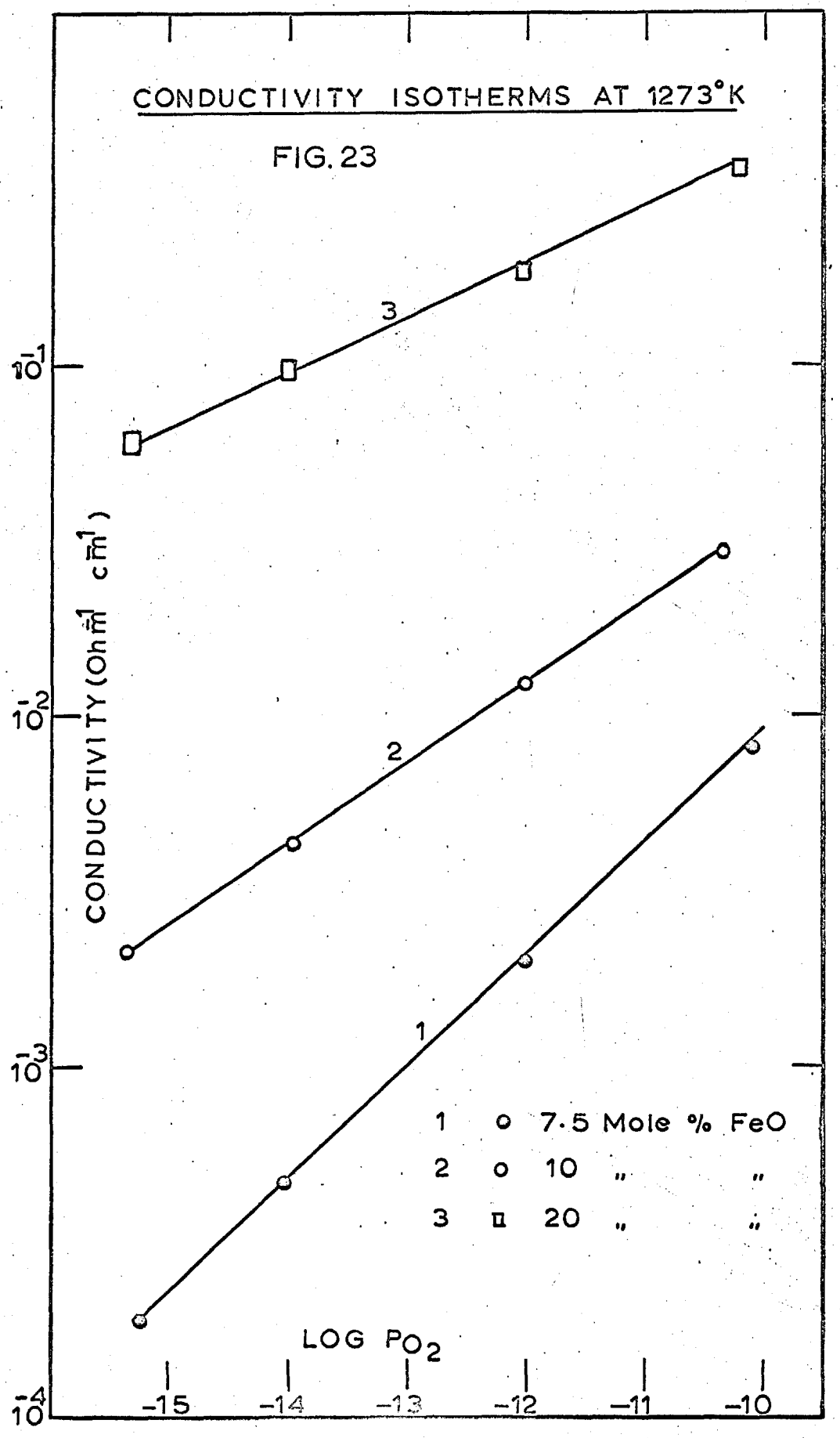
CONDUCTIVITY ISOTHERMS AT 1273°K
FIG. 23
CONDUCTIVITY (Ohm⁻¹ cm⁻¹)
10⁻¹
10⁻²
10⁻³
10⁻⁴
3
2
1
1 o 7.5 Mole % FeO
2 o 10 " "
3 □ 20 " "
LOG P_{O_2}
-15
-14
-13
-12
-11
-10

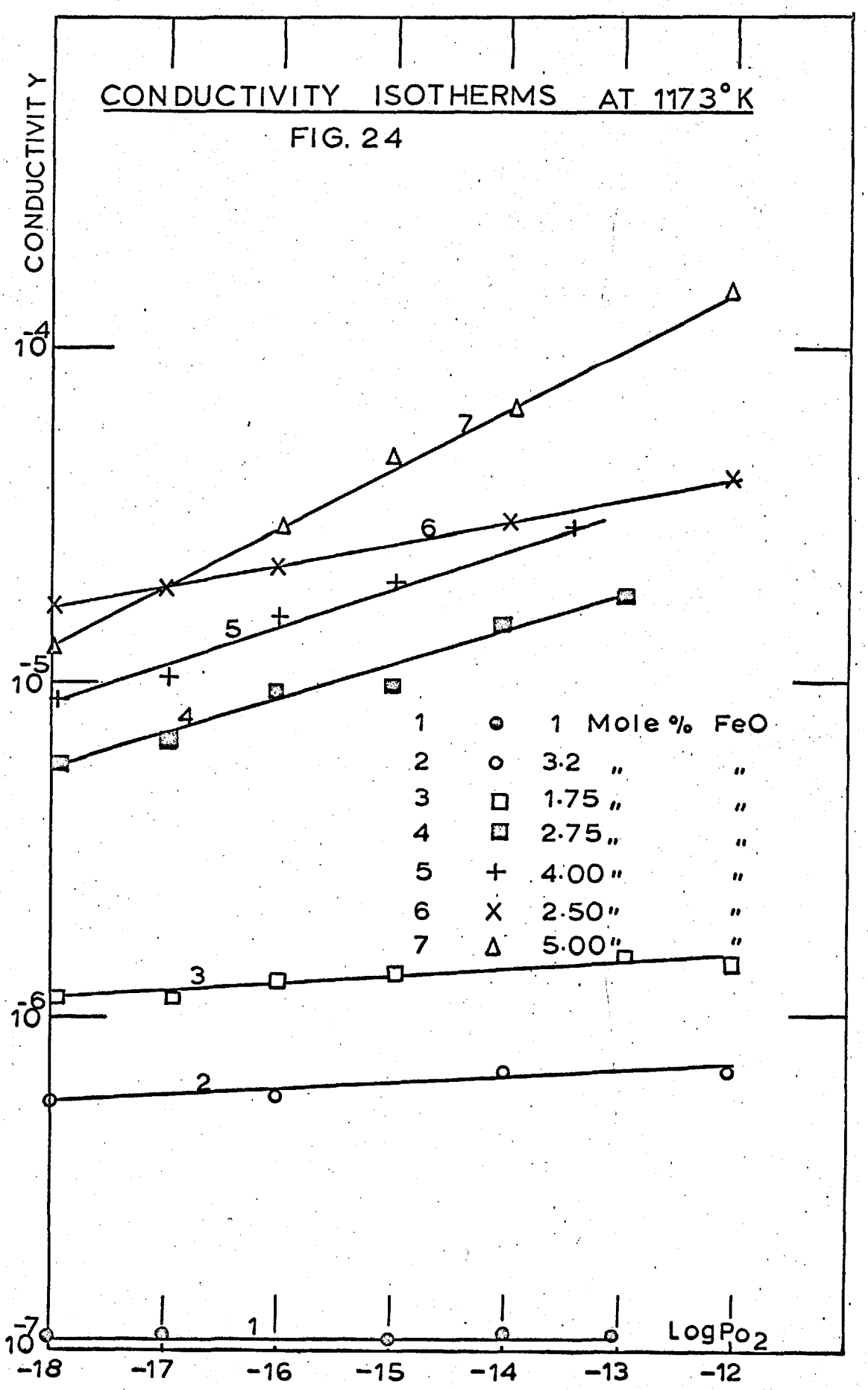
CONDUCTIVITY ISOTHERMS AT 1173°K
FIG. 24
CONDUCTIVITY
10-4
10-5
10-6
10-7
1 Mole % FeO
3·2 " "
1·75 " "
2·75 " "
4·00 " "
2·50 " "
5·00 " "
Log Po2
-18
-17
-16
-15
-14
-13
-12

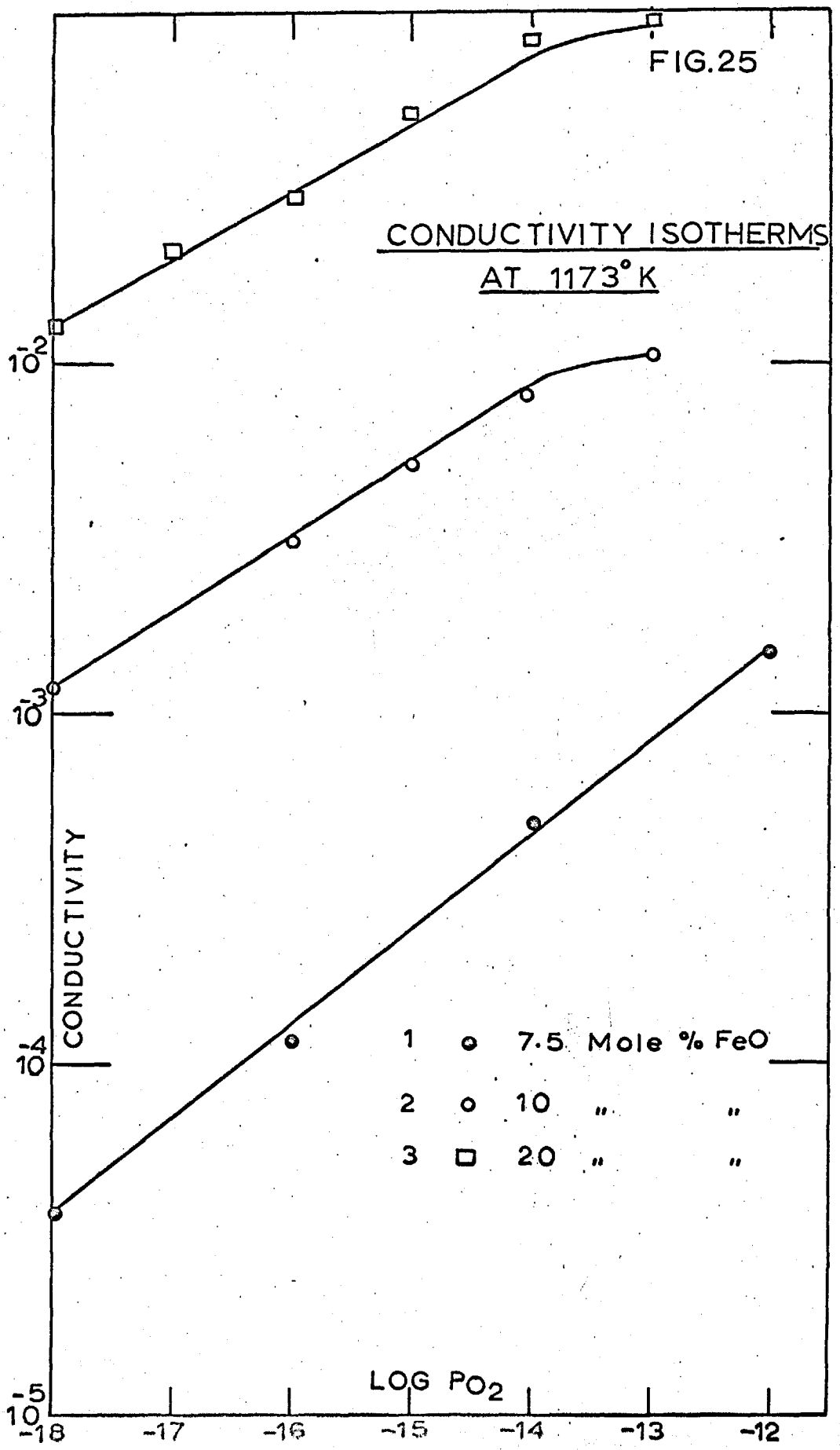
FIG.25
CONDUCTIVITY ISOTHERMS
AT 1173° K
10^{-2}
10^{-3}
10^{-4}
10^{-5}
CONDUCTIVITY
1 o 7.5 Mole % FeO
2 o 10 " "
3 □ 20 " "
LOG P_{O_2}
-18
-17
-16
-15
-14
-13
-12

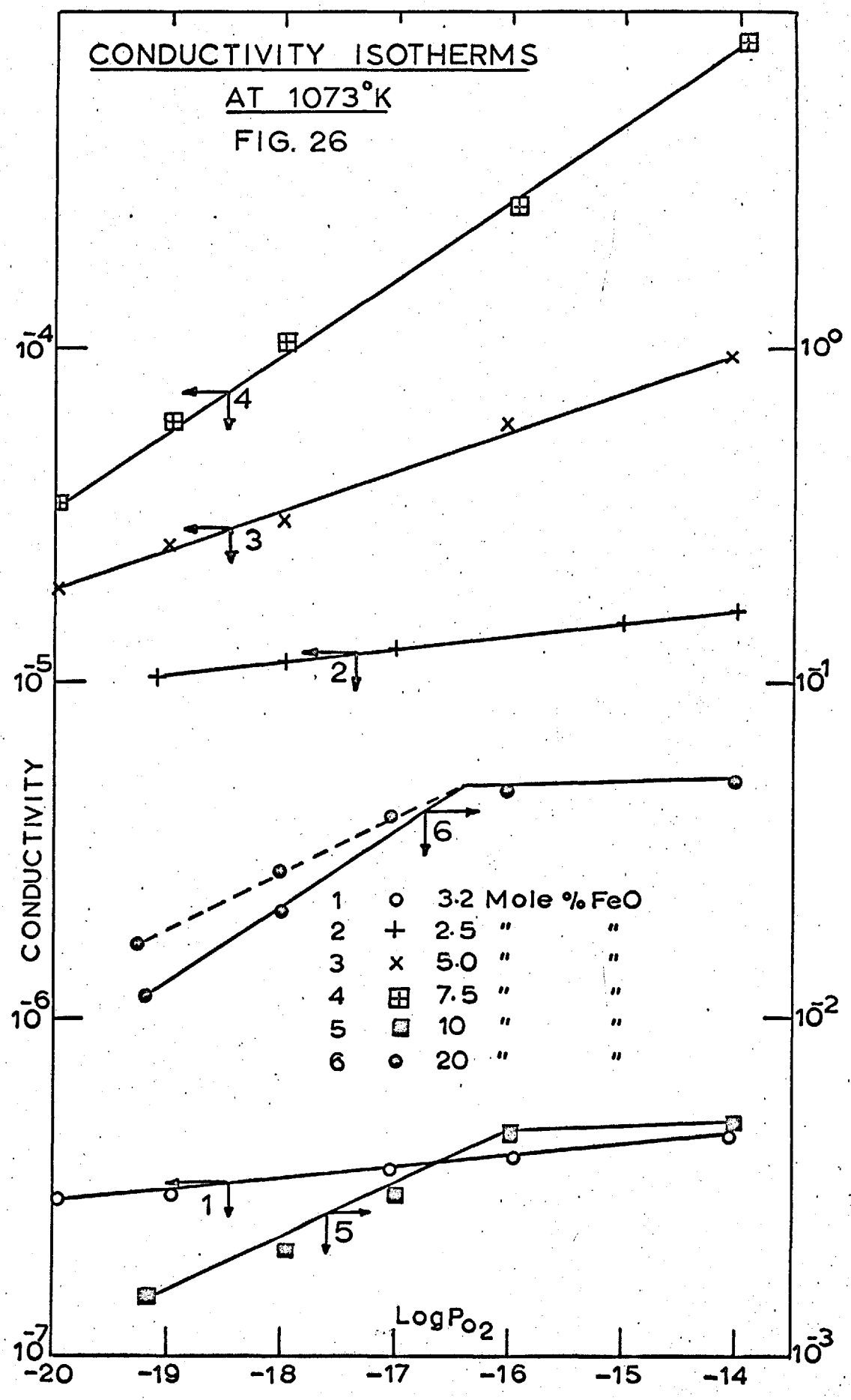
CONDUCTIVITY ISOTHERMS
AT 1073°K
FIG. 26
CONDUCTIVITY
10^{-4}
10^{-5}
10^{-6}
10^{-7}
10^{0}
10^{-1}
10^{-2}
10^{-3}
1 o 3.2 Mole % FeO
2 + 2.5 " "
3 x 5.0 " "
4 ⊞ 7.5 " "
5 ▣ 10 " "
6 o 20 " "
Log P_{O_2}
-20
-19
-18
-17
-16
-15
-14

TABLE 4.4

Summary of the Power Dependence of Conductivity with the Oxygen Partial Pressure (See Fig. 21 to 25).

Temp. ^{o}k	Power dependence at the following compositions (Mole per cent FeO)									
	20	10	75	5	4	3.2	2.75	2.5	1.75	1.0
1273	1/6	1/7	1/4.5	1/3.5	1/10	1/10	I	1/9	1/10	1/10	I
1173	"	1/7	1/3.75	1/7	1/9	1/10	1/10	1/10	I	I
1073	1/6	1/6	1/3.75	1/8	N.D.	1/10	N.D.	1/10	N.D.	N.D.

NOTE I - conducting independent of p_{o_2}

N.D. - not determined.

small amounts of iron. On the other hand the solid solutions containing 7.5, 10 and 20 mole per cent FeO exhibit a power dependence nearly equal to one sixth or a quarter, indicating that the electrical properties of these solid solutions are comparable to that of the pure wustite phase (see Chapter 1 Sec. 1-26). Hence the defect reactions involving the creation of extrinsic positive holes in the solid solutions containing 7.5 mole per cent and above appear to be similar to that of the pure wustite.

4.3 (b) Dependence of Conductivity on the Total Iron Content.

Fig. 27 depicts the variation of electrical conductivity of the solid solutions with the total iron content at constant temperature and oxygen activity. As expected, the conductivity of the solid solutions is much higher than the pure magnesia regardless of the iron content. This is because the magnesium oxide is almost an insulator compared to wustite and addition of FeO to magnesia should therefore increase the electrical con - ductivity of the host lattice. From the Fig. 27 it can be seen that the effect of addition of wustite on the electrical conductivity is not uniform, particularly in the regions of low iron content. The solid solutions containing more than 4.0 mole per cent FeO exhibit a consistant behaviour in that the conductivity increases with increasing iron content though the rate of conductivity change decreases. This change in the rate

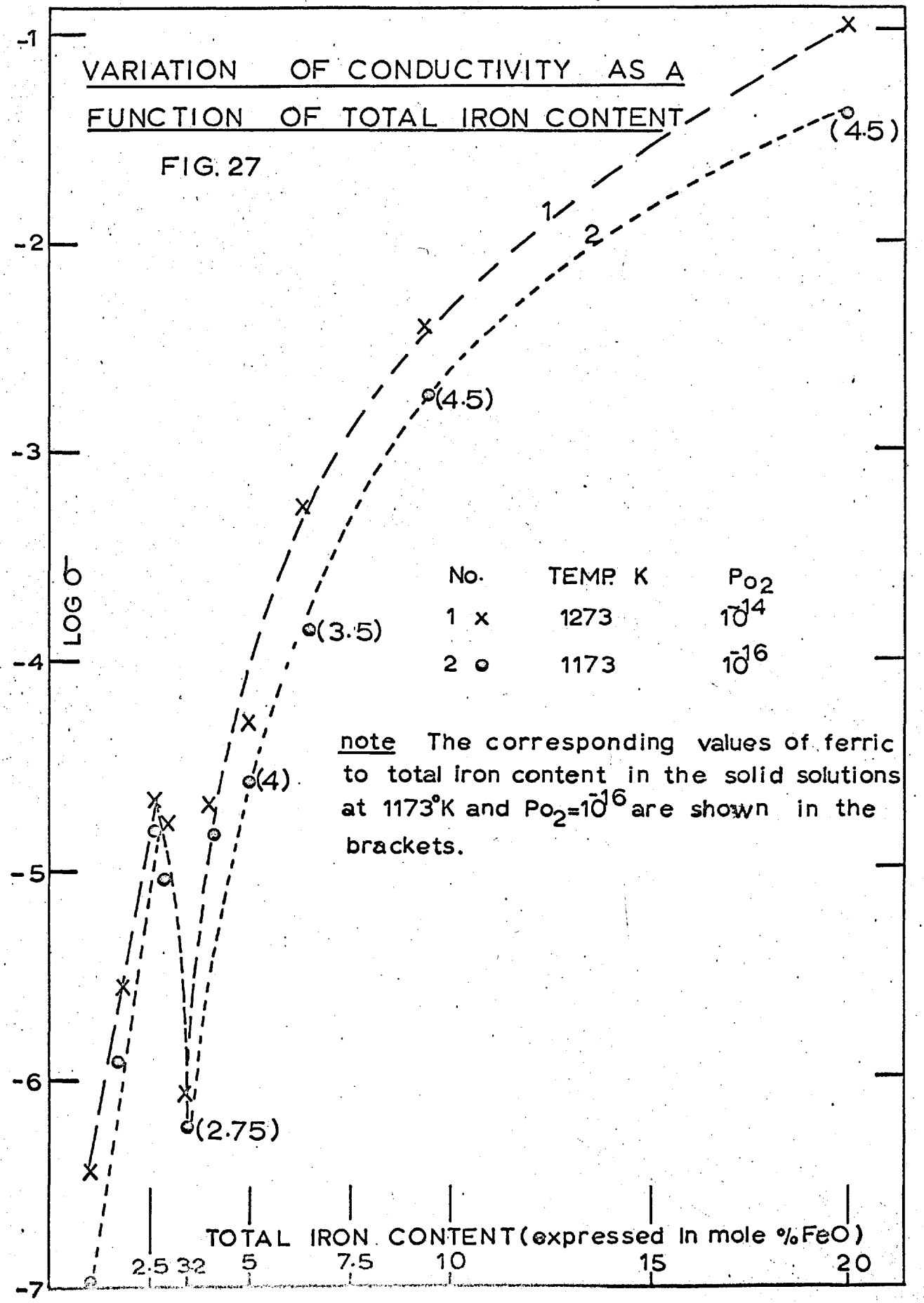
VARIATION OF CONDUCTIVITY AS A FUNCTION OF TOTAL IRON CONTENT
FIG. 27
LOG σ
-1
-2
-3
-4
-5
-6
-7
1
2
(4.5)
(4.5)
(3.5)
(4)
(2.75)
No. TEMP. K P_{O_2}
1 x 1273 10^{-14}
2 o 1173 10^{-16}
note The corresponding values of ferric to total iron content in the solid solutions at 1173°K and $P_{O_2}=10^{-16}$ are shown in the brackets.
TOTAL IRON CONTENT (expressed in mole % FeO)
2.5 3 2 5 7.5 10 15 20

of conductivity increase might be attributed to the attendant changes in the ferric to ferrous ratio in the solid solutions. But it is difficult to support this viewpoint with the present set of data.

However a totally different behaviour is exhibited by the solid solutions containing less than 4 mole per cent FeO. In this composition range addition of FeO has two distinct effects on the conductivity (Fig. 27).

(1) Initially, the conductivity increases on adding small amounts of FeO and this effect continues until the iron oxide content reaches 2.5 mole per cent. The rate of increase in this composition range is such that the conductivity of the solid solution, 2.5 mole per cent FeO, is about 3 - 4 orders of magnitude higher than that of the pure magnesia.

(2) Further increase of iron oxide content actually decreases the conductivity at the same rate, until the solid solution contains 3.2 mole per cent FeO. Beyond this composition conductivity begins to increase. Such a behaviour exhibited by the dilute solutions clearly indicate that the conduction mechanism in these solutions is very much different from those containing high - iron contents. Further it should be recalled that the magnitude of power dependence of conductivity on the oxygen partial pressure is very small for dilute solid solutions whereas solutions containing high iron contents exhibit a large

power dependence. Moreover the same trend is maintained at other temperatures of measurement.

It is interesting to note that Rao and Smakula[60] have observed a non - linear dependence of conductivity with composition in NiO - CoO system and the solid solution containing equimolar proportions of NiO and CoO possess a maximum conductivity. These authors have also observed a marked influence of composition on the conductivity in the dilute solution range. They believe such effects as mentioned above are due probably to the lattice distortion and an increase in the trivalent cation concentration. To what extent these effects would influence the conduction behaviour of the dilute magnesio. wustites, it is not known. Work of Hauffe etal[61] on the electrical conductivity of ZnO as a function of impurity content provides an additional example for an anomalous conduction behaviour of dilute metal - oxide solid solutions. Since the zinc oxide is a metal excess n - type semiconductor containing excess zinc ions in interstitial positions[62,63], substitution of aluminium or chromium ions on zinc sites should increase the conductivity, whereas the addition of Li_2O should decrease. Hauffe etal[61] have found that the conductivity of ZnO. increases with increasing alumina or chromia content up to one mole per cent (of Al_2O_3 or Cr_2O_3) and further increase of Al^{+++} or Cr^{+++} ion concentration up to 4 mole of the oxide has no effect on the conductivity. Beyond

this impurity content conductivity begins to decrease. Similarly incorporation of Li^+ ions on zinc sites decrease the conductivity as expected, but beyond 1 mole per cent of Li_2O conductivity begins to increase. To date, no attempts have been made to explain these anomalous electrical properties observed in dilute oxide solid solutions.

4.3 (c) Calculation of the Conduction Activation Enthalpies.

Calculations have been made of the conduction activation enthalpies for the motion of the hole for the solid solution containing 7.5, 10 and 20 mole per cent using the relation similar to that derived by Mitoff[64] for the conductivity of transition metal oxides due to the migration of the holes via hopping process. When modified slightly for generality, Mitoff's equation can be written in the form

$$\sigma = c' \, p_{O_2}^{1/m} \exp \frac{-\left(\frac{\Delta H_f}{m/2} + \Delta H_{m\oplus}\right)}{RT} \qquad (4.2)$$

where c ' is a constant comprising the lattice constant, jump frequency of the hole, and exponential entropy terms, m is a number $(4 \leq m \leq 6)$, and is taken as an integral value indicative of the degree of ionization of the atomic imperfections. H_f is the activation enthalpy of formation of the holes, and $\Delta H_{m\oplus}$ is the activation enthalpy for motion of the holes. Since ΔH_f is almost equal to the partial heat of solution of oxygen, the

slope of the plot of $\log \sigma / p_{O_2}^{1/m}$ as a function of $1/T\ ^{o}k$ enables one to calculate the activation enthalpy for motion of the holes. One could also calculate the conduction activation enthalpies at a constant carrier concentration using equation (1-30). However due to the lack of data on the variation of the defect concentration with the oxygen partial pressures at temperatures 1073 and 1273 ^{o}k, equation (4.2) was in fact used to calculate the activation enthalpy for motion. The results of such calculations are included in the Fig. 28. The error involved in the calculation can be as high as $\pm$ 20% due largely to the non - intergral values of m and inaccuracy associated with the calculation of the heat of solution of oxygen. The solid solution containing 7.5 mole per cent iron has a much higher activation enthalpy for motion (0.7 ev) than those containing 10 and 20 mole per cent (0.44 to 0.38 ev). The activation enthalpy for motion then obtained lies in the range 0.7 to 0.4 ev (16 to 9.2 K.cals) for solid solutions containing 7.5 to 20 mole per cent FeO and these values are not in accord with those reported by Cutler etal[46]. The activation energy for motion obtained by these authors lies in the range 0.1 to 0.18 ev (2.3 to 4.2 K. cals) for solid solutions containing Fe - Fe neighbours in the next nearest positions and 0.4 to .5 ev for those containing Fe - Mg neighbours on the nearest positions. It could be recalled that the activation enthalpy for motion

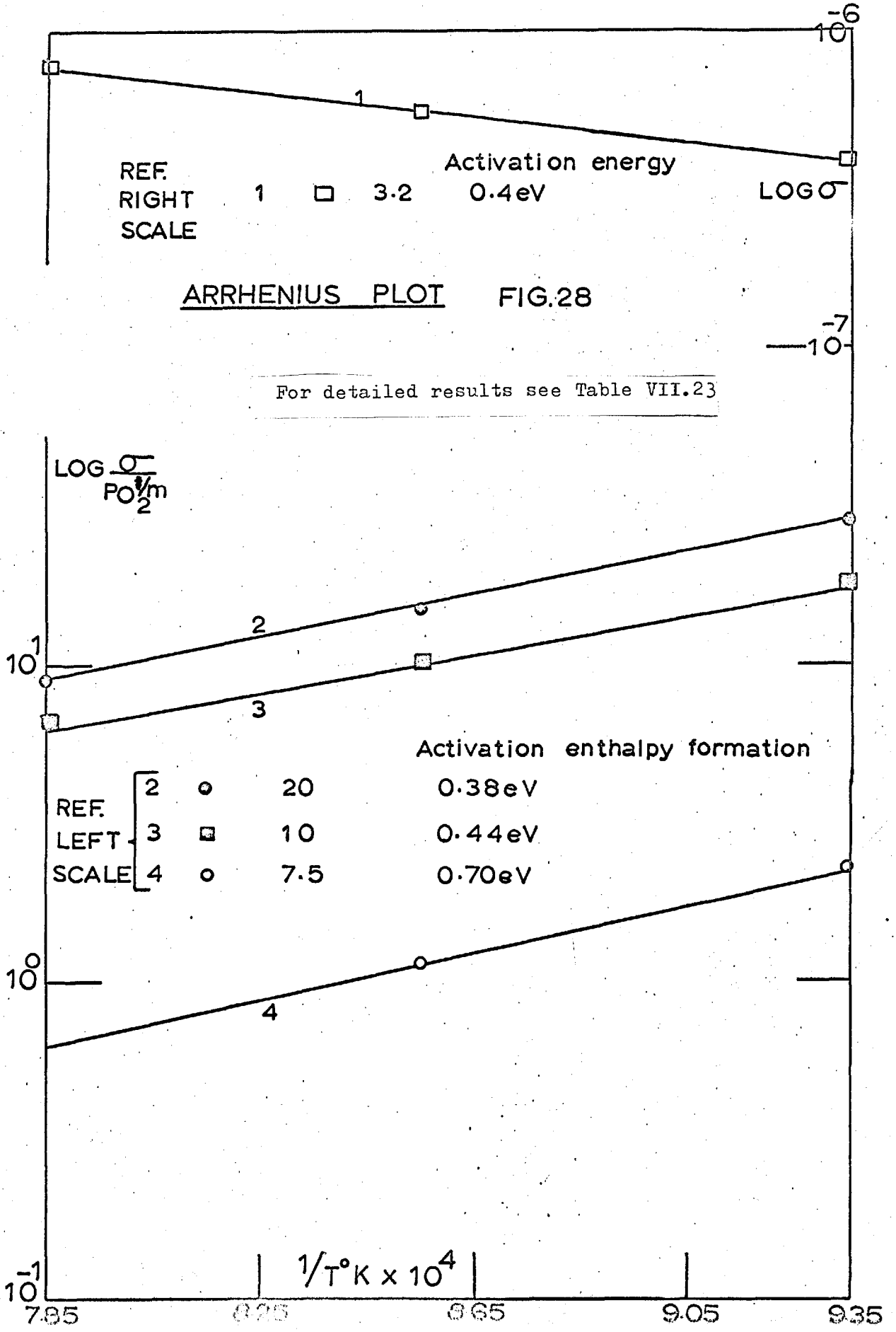

ARRHENIUS PLOT FIG.28

For detailed results see Table VII.23

in pure wustite is very small and has a value of about 0.06 ev (1.5 K.cal). It is difficult to offer any satisfactory explanation for these activation energy data.

Since the solid solutions containing less than 5 mole per cent FeO exhibited a very small dependence of conductivity with the oxygen partial pressure. It does not seem appropriate to use the equation (4.2) for calculation of the activation energy. However, attempts have been made to calculate conduction activation energy using the conventional exponential relation

$$\sigma = \sigma_0 \exp\left(-\frac{\Delta E}{RT}\right) \qquad (4.3)$$

Fig. 28 contains the Arrhenius plot of conductivity as a function of temperature for the solid solution containing 3.2 mole per cent FeO. The conduction activation energy has been found to be 0.4 ev and appears to be in good agreement with Cutler's work.

4.3 (d) Conduction Mechanism in MgO - FeO Solid Solutions.

The present work and the results of Cutler clearly suggest that the conduction mechanism in the solid solutions containing more than 5 mole per cent FeO is different from those containing lesser amounts of iron. The solid solutions containing 7.5, 10 and 20 mole per cent FeO exhibit a large variation in the conductivity with the oxygen partial pressure and a systematic increase in the conductivity with increasing iron content. It appears that the conductivity data obtained in the present work for solid Solutions containing more than 5 mole per cent FeO

may be interpreted in terms of the equation (4.2), thus indicating that the thermally activated hole transfer from Fe^{+++} ion to Fe^{++} ion contributes to conductivity. It will be recalled that the activation enthalpy for such a motion appears to decrease (0.7 to 0.4 ev) as the FeO content is increased (7.5 to 20 mole per cent) but appears to be independent of ferric ion concentration. Additional information on the solid solutions containing higher amounts of iron is provided by the work of Cutler etal[46]. These authors have observed in the solid solutions containing up to 43 mole per cent FeO, the conduction activation energy is relatively independent of the ferric ion concentration, whereas above 54.1 mole per cent FeO it decreased with increasing ferric ion cencentration. All these observations may be interpreted in terms of the changes in polarization energy of the iron ions caused by the surrounding ions in the next nearest positions. The magnitude of the polarization energy at any particular iron ion site may depend upon the number of iron cations in the nearest positions as well as the larger and more polarizable anions. Any Fe^{++} ion that has already trapped a hole and polarized the co-ordinating oxygen ions may well influence the energy necessary for a neighbouring ferrous ion to trap a hole. If so, the conduction activation enthalpy should remain nearly independent of ferric ion concentration in the regions of high magnesium oxide contents, because the number of iron cations in the next

nearest position would be small (compared to the number Mg^{++} neighbours) to cause any significant change in the polarization energy of the nearest iron ions. In the regions of high FeO contents, the number of iron ions in the nearest positions would be more than that of Mg^{++} ions, the polarization energy of the iron ions would then be very much influenced by the surrounding ions, such attendant changes in the polarization energy, due largely to the greater number of iron ions in the next nearest positions should be accompanied by the decrease in the activation enthalpy for motion with increasing ferric ion concentration. At present, a rigorous test of the above model is not feasible due to the lack of data. According to the above model the activation enthalpy for motion in the pure wustite should exhibit a large dependence with the ferric ion concentration. However no such effects have so far been reported. In fact the activation enthalpy for motion in pure wustite (0.05. 0.067 ev) is nearly independent of the defect concentration. This contrasting behaviour may be reconciled by the fact that in pure wustite the intrinsic electronic dis-order is so high that the changes in the polarization energy caused by dissolution of stoichiometric excess of oxygen is not significant enough to influence the conduction activation enthalpy for motion.

Considering the behaviour of the other oxide solid solutions, it may be noted that Heikes and Johnston[4] have obtained a decrease

in the activation enthalpy for motion as the Li^+ content in the solid solution $Li_x Ni_{1-x}O$ is increased. These authors attribute the decrease in the activation enthalpy for motion to the chabges in the elastic properties of the crystal, but offer no theoretical analysis.

Further, the dependence of conductivity on ferric ion concentration is analysed in the light of the model proposed by Tannhauser[17] for wustite (see Chapter 1, Sec. 1-2c). When the ferric ion concentration is small, the plot of log against $\log {}^{n}Fe^{++} \cdot {}^{n}Fe^{+++} / O_2^{=}$ is linear (Fig 29), but the slope is different from that of unity. If the mechanism of electron-exchange between di and trivalent iron ions in the magnesio. wustites (containing at least one Fe-Fe pair in the nearest positions) is similar to that occuring in pure wustite phase, the conductivity should then show a linear dependence with the product of di and tri valent iron cations situated in the neighbourhood of the octahedral sites (cf equation 1.31a). The conductivity data obtained in the present work found to exhibit a non-linear variation with ${}^{n}Fe^{++} \cdot {}^{n}Fe^{+++}/O_2^{=}$ (Fig.29) and such a behaviour may be due to the following reasons:

1) We have assumed that all ferric ions in the solid solutions are situated in the octahedral sites which may not be true.

2) In the solid solutions the number of acceptor sites

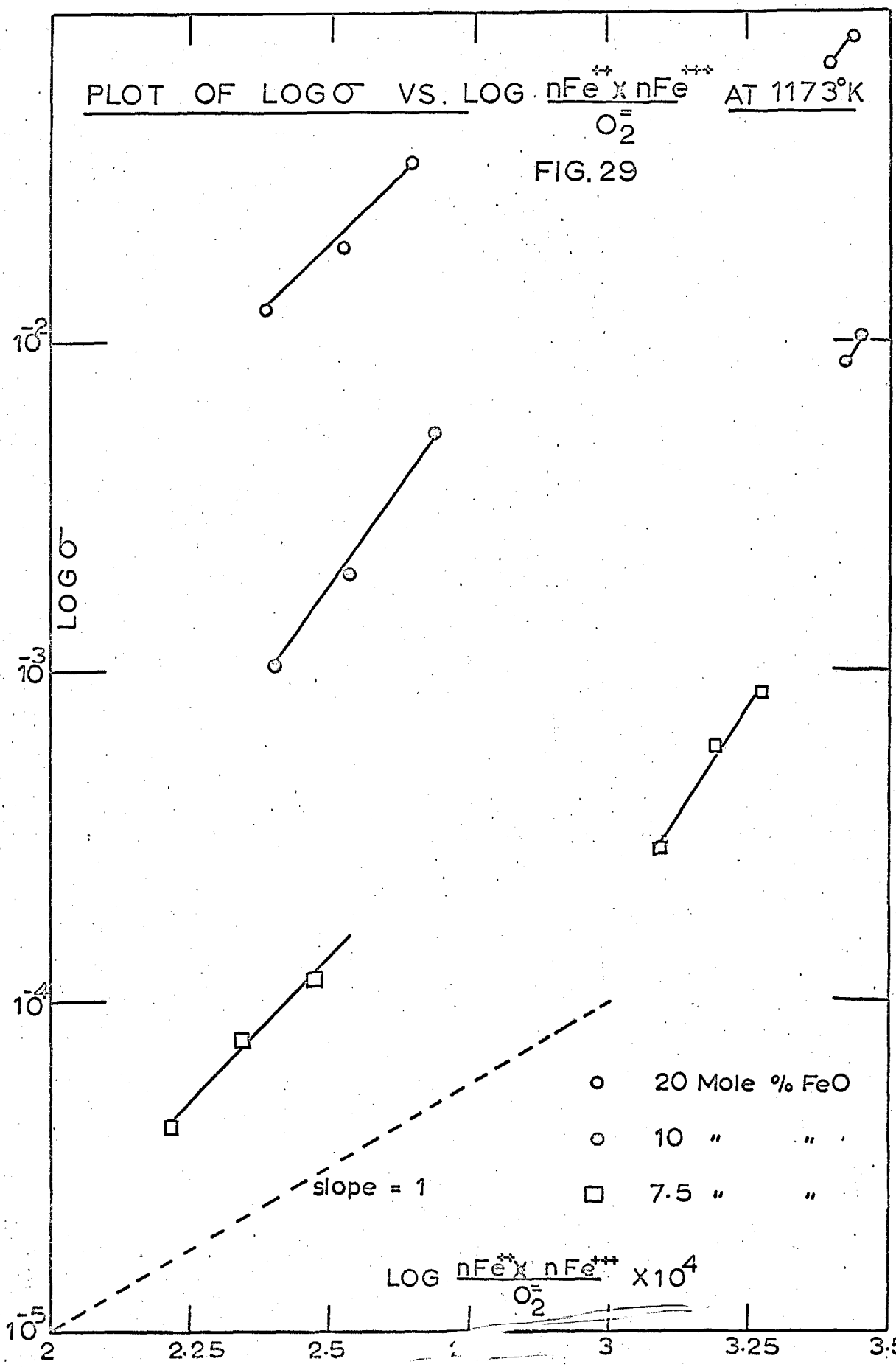
PLOT OF LOG σ VS. LOG $\frac{nFe^{++} \times nFe^{+++}}{O_2^=}$ AT 1173°K
FIG. 29
LOG σ
10^{-2}
10^{-3}
10^{-4}
10^{-5}
20 Mole % FeO
10 " "
7·5 " "
slope = 1
LOG $\frac{nFe^{++} \times nFe^{+++}}{O_2^=} \times 10^4$
2
2·25
2·5
3
3·25
3·5

is small compared to the pure wustite phase. This would not only effect the electron transfer process, but also decreases the probability of finding an acceptor site for the hole.

3) The presence ofaltavalent ions of different nature and radii might cause significant lattice distortion, thus influencing the conductivity-composition relationships.

Using the results of chemical analysis and the conductivity data at $1173^{o}k$, the hole mobilities have been calculated using the equation $\mu = \sigma / ne$ (4.4). Where n is the number of holes per cm^3 (equal to the ferric ion concentration). The calculated mobility is found to increase from 1.5×10^{-6} to 4.5×10^{-4} cm^2/volt sec as the total iron content increases from 5 to 20 mole per cent FeO. The corresponding hole mobility in wustite phase is about 0.11 cm^2/volt sec. Such a low carrier mobility clearly suggests hopping conduction in these solid solutions. Additional evidence in support of this conclusion is provided by the theoretical analysis of the hopping model by Jiro Yamashita[6]. He has suggested that the magnetude of the carrier mobility can be used as one of the guides to understand the conduction mechanism in the semi-conductors. If the carrier mobility is smaller than 1 cm^2/volt sec. conduction mechanism could be satisfactorily interpreted in terms of the hopping model.

Despite the non-linear variation of conductivity with

$n_{Fe^{++}}\ n_{Fe^{+++}}/O_2^{=}$ function, it appears that the conduction process in the MgO - FeO solid solutions containing Fe - Fe pairs in the next nearest positions could be satisfactorily explained in the light of the hopping model. Experimental evidences in support of the above conclusions are, low carrier mobility (10^{-4} cm^2/volt sec.) and the conductivity data appear to fit well with the equation (4.2) derived by Mitoff for hopping conduction.

In the solid solutions containing 1 to 5 mole per cent FeO iron - iron neighbours are no longer present in the next nearest positions and hence conduction mechanism appears to be different. This is indicated by a small power dependence of conductivity with oxygen partial pressure (1/8) and a marked influence of composition (i.e. total iron content) on the conductivity (Fig. 27). Should the conduction process in these dilute solutions involve a thermally activated hole transfer as mentioned above, not only the jump distance for the hole would be large (at least $2x^{o}A$ where x is the nearest anion - cation distance), also the hole has to overcome the screening effect due to magnesium ions in second co-ordination sphere.

However it is difficult to offer a satisfactory explanation for the observed conduction behaviour in the dilute solid solutions. It appears that the conduction mechanism in the dilute solutions is quite complex and requires a systematic theoretical approach.

CONCLUSIONS

The present work has indicated that the non-stoichiometric behaviour of $FeO-MgO-O_2$ system can be described fairly satis - factorily in terms of the defect equilibria usually proposed for the non-stoichiometric behaviour of the oxides. Since the partial heat of solution of oxygen in the solid solutions remains independent across the whole range of composition up to and including $Fe - O_2$ binary system, it appears that the thermodynamics of this ternary system is determined by the entropy changes only. The cation vacancies and ferric ions seem to form a variety of defect complexes.

The conductivity measurements have indicated a p-type semi-conduction in these solid solutions (containing up to 20 mole per cent FeO). It is noted that the total iron content has a marked influence on the dependence of conductivity with the oxygen partial pressure and more so on the magnitude of the conductivity. It appears that in the solid solutions containing 7.5 mole per cent and above, the change carriers are localized on the iron cations and the hopping model seems to be valid.

It is difficult to offer any theoretical explanation for the anomalous conduction behaviour exhibited by the solid solutions contained less than 5 mole per cent FeO.

ACKNOWLEDGEMENTS

I wish to express my sincere gratitude to Professor C.B. Alcock for his valuable advice and encouragement and constant supervision during this work.

I am grateful to Dr. B.C.H. Steele for many helpful discussions and criticisms.

I wish to thank Morganite Ltd., for the financial support which has made this study possible.

Many-sided technical assistance rendered by the staff of the Chemical Metallurgy and the workshop is appreciated.

The outstanding support of the members of the Nuffield research and Ceramics and Nuclear Materials research groups is deeply acknowledged.

I am indebted to my wife for her constant support and co-operation.

G.N.K. IYENGAR.

REFERENCES

1. E.J.W. Verwey etal, Philips Res. Rept., 5, 173 (1950).

2. C. Kittel, "Introduction to Solid Stote Physics", John Wiley & Sons, New York (1961).

3. F.J. Morin, The Bell Syst. Tech. J., 37, 1037 (1958).

4. R.R. Heikes and W.D. Johnston, J. Chem. Phys., 26, 582 (1957).

5. C. Zener, J. Phys. Chem. Solids, 8, 26 (1959).

6. Jiro Yamashita, J. App. Phys., 32, 2215 (1961).

7. A.F. Wells, "Structural Inorganic Chemistry", Clarendon Press, Oxofrd (1962).

8. E.R. Jette and K. Fotte, J. Chem. Phys., 1, 29 (1933).

9. W.C. Hahn and A. Muan, Trans. A.I.M.E., 224, 416 (1962).

10. N.L. Bowen and J.F. Schairer, Am. J. Sci., 5, 29 (1935).

11. L.S. Darken and R.W. Gurry, J. Am. Chem. Soc., 67, 1398 (1946).

12. P.K. Foster and A.J.E. Welsh, Trans. Faraday Soc., 52, 1626 (1956).

13. K. Himmel, R.F. Mehl and C.E. Birchenall, Trans. A.I.M.E., 197, 827 (1953).

14. F.D. Richardson and R.A. Carter, ibid, 200, 1244 (1954).

15. E. Köch and C. Wagner, Z. Phys. Chem., B 32, 439 (1936).

16. J. Aubry and F. Marion, Compt. Rind., 241, 1778 (1955).

17. D.S. Tannhauser, J. Phys. Chem. Solids., 23, 25 (1962).

18. S.M. Ariya and B. Ya Brach, Soviet Physics - Solid State, 2, 2565 (1964).

19. G.G. Mikhalliov and V.A. Kozheuroff, Zh. Fiz, Khim., 39, 775 (1963).

20. G.H. Geiger, R.L. Levin and J.B. Wagner, J. Phys. Chem. Solids., 27, 947 (1966).

21. K. Hauffe and H. Pfeiffer, Z. Metallak, 44, 27 (1953).

22. D.M. Smyth, J. Phys. Chem. Solids, 19, 167 (1961).

23. J.S. Anderson, Proc. Roy. Soc., A 185, 69 (1946).

24. G.G. Libowitz, Prog. Solid State Chemistry, 2, 216 (1965).

25. R.F. Brebrick, J. Phys. Chem. Solids, 18, 116 (1961).

26. S.M. Ariya and M.P. Morozova, J. Genl. Chem., U.S.S.R. 28, 2647 (1957).

27. J. Brynestad and H. Flood, Z. Electro Chem., 62, 953 (1958).

28. W.L. Roth, Acta. Cryst., 13, 140 (1960).

29. P. Raccan etal, Mem. Scient. Rev. Metall., 62, 1 (1965).

30. A. Lempicki, Proc. Phyl, Soc. (London), B 66, 28 (1953).

31. E. Yamaka and K. Sawamato, J. Phys. Soc. Japan, 10, 176 (1955).

32. R. Mansfield, Proc. Phyl. Soc. (London), B 66, 612 (1953).

33. S.P. Mitoff, J. Chem. Phys., 31, 1261 (1959).

34. H. Schmalzried, ibid 33, 940 (1960).

35. S.P. Mitoff, ibid 36, 1383 (1962).

36. S.F. Paignev and A.D. Neuimim, Soviet Physics - Solid State, 4, 629 (1962).

37. R. Lindner and G.D. Parfitt, J. Chem. Phys., 26, 182 (1957).

38. Y. Oishi and W.D. Kingery, ibid 33, 905 (1960).

39. M.D. Davies, ibid 38, 1047 (1963).

40. B. Phillips, S. Somiya and A. Muan, J. Am. Ceram. Soc., 44, 167 (1961).

41. D. Woodhouse and J. White, Trans. Bri. Ceram. Soc., 54, 383 (1955).

42. A. Berthet, Ph. D. Thesis, University of Nancy, (1963).

43. L.G. Schmahl, B. Frisch and G. Stock, Arch. Eisenhüttenws, 32, 297 (1961).

44. Y.I. Gerasimov and A.V. Shaskina, Zh. Fiz. Khim., 27 399 (1953).

45. M.P. Morozova and G.D. Korlovskaya, Ser. Fitz. Khim., 1, 117 (1960).

46. K.W. Hanson and I.B. Cutler, J. Am. Ceram. Soc., 49, 100 (1966).

47. E.R. Rigby and I.B. Cutler, ibid, 48, 95 (1965).

48. W.L. Schaefer and G.W. Brindley, J. Phys. Chem. Solids, 24, 919 (1963).

49. G.W. Gloves and M.E. Fine, J. App. Phys., 35, 3587 (1965).

50. J. Weissbart and R. Ruka, Rev. Sci. Instruments, 32, 593 (1961).

51. T.W. Penrice, Powder Metallurgy, 1-2, 79 (1958).

52. B.C.H. Steele, Ph.D. Thesis, University of London (1965).

53. O. Kubaschewski and E. Li. Evans, "Metallurgical Thermochemistry", Pergoman, 3rd edition (1962).

54. A. Kubik, Ph. D. Thesis, University of London (1960).

55. L.L. Seigle, Trans A.I.M.E., 206, 91 (1956).

56. J.T. Jones and I.B. Cutler, J. Am. Ceram. Soc., 49, 57[illegible]

57. S. Aronson and J.C. Clayton, J. Chem. Phys., 32, 749 (1960).

58. L.E.J. Roberts etal, "Proceedings of the Second United Nations International Conference on the Peaceful use of Atomic Energy", Geneva, 28, 215 (1958).

59. B.J. Wuensch and T. Vasilos, J. Chem. Phys., 36, 2917 (1962).

60. K.V. Rao and A. Smakula, J. App. Phys., 36, 2031 (1965).

61. K. Hauffe and A.L. Vierk, Z. Physik. Chem., 196, 160 (1950).

59a. J.W. Orton et al, Dis. Faraday Soc, T26, 66 (1958)

60a. H. Flood et al, Acta Chemica Scandinavica, 15, 1624 (1961)

62. H.H. Baumbach and C. Wagner, ibid, B 22, 199 (1933).

63. D.G. Thomas, J. Phys. Chem. Solids, 3, 229 (1957).

64. S.P. Mitoff, J. Chem. Phys., 35, 882 (1961).

APPENDIX I

Comparisons of various notations of centers for the case of MgO containing vacancies.*

IONIC NOTATION	ATOMIC NOTATION	SCHOTTKY'S NOTATION	REES'S NOTATION	EFFECTIVE CHARGE
MgO	$Mg^{2+}\ O^{2+}$	MgO	$Mg^{2+}\ O^{2-}$	
V_{Mg}	$V_c 2+$	$Mg\square^{x}$	$(P_2/\square^{+})$	0
V_{Mg}'	$(V_c+)'$	$Mg\square'$	$(P/\square^{+})$	-1
V_{Mg}''	$(V_c)''$	$Mg\square''$	$\square^{+}$	-2
V_O	$V_A=$	$O\square^{x}$	$(e_2/\square^{-})$	0
V_O'	$(V_A-)^{\bullet}$	$O\square^{\bullet}$	$(e/\square^{-})$	+1
V_O''	$(V_A)^{\bullet\bullet}$	$O\square^{\bullet\bullet}$	$\square^{-}$	+2

* Ref. F.A. Kröger and H.J. Vink, Solid State Physics, 3, 310 (1956).

APPENDIX II

Calculation of the energy requirements for the various electronic transitions in wustite.

An attempt has been made to propose an energy level diagram for wustite, similar to that proposed by Morin[1] for nickel oxide. The charge carriers in wustite are produced by the following reactions, in which the electronic states represented, are separated by large distances in the crystals:

$$Fe^{++}(3d^6) + O^{=}(2p^6) = Fe^{+}(3d^7) + O^{-}(2p^5) \qquad (1)$$

$$Fe^{++}(3d^6) + Fe^{++}(3d^6) = Fe^{+}(3d^7) + Fe^{+++}(3d^5) \qquad (2)$$

$$V_{Fe^{++}} - Fe^{+++}(3d^5) + Fe^{++}(3d^6) = V - Fe^{++}(3d^6) + Fe^{+++}(3d^5) \qquad (3)$$

$$Fe^{+++}(3d^5) + O^{=}(2p^6) = Fe^{++}(3d^6) + O^{-}(2p^5) \qquad (4)$$

These reactions represent:

1) The formation of a hole in the 2 p band and an electron in 3 d levels.

2) The formation an electron-hole pair in the 3 d levels.

3) The trapping of an electron by the ferric ion situated near the vacancy with the formation of a hole in the 3 d levels.

4) The trapping of an electron by the ferric ion and the formation of a hole in 2 p bond.

Consider first, the energy required to remove an electron from $O^{=}$ ion and place it on a distant Fe^{++} ion site in the lattice as shown in the reaction (1). The total energy required for the

transition $O^- + e = O^=$ have been to be $^-9.7$ ev[20]. This energy is plotted relative to the $2p^5$ level plus an electron on the left of the diagram (1). The ionization potential of Fe^+ ($3d^7$) is 16.2 ev and is plotted relative to $3d^6$ level. When the ions are brought together to form the lattice, the energy level of the negitive ion is depressed and that of positive is raised, both by an amount equal to the Madelung potential, which is 23.62 ev for wustite. These levels are now moved to -13.92 ev ($2p^5$) and +7.4 ev ($3d^7$). The difference in the energy between these two levels, 21 12 ev is the energy required for the reaction (1). Since the above reaction (1) is carried out in a dielectric, the energy required is reduced by a factor, equal to the dielectric constant of the lattice. Taking this value as 20 for wustite, the energy required for the reaction (1) is found to be 1.05 ev. This energy is shown (on the enlarged scale) on the right of the diagram (1).

Similarly the calculations have been of the energy requirements for the reactions (2) and (4) using the appropriate data. The corresponding energies are shown on the right of the diagram.

Energy required for the reaction (3) can be calculated as follows. In wustite each vacant cation site is surrounded by twelve Fe^{++} ions and two of ferrous ions (Fig. 3a) yield an electron each to form Fe^{+++} ions to compensate for the absence of the ferrous ion. From the Fig. 3a, it follows that each Fe^{+++} ion is surrounded by a normal lattice minus one Fe^{++} ion at a

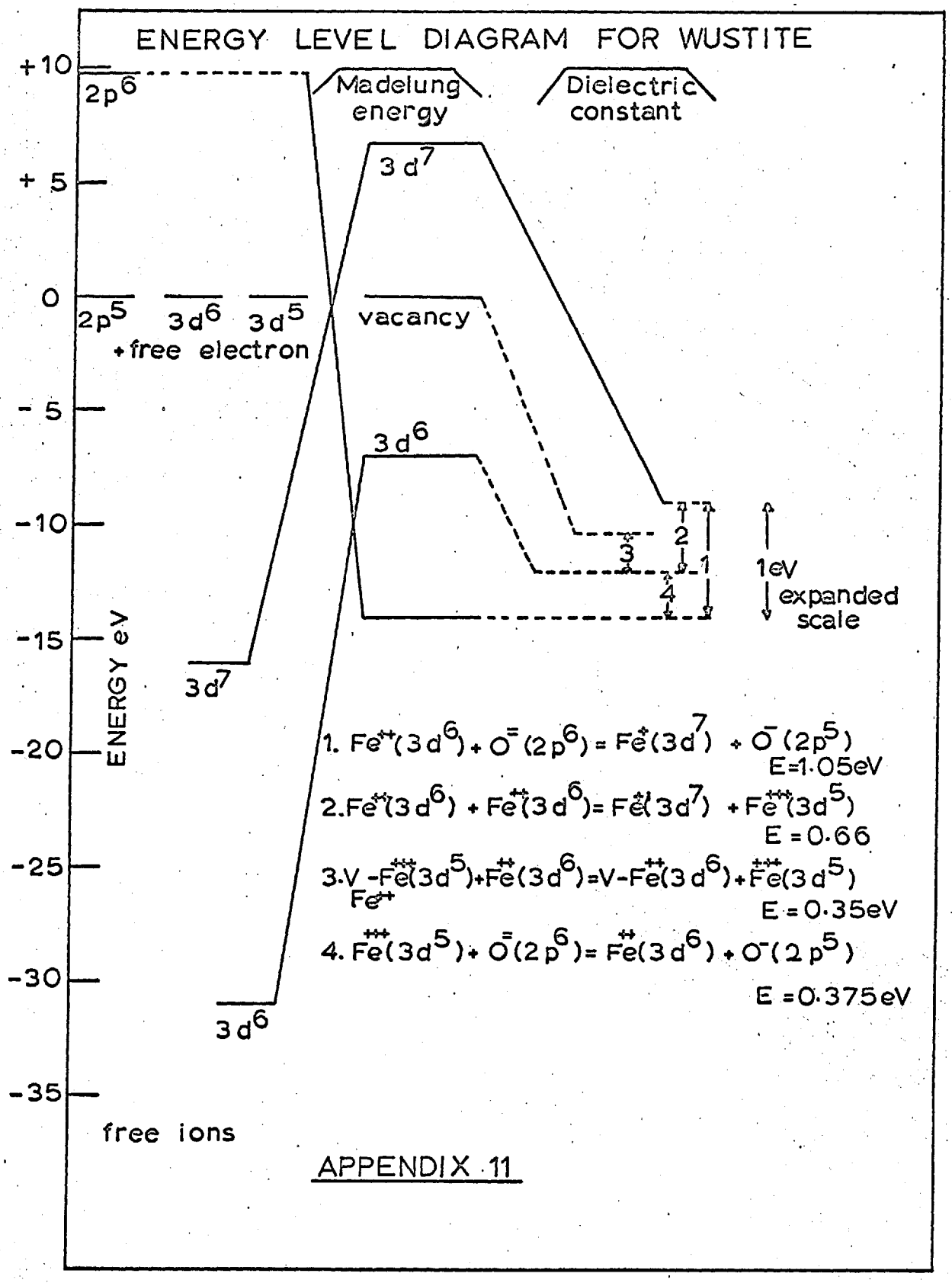
ENERGY LEVEL DIAGRAM FOR WUSTITE
+10
+ 5
0
- 5
-10
-15
-20
-25
-30
-35
ENERGY eV
2p6
Madelung energy
Dielectric constant
3d7
2p5
3d6
3d5
+free electron
vacancy
3d6
3d7
3d6
2
3
1
4
1eV
expanded scale
1. Fe++(3d6) + O=(2p6) = Fe+(3d7) + O-(2p5)
E=1.05eV
2. Fe++(3d6) + Fe++(3d6) = Fe+(3d7) + Fe+++(3d5)
E = 0.66
3. V-Fe+++(3d5) + Fe++(3d6) = V-Fe++(3d6) + Fe+++(3d5)
Fe++
E = 0.35eV
4. Fe+++(3d5) + O=(2p6) = Fe++(3d6) + O-(2p5)
E = 0.375eV
free ions

APPENDIX 11

distance equal to $a\sqrt{2}/2$ plus one positive charge (Fe^{+++}) situated at a distance $a\sqrt{2}$ where a is the lattice constant of wustite (i.e. a = 4.2 ^{o}A). Hence the potential at one Fe^{+++} site is the sum of the normal Madelung potential-plus $2e^2/a\sqrt{2}/2 - e^2/a\sqrt{2} = 23.82 + 9.78 - 2.41 = 31.2$ ev. Thus the level of this ion is raised to 7.4 ev above the normal $3(d^6)$ ions. Dividing this energy (7.4 ev) by the dielectric constant yields 0.35 ev which is the energy required for the reaction (3). All these energies are shown in the diagram (1). From these calculations we can infer that the energy requirements for the reactions (3) and (4) are nearly the same.

1 F.J. Morin, The Bell Syst. Tech. J. 37, 1037 (1958).

2. "Atomic energy levels" N.B.S. Circular 467 vols. (1949)

APPENDIX III

Impurity Contents in the Gases Used.

Gas Used	Purity %	Impurity Contents p.p.m.			
		O_2	GO_2	CO	N_2
H_2	99.9	10	10	10	0.01%
CO_2		H_2O	N_2	O_2	CO
		30	15	5	½
CO	99.0	O_2	CO_2		N_2
		0.15.1	0.2.1		0.6%

APPENDIX IV

Calculation of the oxygen partial pressure in the gas phase.

The oxygen partial pressure of the gas phase at equilibrium, can be calculated from the composition of the ingoing gas (e.g. CO_2^i/H_2^i in the present case) and the standard free energies of formation of the gaseous species, at known temperature. The reaction between H_2 and CO_2 can be represented

$$H_2 + CO_2 = H_2O + CO \qquad (5)$$

Thus it follows from stoichiometry,

$$\frac{p_{CO_2}^i}{p_{H_2}^i} = \frac{p_{CO} + p_{CO_2}}{p_{H_2} + p_{H_2O}} \qquad (6)$$

Where $p_{CO_2}^i$ and $p_{H_2}^i$ represent the partial pressurs of the ingoing CO_2 and H_2 respectively and p_{H_2O}, p_{CO}, p_{H_2} and p_{CO_2} represent the corresponding partial pressures at equilibrium.

From the reaction (5)

$$p_{H_2O} = p_{CO} \qquad (7)$$

hence the equation (6) can be written as

$$\frac{p_{CO_2}^i}{p_{H_2}^i} = \frac{1 + p_{CO_2}/p_{CO}}{1 + p_{H_2}/p_{H_2O}} \qquad (8)$$

The equilibrium constant for the reaction (5) is given by the equation (9)

$$k_5 = \frac{p_{H_2O}}{p_{H_2}} \quad \frac{p_{CO}}{p_{CO_2}} \qquad (9)$$

From the above equation

$$\frac{p_{H_2}}{p_{H_2O}} = \frac{1}{k_5} \quad \frac{p_{CO}}{p_{CO_2}} \qquad (10)$$

Considering the reaction,

$$CO + \tfrac{1}{2}O_2 = CO_2 \qquad (11)$$

and the corresponding equilibrium constant

$$k_{11} = \frac{p_{CO_2}}{p_{CO}} \quad \frac{1}{p_{O_2}} \quad \tfrac{1}{2}$$

or

$$\frac{p_{CO_2}}{p_{CO}} = k_{11} \; p_{O_2}{}^{\frac{1}{2}} \qquad (12)$$

substituting equation (10) in the equation (8) we get

$$\frac{p_{CO_2}^{i}}{p_{H_2}{}^{i}} = \frac{\left(1 + \frac{p_{CO_2}}{p_{CO}}\right)}{\left(1 + \frac{1}{k_5} \frac{p_{CO}}{p_{CO_2}}\right)}$$

or

$$= \frac{\frac{p_{CO_2}}{p_{CO}} \left(1 + \frac{p_{CO_2}}{p_{CO}}\right)}{\left(\frac{1}{k_5} + \frac{p_{CO_2}}{p_{CO}}\right)} \qquad (13)$$

From equations (12) and (13) it follows

$$\frac{p_{CO_2}^i}{p_{H_2}^i} = k_{11}\, p_{O_2}^{1/2} \left[\frac{1 + k_{11}\, p_{O_2}^{1/2}}{\frac{1}{k_5} + k_{11}\, p_{O_2}^{1/2}} \right] \qquad (14)$$

The equilibrium constants k_5 and k_{11} at various temperatures were calculated using the following thermodynamic data.*

$$\Delta G^\circ_{H_2O} = -58900 + 13.1\, T$$

$$\Delta G^\circ_{CO_2} = -94200 + 0.2\, T$$

and $$\Delta G^\circ_{CO} = -26700 - 20.75\, T$$

Thus the oxygen partial pressure at equilibrium, can be calcula - ted from known cold gas composition, using the equation (14) and knowing apprcpriate thermodynamic data.

* Taken from O. Kubaschewski and E. Li. Evans, "Metallurgical Thermochemistry" Pergoman, 3rd. ed.(1962).

APPENDIX V

Chemical analysis.

As mentioned earlier (see chapter 2, sec. 2.4 d) both colorimetric and volumetric methods were used to determine the relative amounts of ferrous and ferric iron in the equilibrated and subsequently quenched samples.

a. Spectrophotometric method.

After dissolving the quenched and well ground sample in conc. hydrochloric acid under oxygen-free nitrogen, the solution was cooled and diluted to a known volume (250 or 500 ml.) Aliquot portion containing 0.2 to 1.0 mg. of iron (5 or 10 ml.) was transferred to 100 ml. flask. The required amount of buffer (0.2 or 2 M sodium acetate) was added followed by 8 ml. of hydroxylamine hydrochloride (as a reducing agent) and 10 ml. of O. phenonthroline (prepared by dissolving 0.25 gms. of the reagent in 100 ml. warm demineralized water and subsequently cooled). After standing the solution for an hour the solution was made up to 100 ml. and the optical density was then determined in the Unicam spectrophotometer at 516μ wavelength using a blue filter. The iron content in the solution was obtained from a previously calibration chart. The total iron content was thus determined.

The ferrous iron content was determined as follows. A suitable aliquot (5 or 10 ml. of the stock solution) was treated with 10 ml. of O. phenonthroline reagent followed by a few drops

of dilute sulphuric acid and finally buffered with potassium hydrogen phthalate at pH 3.9 solution, was allowed to stand for an hour and finally diluted to 100 ml. and the ferrous iron content was determined as explained above.

The ferric ion content was found by the difference between the first and the second measurements. The analysis was repeated for concordant values.

b. Volumetric method.

The solution obtained by dissolving the quenched sample as explained above was acidified with 25.30 ml. of dilute sulphuric acid. 5ml. of ortho-phospharic acid was then added and followed by a few drops of barium diphemyl amine as an internal indicator. The solution was titrated against standard potassium dichromate of suitable strength.*

The total iron content was determined by reducing the above solution with stannous chloride in hot condition. The excess stannous chloride was destroyed by adding a requisite amount of saturated solution of mercuric chloride to the well cooled solution. The iron content was determined in the usual manner.

* Potassium dichromate solution of 0.01 to 0.02 N strength was used depending the composition of the sample.

APPENDIX VI

Results of chemical analysis.

Standard solutions used.

1) 0.025 mg/ml of iron (Fe^{++}).

2) 0.025 mg/ml of iron (Fe^{+++}).

3) 0.01 and 0.02 N $K_2Cr_2O_7$ solution.

Symbols Used.

OD_1 = optical density at 515μ to give total iron as ferrous iron using Hydroxylamine hydrochloride as a reducing agent.

OD_2 = optical density to give ferrous iron only (at 515μ).

V_1 = Titre value of dichromate before reduction to give the value for Fe^{++}.

V_2 = Titre value of dichromate after reduction with $SnCl_2$ to give the value for total iron.

W = weight of the sample taken.

NOTE.

Total and the mean total iron contents are expressed in weight per cent, whereas the nominal composition of the sample is expressed in mole % FeO.

Comp. Mole % FeO.	Total iron content Wt. % Fe.
3.2	4.32
5.00	6.68
7.50	9.79
10.00	12.71
20.00	24.05

TABLE VI.1. Calibration chart.

EXPT.A			EXPT.B			EXPT.C				
Vol. of solution taken mls.	Iron content mgs.	OD_2	Vol. of solution taken mls.	Iron content mgs.	OD_1	Vol. of Fe^{++} sol. taken	Vol. of Fe^{+++} sol. taken	Total iron content	OD_1	OD_2
10	0.25	0.25	2	0.05	0.051	19.00	1.00	0.50 (95%)	0.474	0.497
20	0.50	0.501	8	0.20	0.201	16.00	4.00	" (80%)	0.402	0.501
30	0.75	0.750	20	0.50	0.50	12.00	8.00	" (60%)	0.301	0.500
40	1.00	0.98	28	0.70	0.70	8	12.00	" (40%)	0.200	0.501
						4	16	" (20% Fe^{++})	0.097	0.500
						0	20	"	0.000	0.500

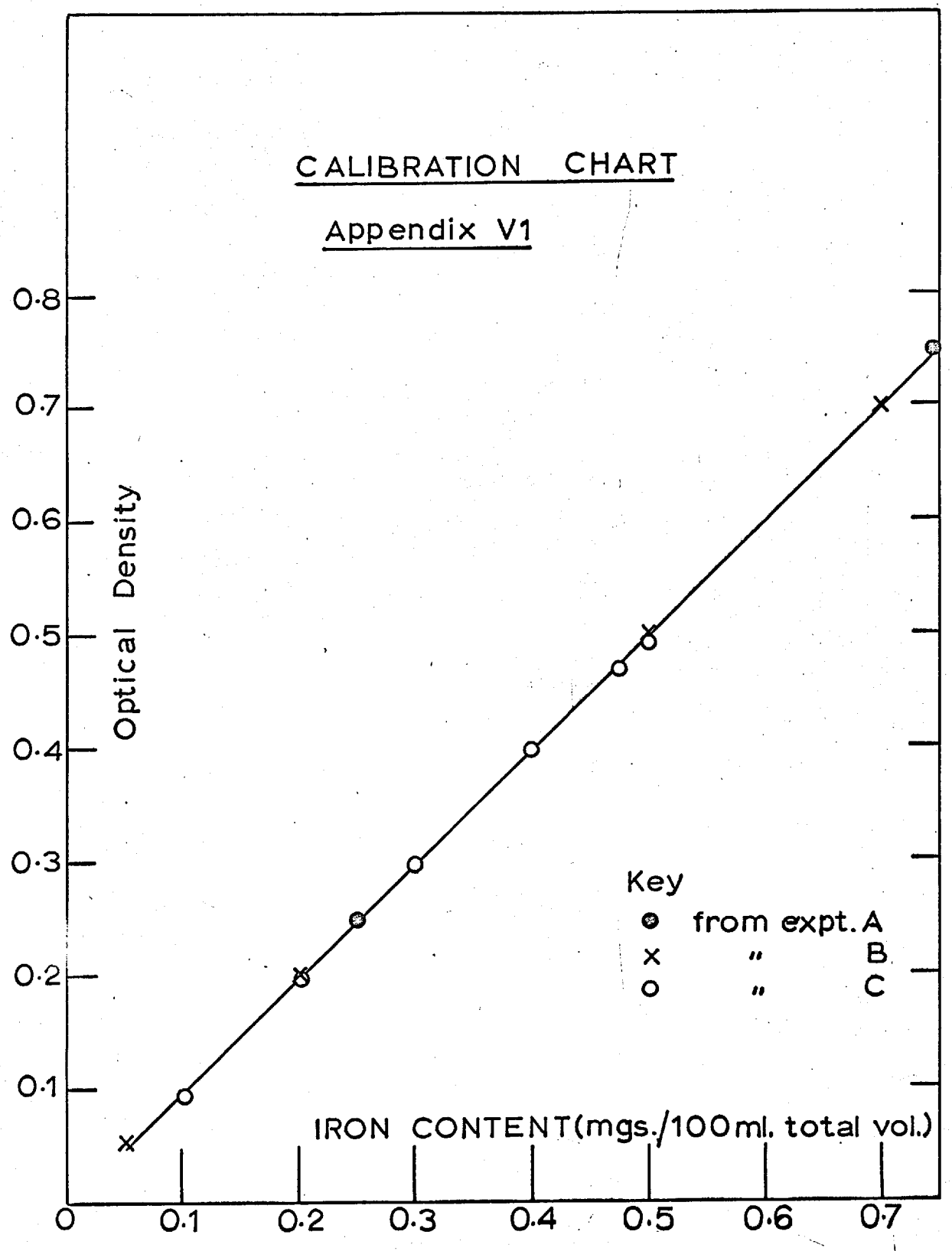
CALIBRATION CHART
Appendix V1
Optical Density
0·8
0·7
0·6
0·5
0·4
0·3
0·2
0·1
0
0.1
0.2
0.3
0.4
0.5
0.6
0.7
IRON CONTENT (mgs./100 ml. total vol.)
Key
from expt. A
" B
" C

TABLE VI .2. Experiments to test the method of analysis.

Sample	W gms.	V_1 mls.	V_2 mls.	$\frac{n_{Fe^{++}}}{n_{Fe^{+++}}+n_{Fe^{++}}}$ %	$N_{K_2Cr_2O_7}$	Iron content wt.%
Metallic iron	0.5122 * Dissolved in HCl/N_2 diluted to 250ml.	18.30	18.35	100	0.02 1ml=1.117 mg Fe	0.512 -100.
		18.30	18.30			
Magnetite	0.5681 *	12.35	36.9	33.33	"	72.2%
		12.30	36.95			
		12.30	36.85			
Solid solution of FeO in MgO (3.2ml.% FeO)	0.2001	-	15.30		0.01	4.29
	0.2708	20.6	20.8	99.0	"	4.31
" " "	0.1015	-	21.8	99.5	0.02	24.1
(20ml.% FeO).	0.1050	22.3	22.5			23.95

* 25ml. was taken for each analysis.

TABLE VI.3. Results of chemical analysis Temp. 1173°K

Comp. mole % FeO	P_{O_2} atm.	W gms.	Dilution ml.	Vol. taken ml.	OD_2	OD_1	$\frac{n_{Fe^{+++}}}{n_{Fe^{++}}+n_{Fe^{+++}}}$ %	Total iron content wt.%	Mean iron content wt.%	Mean $\frac{n_{Fe^{+++}}}{n_{Fe^{++}}+n_{Fe^{+++}}}$ %
3.2	10^{-18}	0.0971	100	10	0.420	0.409	2.6	4.32		2.7±0.1
		0.1225			0.530	0.515	2.8	4.32		
"	10^{-17}	0.1340	"	"	0.580	0.565	2.69	4.31		2.71±0.02
		0.1041			0.445	0.433	2.74	4.27	4.34	
"	10^{-16}	0.1141	"	"	0.500	0.485	2.84	4.39	±0.04	2.77±0.07
		0.0842			0.370	0.360	2.70	4.40		
"	10^{-15}	0.1265			0.550	0.510	7.30	4.35		7.45±0.15
		0.1370			0.59	0.545	7.6	4.31		
"	10^{-14}	0.1145	"	"	0.490	0.380	22.5	4.28		21.85±.65
		0.1090			0.470	0.371	21.2	4.31		

TABLE VI.4. Results of chemical analysis. Temp. 1173°K

Comp. mole % FeO	P_{O_2} atm.	W gms.	V_1 mls.	V_2 mls.	$\frac{n_{Fe^{+++}}}{n_{Fe^{++}}+n_{Fe^{+++}}}$ %	Dichromate strength N	Total iron content wt.%	Mean total iron content wt.%	Mean $\frac{n_{Fe^{+++}}}{n_{Fe^{++}}+n_{Fe^{+++}}}$ %
3.20	10^{-18}	0.2041	15.40	15.80	2.60	0.01	4.32	4.33 ±0.07	2.7±0.1
		0.2081	15.65	16.10	2.80		4.30		
	10^{-17}	0.2250	17.30	17.80	2.80		4.40		2.65±0.15
		0.1565	11.70	12.00	2.50		4.28		
	10^{-16}	0.1815	13.90	14.30	2.80		4.41		2.65±0.15
		0.2578	19.50	20.00	2.50		4.34		
	10^{-15}	0.2221	15.60	16.90	7.70		4.25		7.6±0.1
		0.2580	18.50	20.00	7.50		4.30		
	10^{-14}	0.2210	13.40	17.10	21.75		4.31		22.87±0.12
		0.2511	15.60	20.00	22.00		4.45		
	10^{-13}	0.2001	11.50	15.20	23.00		4.20		23.00
		0.2240	13.70	17.80	23.00		4.40		

TABLE VI.5. Results of chemical analysis Temp. 1173°K

Comp. mole % FeO	P_{O_2} atm.	W gms.	Dilution ml.	Vol.taken ml.	OD_2	OD_1	$\frac{n_{Fe^{+++}}}{n_{Fe^{++}}+n_{Fe^{+++}}}$ %	Total iron content wt.%	Mean total iron content wt.%	Mean $\frac{n_{Fe^{+++}}}{n_{Fe^{++}}+n_{Fe^{+++}}}$ %
2.00	10^{-18}	0.1195			0.400	0.384	4.0	6.67		4.1 ± 0.1
		0.1415			0.475	0.455	4.20	6.71		
"	10^{-17}	0.1530	500	25	0.500	0.480	4.00	6.65	$6.67\pm$	3.95 ± 0.05
		0.1380			0.465	0.446	3.9	6.74		
"	10^{-16}	0.1230			0.410	0.3920	4.40	6.64	±0.04	4.2 ± 0.2
		0.1501			0.500	0.480	4.00	6.65		
"	10^{-15}	0.1395			0.460	0.360	21.75	6.59		22 ± 0.25
		0.1405			0.470	0.365	22.25	6.67		
"	10^{-14}	0.1420	"	"	0.475	0.360	22.80	6.68		22.75 ± 0.150
		0.1401			0.467	0.360	22.90	6.70		

TABLE VI.6. Results of chemical analysis Temp. 1173°K

Comp. mole % FeO	p_{O_2} atm.	W gms.	V_1 mls.	V_2 mls.	$\frac{n_{Fe^{+++}}}{n_{Fe^{++}}+n_{Fe^{+++}}}$ %	Dichromate strehgth N	Total iron content wt.%	Mean total iron content wt.%	Mean $\frac{n_{Fe^{+++}}}{n_{Fe^{++}}+n_{Fe^{+++}}}$ %
5.00	10^{-18}	0.1385	16.20	16.90	4.20		6.81	6.70 $\pm$0.08	4.1$\pm$0.1
		0.1250	14.40	15.00	4.00		6.71		
	10^{-17}	0.1500	17.30	18.00	3.90		6.68		3.95$\pm$0.05
		0.1669	19.20	20.80	4.00	0.0 IN	6.69		
	10^{-16}	0.1530	17.55	18.30	4.10		6.65		4.00$\pm$0.1
		0.1610	18.75	19.30	3.90		6.70		
	10^{-15}	0.1530	13.15	18.10	22.90		6.61		23.00
		0.1690	15.40	20.0	23.00		6.60		
	10^{-14}	0.1610	14.80	19.50	24.00		6.76		24.0
		0.1360	12.15	16.00	24.00		6.60		
	10^{-13}	0.1580	14.00	19.20	27.00		6.68		27.00$\pm$0.1
		0.1410	12.70	17.20	26.90		6.81		

TABLE VI.7. Results of chemical analysis Temp. 1173°K

Comp. mole % FeO	p_{O_2} atm.	W gms.	Dilution mls.	Volume taken mls.	OD_2	OD_1	$\frac{n_{Fe^{+++}}}{n_{Fe^{++}}+n_{Fe^{+++}}}$ %	Total iron content wt.%	Mean total iron content wt.%	Mean $\frac{n_{Fe^{+++}}}{n_{Fe^{++}}+n_{Fe^{+++}}}$ %
7.50	10^{-18}	0.1121	250	10	0.435	0.428	1.61	9.71		1.7±0.10
		0.1429			0.553	0.543	1.81	9.69		
"	10^{-17}	0.1220	"	"	0.475	0.465	2.10	9.75	9.73 ±0.02	2.2±0.1
		0.1550			0.605	0.591	2.31	9.74		
	10^{-16}	0.1321			0.516	0.501	2.90	9.74		3.00±0.1
		0.1161			0.450	0.436	3.10	9.71		
	10^{-15}	0.1106	"	"	0.431	0.371	13.80	9.76		139±0.1
		0.1003			0.400	0.345	14.00	9.72		
	10^{-14}	0.1120	"	"	0.435	0.360	16.2	9.71		16.1±0.1
		0.1205			0.470	0.395	16.00	9.77		

TABLE VI.8. Results of chemical analysis Temp. 1173°K

Comp. Mole % FeO	p_{O_2} atm.	W gms.	V_1 mls.	V_2 mls.	$\frac{n_{Fe^{+++}}}{n_{Fe^{++}} + n_{Fe^{+++}}}$ %	Dichromate strength N	Total iron content wt.%	Mean total iron content wt.%	Mean $\frac{n_{Fe^{+++}}}{n_{Fe^{+++}} + n_{Fe^{++}}}$ %
7.50	10^{-18}	0.1371	23.50	24.00	1.90	0.01	9.80		2.0 ± 0.1
		0.1640	28.00	28.60	2.10		9.70		
	10^{-17}	0.1411	23.95	24.50	2.10		9.70		2.2 ± 0.1
		0.1116	19.350	19.80	2.30		9.90		
	10^{-16}	0.1491	25.10	25.90	3.10		9.71	9.74 ± 0.07	$3 \pm$
		0.1151	19.40	20.00	3.00		9.71		
		0.1210	20.50	21.20	3.0		9.80		
	10^{-15}	0.1140	17.10	19.80	13.90		9.68		14.00 ± 0.10
		0.1520	22.7	26.50	14.10		9.71		
	10^{-14}	0.1445	21.10	25.10	15.91		9.70		16.10 ± 0.1
		0.1594	23.60	28.10	16.10		9.81		
	10^{-13}	0.1470	20.10	25.60	21.40		9.75		21.55 ± 0.15
		0.1580	21.40	27.50	21.70				

TABLE VI.9. Results of chemical analysis Temp. 1173°K

Comp. mole %FeO	P_{O_2} atm.	W gms.	Dilution mls.	Volume taken mls.	OD_2	OD_1	$\frac{n_{Fe^{+++}}}{n_{Fe^{++}}+n_{Fe^{+++}}}$ %	Total iron content wt.%	Mean total iron content wt.%	Mean $\frac{n_{Fe^{+++}}}{n_{Fe^{++}}+n_{Fe^{+++}}}$ %
	10^{-18}	0.1600	500	10	0.405	0.395	2.42	12.65		2.41±0.1
		0.1955			0.495	0.473	2.43	12.68		
	10^{-17}	0.1875	"	"	0.455	0.440	3.3	12.71		3.5±0.2
10.00		0.1785			0.410	0.395	3.7	12.69	12.7±0.040	
"	10^{-16}	0.1870			0.455	0.435	4.4	12.80		4.5±0.1
		0.1956	"	"	0.500	0.477	4.6	12.81		
	10^{-15}	0.1871			0.475	0.275	41.7	12.69		41.9±0.20
		0.1771			0.450	0.260	42.1	12.71		
	10^{-14}	0.1971	"	"	0.500	0.280	43.8	12.69		44.0±0.20
		0.1694			0.430	0.240	44.2	12.69		

TABLE VI.10. Results of chemical analysis Temp. 1173°K

Comp. mole % FeO	P_{O_2}	W gms.	V_1 mls.	V_2 mls.	$\frac{n_{Fe^{+++}}}{n_{Fe^{++}}+n_{Fe^{+++}}}$ %	Dichromate strength N	Total iron content wt.%	Mean total iron content wt.%	Mean $\frac{n_{Fe^{+++}}}{n_{Fe^{++}}+n_{Fe^{+++}}}$ %
10.00	10^{-18}	0.1491	16.45	16.90	2.62	0.02	12.70	12.71 ±0.05	2.50±0.12
		0.1901	20.50	21.00	2.38		12.50		
	10^{-17}	0.1571	17.45	18.10	3.6		12.71		3.5±0.10
		0.1551	17.10	17.70	3.4		12.61		
	10^{-16}	0.1371	14.85	15.50	4.2		12.64		4.5±0.30
		0.1265	13.9	14.60	4.8		12.89		
	10^{-15}	0.1620	11.00	18.60	40.8		12.80		41.0±0.20
		0.1771	11.75	20.00	41.2		12.61		
	10^{-14}	0.1600	9.80	18.20	46.00		12.70		46.00
		0.1510	9.35	17.10	46.16		12.61		
	10^{-13}	0.1810	10.80	20.50	48.1		12.70		47.9±0.2
		0.1550	9.50	18.00	47.7		12.90		

TABLE VI.11. Results of chemical analysis Temp. 1173°K

Comp mole % FeO	p_{O_2} atm.	W gms.	Dil. mls.	Vol. taken mls.	OD_2	OD_1	$\frac{n_{Fe^{+++}}}{n_{Fe^{++}}+n_{Fe^{+++}}}$ %	Total iron content wt.%	Mean iron cont. %	Mean $\frac{n_{Fe^{++}}}{n_{Fe^{++}}+n_{Fe^{+++}}}$ %
	10^{-18}	0.2091	500	10.00	0.400	0.390	2.50	23.90		2.44 ± 0.06
		0.2401			0.462	0.451	2.38	24.00		
20.00	10^{-17}	0.2321	"		0.448	0.435	3.42	24.10	24.01 $\pm$0.10	3.5 ± 0.1
		0.2155			0.412	0.400	3.45	24.05		
		0.2201			0.425	0.411	3.6	23.95		
"	10^{-16}	6.1972	"		0.377	0.360	4.4	24.12		4.5 ± 0.10
		0.2260			0.435	0.415	4.6	24.10		
"	10^{-15}	0.2132	"		0.410	0.203	50.3	24.10		50.4 ± 0.1
		0.2232			0.420	0.211	50.5	23.80		
	10^{-14}	0.2093	"		0.402	0.202	49.7	24.10		49.65 ± 1.10
		0.2075			0.396	0.200	49.6	23.90		

Made up to 250 ml. Since the calibration was made on the basis of 10 ml. the OD_1 should be multiplied by 2.5 to give total iron.

TABLE VI. 12. Results of chemical analysis Temp. 1173°K

Comp. mole % FeO	P_{O_2} atm.	W gms.	V_1 mls.	V_2 mls.	$\frac{n_{Fe^{+++}}}{n_{Fe^{++}}+n_{Fe^{+++}}}$ %	Dichromate strength N	Total iron content wt.%	Mean total iron content wt.%	Mean $\frac{n_{Fe^{+++}}}{n_{Fe^{++}}+n_{Fe^{++}}}$ %
20.0	10^{-18}	0.0865	18.10	18.60	2.41	0.02	24.10	24.1±0.05	2.5±0.1
		0.1160	24.45	25.10	2.59		24.2		
	10^{-17}	0.1350	28.15	29.20	3.60		24.1		3.7±0.1
		0.1321	27.75	28.50	3.80		24.05		
	10^{-16}	0.1271	26.25	27.40	4.20		24.10		4.5±0.3
		0.1131	23.80	25.00	4.80		24.20		
	10^{-15}	0.1250	14.00	27.00	48.10		24.10		48.0±0.10
		0.1260	14.00	26.90	47.91		23.95		
	10^{-14}	0.1170	12.55	25.10	50.0		23.9		50±
		0.1210	13.00	26.00	50.0		24.10		
	10^{-13}	0.1250	13.4	27.00	50.40		24.10		50±
		0.1141	12.1	24.4	50.60		23.95		

TABLE VI.13. Results of chemical analysis. Temp. 1323°K

Comp. mole % FeO	p_{O_2} atm.	W gms.	V_1 mls.	V_2 mls.	$\frac{n_{Fe^{+++}}}{n_{Fe^{++}}+n_{Fe^{+++}}}$ %	Dichromate strength N $K_2Cr_2O_7$	Total iron content %	Mean total iron content %	Mean $\frac{n_{Fe^{+++}}}{n_{Fe^{++}}+n_{Fe^{+++}}}$ %
3.2	10^{-16}	0.2481	18.7	19.1	2.1	0.01	4.32		2.4±0.3
		0.2001	15.4	19.8	2.7		4.41		
	5×10^{-15}	0.2320	17.1	17.50	2.00	"	4.20		2.2±0.2
		0.2160	16.30	16.70	2.40		4.30		
	5×10^{-14}	0.2400	17.95	18.40	2.2		4.28		2.3±0.1
		0.2710	20.30	20.80	2.4		4.31	4.33±0.09	
	5×10^{-13}	-	-	-	-	-	-	-	-
	5×10^{-12}	0.2200	16.20	17.30	5.20	"	4.40		5.55±0.25
		0.1740	14.00	14.30	2.10		4.70		
		0.2010	16.00	17.00	5.90		4.30		
	5×10^{-11}	0.2290	15.7	17.70	11.30		4.30		11.6±0.30
		0.1941	14.1	16.00	11.90		4.48		
	5×10^{-10}	0.2191	14.50	16.60	12.70		4.21		12.9±0.20
		0.2471	16.60	19.10	13.10		4.34		

TABLE VI.14 — Results of chemical analysis — Temp. 1323°K

Comp., mole % FeO	p_{O_2} atm.	W gms.	V_1 mls.	V_2 mls.	$\frac{n_{Fe^{+++}}}{n_{Fe^{++}}+n_{Fe^{+++}}}$ %	Dichromate strength N	Total iron content wt.%	Mean total iron content wt.%	Mean $\frac{n_{Fe^{+++}}}{n_{Fe^{++}}+n_{Fe^{+++}}}$ %
5.00	10^{-16}	0.1590	18.50	19.1	3.60	0.01	6.68		3.8±0.2
		0.1550	17.95	18.70	4.00		6.75		
	5×10^{-15}	0.1270	15.10	15.70	3.80		6.92		3.95±0.15
		0.1420	16.40	17.10	4.10		6.71		
	5×10^{-14}	0.1265	14.40	15.00	4.00		6.61	6.71±0.11	4.1±0.2
		0.1208	14.15	14.80	4.40		6.84		
		0.1495	17.25	18.00	3.90		6.72		
	5×10^{-13}	0.1430	16.85	17.50	3.70		6.91		3.9±0.2
		0.1440	16.40	17.10	4.10		6.61		
	5×10^{-12}	0.1515	16.85	18.20	7.4		6.70		7.2±0.1
		0.1530	17.65	19.00	7.2		6.90		
		0.1510	16.30	18.00	7.1		6.65		
	5×10^{-11}	0.1371	15.05	16.20	7.1		6.20		7.25±0.15
		0.1391	16.00	17.30	7.4		6.67		
	5×10^{-10}	0.1601	16.00	19.30	17.1		6.70		17.5±0.3
		0.1496	15.00	19.20	17.6		6.60		
		0.1501	15.60	19.00	17.9		6.60		

TABLE VI.15 Results of chemical analysis Temp. 1323°K

Comp. mole % FeO	p_{O_2} atm.	W gms.	V_1 mls.	V_2 mls.	$\frac{n_{Fe^{+++}}}{n_{Fe^{++}}+n_{Fe^{+++}}}$ %	Dichromate strength N	Total iron content wt.%	Mean total iron content wt.%	Mean $\frac{n_{Fe^{+++}}}{n_{Fe^{++}}+n_{Fe^{+++}}}$ %
7.50	10^{-16}	0.1440	23.9	25.00	4.10	0.01	9.71	9.75 ± 0.07	4.00±0.1
		0.1596	26.9	28.00	3.90		9.78		
	5×10^{-15}	0.1355	22.60	23.50	3.8		9.69		4.00±0.2
		0.1570	26.15	27.30	4.2		9.70		
	5×10^{-14}	0.1480	25.00	26.20	4.6		9.87		4.4±0.2
		0.1560	25.90	27.00	4.20		9.70		
	5×10^{-13}	0.1140	19.15	20.00	4.10		9.78		4.10
		0.1254	21.20	22.10	4.10		9.71		
	5×10^{-12}	0.1473	23.50	25.50	7.90		9.72		7.00±0.1
		0.1501	24.35	26.50	8.10		9.86		
	5×10^{-11}	0.1216	19.20	21.50	10.70		9.82		10.7
		0.1179	18.20	20.60	10.70		9.75		
	5×10^{-10}	0.1105	16.10	19.20	16.20		9.71		16.5±0.3
		0.1240	18.30	22.00	16.80		9.67		

TABLE VI.16. Results of chemical analysis Temp. 1323°K

Comp. mole % FeO	p_{O_2} atm.	W gms.	V_1 mls.	V_2 mls.	$\frac{n_{Fe^{+++}}}{n_{Fe^{++}}+n_{Fe^{+++}}}$ %	Dichromate strength N	Total iron content wt.%	Mean total iron content wt.%	Mean $\frac{n_{Fe^{+++}}}{n_{Fe^{++}}+n_{Fe^{+++}}}$ %
10.00	10^{-16}	0.1631	18.40	18.70	1.40	0.02	12.80		
		0.1621	36.45	36.80	0.96	0.01	12.60		1.12 ± 0.12
		0.1540	34.65	35.00	1.00	"	12.65		
	5×10^{-15}	0.1381	31.55	32.00	1.40	"	12.85	12.72 $\pm$0.10	
		0.1333	29.70	30.00	1.00	"	12.55		1.2 ± 0.2
	5×10^{-14}	0.1845	20.45	21.00	2.50		12.70		
		0.2170	24.40	25.00	2.40		12.90		2.45 ± 0.05
	5×10^{-13}	0.2056	22.45	23.20	3.20		12.61		
		0.2070	22.70	23.80	3.4	"	12.70		3.3 ± 0.1
	5×10^{-12}	0.1878	19.55	21.10	7.40		12.58		
		0.2101	22.25	24.00	7.30		12.80		7.35 ± 0.05
	5×10^{-11}	0.2050	20.30	23.10	12.10		12.60		
		0.2070	20.60	23.60	12.70		12.70		
	5×10^{-10}	0.2220	21.25	25.00	15.00		12.60		
		0.2291	21.50	26.50	15.00		12.90		15.05 ± 0.05

TABLE VI.17 Results of chemical analysis Temp. 1323°K

Comp. mole % FeO	p_{O_2} atm.	W gms.	V_1 gms.	V_2 gms.	$\frac{n_{Fe^{+++}}}{n_{Fe^{++}}+n_{Fe^{+++}}}$ %	Dichromate strength N	Total iron content wt.%	Mean total iron content wt.%	Mean $\frac{n_{Fe^{+++}}}{n_{Fe^{++}}+n_{Fe^{+++}}}$ %
20	10^{-16}	0.1117	24.25	24.50	1.02	0.02	24.4	24.10 ±0.15	1.2±0.2
		0.1001	21.10	21.40	1.40		24.1		
	5×10^{-15}	0.1259	26.55	26.90	1.30		23.9		1.2±0.1
		0.1220	25.90	26.20	1.10		24.10		
	5×10^{-14}	0.1067	22.40	23.10	3.20		24.20		3.00±0.20
		0.1081	22.75	23.40	2.80		24.10		
	5×10^{-13}	0.1161	23.70	25.00	5.20		24.10		5.10±0.10
		0.1087	21.90	23.10	5.00		23.9		
	5×10^{-12}	0.1194	20.80	24.40	14.80		23.9		15.00±0.20
		0.1022	18.40	21.70	15.20		23.8		
	5×10^{-11}	0.1171	18.1	25.10	28.00		23.90		28.05±0.05
		0.1231	19.40	27.00	28.10		23.7		
	5×10^{-10}	0.1001	8.65	21.10	58.10		23.70		58.2±0.10
		0.1179	10.45	25.10	58.30		23.9		

TABLE VI.18 Results of chemical analysis Temp. 1473°K

Comp. Mole % FeO	Run No.	P_{O_2} atm.	W gms.	V_1 mls.	V_2 mls.	Dichromate strength $NK_2Cr_2O_7$	$\frac{n_{Fe^{+++}}}{n_{Fe^{+++}}+n_{Fe^{++}}}$ %	Total iron content %	Mean total iron content %	Mean $\frac{n_{Fe^{+++}}}{n_{Fe^{++}}+n_{Fe^{+++}}}$ %
3.2	52	10^{-14}								
	53									
"	54	5×10^{-13}	0.2141	16.80	17.2	0.01	2.9	4.49	4.40 ±0.07	2.56±0.34
	55		0.1960	14.55	15.00		2.7	4.27		
	56		0.2120	16.35	16.70		2.1	4.44		
"	57	10^{-11}	0.1960	15.05	15.50	0.01	2.9	4.41		2.7±0.2
	58		0.1930	15.60	16.00		2.5	4.61		
"	59	10^{-10}	0.2131	16.45	16.90		2.4	4.41		2.65±0.25
	60		0.2480	18.60	19.10		2.9	4.29		
"	61	10^{-9}	0.221	16.80	17.9	0.01	6.10	4.51		6.00±0.10
	62		0.235	16.75	17.8		5.90	4.21		
"	63	10^{-8}	0.2091	14.30	16.30		12.3	4.34		12.55±0.25
	64		0.1971	13.5	15.40		12.8	4.31		
"	65	5×10^{-8}	0.2120	14.4	17.40		17.3	4.31		17.6±0.30
	66		0.2031	13.2	16.10		17.9	4.41		

TABLE VI.19 Results of chemical analysis Temp. 1473°K

Comp. mole % FeO	p_{O_2} atm.	W gms.	V_1 mls.	V_2 mls.	$\frac{n_{Fe^{+++}}}{n_{Fe^{++}}+n_{Fe^{+++}}}$ %	Dichromate strength	Total iron content wt.%	Mean total iron content wt.%	Mean $\frac{n_{Fe^{+++}}}{n_{Fe^{++}}+n_{Fe^{+++}}}$ %
	10^{-14}	-	-	-	-	-	-	-	-
5.00	5×10^{-13}	0.1581	18.30	19.00	3.70	0.01	6.70		
		0.1545	17.75	18.50	4.10	"	6.71		3.9 ± 0.2
		0.1601	-	-	-	-			
	10^{-11}	0.1245	14.40	15.00	4.00		6.71		4.00
		0.1251	14.85	15.50	3.90		6.81	6.70 ±0.10	
	10^{-10}	0.1471	17.35	18.10	4.20		6.84		4.3 ± 0.1
		0.1416	16.25	17.00	4.40		6.71		
	10^{-9}	0.1455	16.00	17.5	8.30		6.72		8.5 ± 0.2
		0.1545	17.00	18.60	8.65		6.71		
	10^{-8}	0.1470	15.20	17.70	14.10		6.68		14.10
		0.1330	13.75	16.00	14.10		6.71		
	5×10^{-8}	0.1454	14.50	17.50	17.10		6.71		17.2 ± 0.1
		0.1635	16.30	19.00	17.3		6.52		

TABLE VI.20 Results of chemical analysis Temp. 1473°K

Comp. mole % FeO	p_{O_2} atm.	W grm.	V_1 mls.	V_2 mls.	$\frac{n_{Fe^{+++}}}{n_{Fe^{++}}+n_{Fe^{+++}}}$ %	Dichromate strength N	Total iron content wt.%	Mean total iron content wt.%	Mean $\frac{n_{Fe^{+++}}}{n_{Fe^{++}}+n_{Fe^{+++}}}$ %
	10^{-14}	-	-	-	-	-	-	-	-
7.5	5×10^{-13}	0.1494	25.25	26.00	2.90	0.01	9.71		3.0 ± 0.1
		0.1282	21.80	22.50	3.10	"	9.79		
	10^{-11}	0.1150	19.40	20.00	3.00		9.75		
		0.2022	34.50	35.6	3.10	"	9.85		3.0 ± 0.1
		0.1280	21.75	22.40	2.90		9.71	9.74 ± 0.09	
	10^{-10}	0.1175	19.75	20.40	3.10		9.71		3.05 ± 0.05
		0.1341	22.60	23.30	3.00		9.78		
	10^{-9}	0.1185	19.60	21.00	6.70		9.90		6.8 ± 0.1
		0.1201	20.20	21.70	6.90		9.80		
	10^{-8}	0.1175	17.20	20.20	14.90		9.65		15 ± 0.1
		0.1295	19.10	22.40	15.10		9.71		
	5×10^{-8}	0.1245	15.65	21.60	27.70		9.62		28 ± 0.3
		0.1261	15.75	22.10	28.30		9.79		

TABLE VI.21 Results of chemical analysis Temp. 1473°K

Comp. mole % FeO	p_{O_2} atm.	W gms.	V_1 mls.	V_2 mls.	$\frac{n_{Fe^{+++}}}{n_{Fe^{++}}+n_{Fe^{+++}}}$ %	Dichromate strength N	Total iron content wt.%	Mean total iron content wt.%	Mean $\frac{n_{Fe^{+++}}}{n_{Fe^{++}}+n_{Fe^{+++}}}$ %
10.00	10^{-14}	0.1791	19.50	20.10	3.00	0.02	12.50		3.05±0.05
		0.1561	17.15	17.70	3.10		12.70		
	5×10^{-13}	0.1871	20.50	21.20	3.3		12.61	12.72 ±0.12	3.35±0.05
		0.1725	18.45	19.10	3.4		12.48		
	10^{-11}	0.2115	23.40	24.20	3.3		12.76		3.6±0.30
		0.1811	19.85	20.60	3.9		12.71		
	10^{-10}	-	-	-	-	-	-	-	-
	10^{-9}	0.1870	18.55	21.20	12.4		12.68		12.5±0.1
		0.1960	19.60	22.4	12.6		12.78		
	10^{-8}	0.1740	14.60	20.10	30.5		12.96		31.0±0.5
		0.1970	15.20	22.40	31.5		12.61		
	5×10^{-8}	0.1891	11.35	21.00	45.9		12.81		46.0±0.10
		0.2141	12.90	23.90	46.1		12.59		

TABLE VI.22 Results of chemical analysis Temp. 1473°K

Comp. mole % FeO	p_{O_2} atm.	W gms.	V_1 mls.	V_2 mls.	$\frac{n_{Fe^{+++}}}{n_{Fe^{++}}+n_{Fe^{+++}}}$ %	Dichromate strength N	Total iron content wt.%	Mean total iron content wt.%	Mean $\frac{n_{Fe^{+++}}}{n_{Fe^{++}}+n_{Fe^{+++}}}$ %
20.00	10^{-14}	0.0963	19.85	20.70	4.10		24.10		4.2 ± 0.1
		0.1075	22.20	23.20	4.30		24.20		
	5×10^{-13}	0.0991	20.50	21.4	4.20	0.02	24.10		4.15 ± 0.05
		0.1016	20.95	21.80	4.10		24.00		
	10^{-11}	0.1021	21.10	22.0	4.10		24.10	24.02 ± 0.05	4.16 ± 0.05
		0.1080	22.2	23.20	4.30		23.95		
	10^{-10}	0.1110	21.80	23.80	8.40		24.00		8.5 ± 0.1
		0.1041	19.20	21.00	8.60		23.80		
	10^{-9}	0.0944	14.50	20.20	28.10		24.10		28.05 ± 0.05
		0.1120	17.6	24.40	28.00		24.20		
	10^{-8}	0.0927	13.3	20.00	33.30		24.20		33.0 ± 0.30
		0.1141	16.60	24.60	32.70		24.09		
	5×10^{-8}	0.1062	11.55	23.10	50.10		24.20		50
		0.1041	11.30	22.60	50.00		24.10		

APPENDIX VII

Calculation of the activation energies

Using the relation

$$\sigma = c\, p_{O_2}^{1/m} \exp. \left(- \frac{\frac{\Delta H_f}{m/2} + \Delta H_{m\,\oplus}}{RT} \right)$$

The activation enthalpy for motion of the positive holes has been calculated from the slope of the plot log $(\sigma / p_{O_2}^{1/m})$ as a function $^{1}/_{T}{}^{o}K$. The following table summarize the results thus obtained.

Comp. mole % FeO	slope x 4576 = $-\left(\frac{\Delta Hf}{m/2} + \Delta H_{m\,\oplus}\right)$ k cals.	$\Delta H_f = \Delta H^{1}/2\theta_2$ k.cals	m	$\Delta H_{m\,\oplus}$
20.00	+14.70	-70 ± 5.0	6	8.7 ± 1.67
10.00	+14.10	-70 ± 5.0		10 ± 2.00
7.50	+17.60	-68 ± 0.5	4	16.4 ± 2.5